BER Analysis of UWB and mm-Wave Communication Systems Adhering to IEEE 802.15 WPAN Standards

A

Thesis submitted

for the award of the degree of

Doctor of Philosophy

By

Anand Agrawal

Department of Electronics and Electrical Engineering

Indian Institute of Technology Guwahati

Guwahati - 781 039, Assam, India

February 2018

Dedicated to

My Beloved Grandparents,

Late Dwarika Prasad Agrawal

and

Smt. Shanti Devi Agrawal

My Parents,

Shri Munna Lal Agrawal

and

Smt. Munni Devi Agrawal

Certificate

This is to certify that the thesis entitled "**BER Analysis of UWB and mm-Wave Communication Systems Adhering to IEEE 802.15 WPAN Standards**", submitted by **Anand Agrawal** (126102011), a research scholar in the *Department of Electronics and Electrical Engineering, Indian Institute of Technology Guwahati*, for the award of the degree of **Doctor of Philosophy**, is a record of an original research work carried out by him under my supervision and guidance. The thesis has fulfilled all requirements as per the regulations of the institute and in my opinion has reached the standard needed for submission. The results embodied in this thesis have not been submitted to any other University or Institute for the award of any degree or diploma.

Date:

Place: Guwahati.

Prof. Rakhesh Singh Kshetrimayum
Dept. of Electronics and Electrical Engg.
Indian Institute of Technology Guwahati
Guwahati, Assam, India - 781 039.

Dr. A. Rajesh
Associate Professor
Dept. of Electronics and Electrical Engg.
Indian Institute of Technology Guwahati
Guwahati, Assam, India - 781 039.

Acknowledgements

This dissertation would not have been possible without the guidance and the help of several individuals who in one way or another contributed and extended their valuable assistance in the preparation and completion of this study.

First and foremost, I feel it is a great privilege in expressing my deepest and most sincere gratitude to my main supervisor Prof. Rakhesh Singh Kshetrimayum, for his excellent guidance throughout my study. His kindness, dedication, hard work and attention to detail have been a great inspiration to me. My heartfelt thanks to you sir for the unlimited support and patience shown to me. I also remain indebted for all his help in patiently and carefully correcting my all manuscripts. At the same time, I want to thank my co supervisor, Dr. A. Rajesh for his special way of inspiring me. His deep insights, suggestions and discussions helped me at various stages of my research. I have no doubts that finishing my degree in a proper and timely manner was impossible without your suggestions and advices.

I would like to thank my doctoral committee members Prof. Prabin kumar Bora, Dr. Smarajit Das and Dr. K.V. Srikanth for sparing their precious time to evaluate the progress of my work. I express my heartfelt thanks to Prof. Anup Kumar Gogoi and Prof. Prabin kumar Bora for providing valuable suggestions on during my progress seminars. My special thank to Dr. P. R. Sahu, IIT Bhubaneswar, to gave me this opportunity and his valuable guidance in very initial phase of my PhD program. I thanks to Mr. Sanjib Das, Mr. Mukut Baruah, Mr. Uday S. Uzir, Ms. Jharana Rani and other staff members of department of electronics and electrical engineering, for maintaining an excellent computing facility and proving various resources useful my research work.

I am very thankful to prof. Chi-Chao Chao for inviting me to the National Tsing Hua University, Hsinchu Taiwan for student exchange in the fall of 2015. I am highly grateful to Hsin-yueh Hsu, Kyo patty, Youchi, Mayuresh, Tarique, Dinesh and Dhruv for the memorable

and joyful moments we shared together.

I had a great time with my many friends and seniors at IIT Guwahati, including (but not limited to) Dr. Murli, Dr. Brijesh, Dr. Somen, Dr. Sikandar, Shivanshu, Santosh, Ashish, Anamika dey, Sunil, Ramesh, Krishna, Venkata, Ripudaman, Ramanand, Mohit, Anirban, and the list goes on. I am also indebted to the my labmates Kukil, Himangshu, Mrinmoy, Dibyajyoti, Jitendra, Mohan, Niladri, Manoranjan and Darpan for their continuous support, help and wonderful memories they provided. My special thanks to Mrinmoy Bharadwaj for his invaluable helping hands. I thank my badminton buddies: Swapnali madam, Anamika madam, Nandan das, Shyam, Dipjyoti, Mukul, Kisor, Pankaj, Subrat, Basant, Arun, Vinod, Shatrughan, Uttam, Siddesh, Purushottam, Jitendra and others for making me cheerful during my stay. I wish to thank Mr. Dibyajyoti Das for helping me get through the difficult times and caring, suggestions he provided. My best buddies in school (Nitin, Deepak and Kailash) deserve special mention for various reasons and activities we did together.

I take this opportunity to sincerely acknowledge the Ministry of Human Resource Development (MHRD), Government of India, New Delhi, for providing financial assistance which buttressed me to perform my work comfortably.

Last but not least, I would like to to pay high regards to my parents, my uncles and aunties who raised me with a love of science, taught me and supported me in all my pursuits. I am deeply thankful to my sweet and caring sisters: Suman, Manju, Sunita, Ruby, Neeru, Seema and Muskaan, my brother in-laws: Manoj Bansal, Gopal Garg and Rajeev Gupta for their love, support, and sacrifices. This thesis will be incomplete without acknowledging my sweet nephew: Saksham, Aayu, Aman and Jatin and lovable niece Anushka, their smile are the secrete of my positive energy. I always indebted to my maternal uncle (Ashok Goyal) and maternal aunt (Usha Goyal) for their regular guidance and motivations. I thanks to my uncles: Ashok Agrawal, Suresh Agrawal, Rajendra Agrawal and aunties: Rakhi Agrawal and Usha Agrawal whose presence always gave me strength to pursuit mt study outside home. I thanks

to all my family members and relatives for their continuous support and encouragement. I dedicate this thesis to the memory of my grandfather Late shree Dwarika Prasad Agrawal, whose role in my life was, and remains, immense.

Anand Agrawal

Abstract

To be able to connect wirelessly to the internet is nowadays a basic part of daily activity and the number of wireless devices accessing wireless networks are increasing rapidly. However, the significant growth in the number of wireless devices along with the development of new high-rate applications and scarcity of microwave frequency spectrum are the major challenges. A promising way to increase the amount of available bandwidth is to utilize the higher frequency spectrum. Ultra- wideband (UWB) and Millimeter wave (mm-Wave) are the potential technologies for high-rate and short distance wireless communication. Both technologies have received great attention due to the license-free utilization of wide available frequency spectrum. Apart from the benefits, wide frequency spectrum has introduced few additional challenges in the typical Saleh-Valenzuela (S-V) channel model. One of the challenges in the modified S-V channel model is the distribution of multipath gain coefficients are lognormal rather than Rayleigh. As we know that, a lognormal random variable has no closed-form expressions of its cumulative distribution function, moment generating function and characteristic function, which are required to find the closed-form BER expression of wireless systems for such channels. For this reason, a lot of research has to be conducted to find the computable BER formulae for such wireless communication systems. Therefore, the thesis focuses on the derivation of computable BER formulae of UWB and mm-Wave wireless communication systems. Firstly, we present an approximate model of a square of lognormal shadowing by a Mixture of Gamma (MG)

distributions by using a moment-matching with non-linear curve fitting method. Using this approximation, we derive the characteristic function based computable BER formula of UWB system over the IEEE 802.15.3a channel model. Secondly, we derive an expression of BER for transmit antenna selection with maximal ratio combining (TAS/MRC) scheme based UWB-MIMO system, where the parameters of MG approximation are estimated by using the Expectation Maximization algorithm. Third, we evaluate the average BER for relay based UWB and LR-UWB systems over the IEEE 802.15.3a and the IEEE 802.15.4a channel models, respectively. In the analysis, each node is equipped with multiple antennas and the antenna selection scheme is performed at the source and the relay nodes. Next, we analyse the performance of antenna beamforming based mm-Wave MIMO system over the IEEE 802.15.3c channel at 60 GHz band. Besides, we show the impact of Rake's fingers on the BERs and suggest the sufficient number of Rake's fingers required to capture the maximum signal energy carried by multipath components in the various channel environments. We also show the effects of various parameters of the UWB and mm-Wave channel models on the performance. All the derived analytical expressions reported in this thesis are validated by the Monte-Carlo simulation results.

Contents

List of Figures

List of Tables

List of Acronyms and Abbreviations

AF	Amplify and Forward
Ana	Analytical
AOA	Angle of Arrival
AOD	Angle of Departure
AWGN	Additive White Gaussian Noise
BER	Bit Error Rate
BPSK	Binary Phase Shift Keying
BW	Band Width
CC	Cooperative Communication
CDF	Commutative Distribution Function
CF	Characteristic Function
CIR	Channel Impulse Response
CM	Channel Model
CPE	Conditional Probability of Error
CSI	Channel State Information
DF	Decode and Forward
EM	Expectation Maximization
ETSI	European Telecommunication Standards Institute
FCC	Federal Communications Commission
HPBW	Half Power Beam Width

i.i.d	Independent and Identically Distributed
IEEE	Institute of Electrical and Electronics Engineers
LN	Lognormal
LOS	Line-of-Sight
LR-UWB	Low Rate Ultra-Wideband
MG	Mixture of Gamma Distributions
MGF	Moment Generating Function
MIMO	Multiple-Input-Multiple-Output
mm-Wave	Millimeter-Wave
MSE	Mean Square Error
NLOS	Non-Line-of-Sight
PDF	Probability Density Function
PDP	Power Delay Profile
PSD	Power Spectral Density
QoS	Quality of Service
RVs	Random Variables
Rx	Receiver
Sim	Simulation
SISO	Single-Input-Single-Output
SNR	Signal to Noise Ratio
TAS/MRC	Transmit Antenna Selection with Maximal-Ratio Combining
TOA	Time of Arrival
TOD	Time of Departure
Tx	Transmitter
ULA	Uniform Linear Array
UWB	Ultra-Wideband

WPAN Wireless Personal Area Network

List of Symbols

N_t	Number of antennas at the transmitter
N_r	Number of antennas at the receiver
T_c	Chip duration
T_m	Arrival time of m^{th} cluster
$\tau_{r,m}$	Arrival time of r^{th} ray within the m^{th} cluster
L	Number of fingers of Rake receiver
p_e	Probability of error
$f_X(.)$	Probability density function of random variable X
$\mathbb{E}[.]$	Expectation operation
$F_X(.)$	Cumulative distribution function of random variable X
$\psi_X(\cdot)$	Characteristic function of random variable X
$\eta_X(.)$	Moment generating function of random variable X
$\mathcal{E}$	Energy captured by Rake receiver
Λ	Cluster arrival rate
λ	Rays arrival rate
Γ	Cluster power decay factor
γ	Rays power decay factor
$\mathbb{C}^{m\times n}$	A matrix of dimension $m \times n$
$\lvert.\rvert$	An absolute value or Modulus
$\lVert.\rVert_2$	2-norm of vector
$(.)^*$	Conjugate operation
$I_A(.)$	Indicator function of event $\{A\}$

1

Introduction

Contents

1.1 Introduction

During the last decade, wireless communications especially indoor or short distance communications have been penetrating into our society profoundly and making human life easier and smarter. The continuous advancements in technology, the increasing popularity of smartphones, scarcity of lower frequency spectrum and many more have encouraged the scientific and industrial communities to explore the possibilities of communications at higher frequency spectrum such as Millimeter-wave (mm-Wave) band or previously unallocated frequency spectrum like Ultra-wideband (UWB). The large available bandwidth of licence-exempted spectrum along with a few other favorable factors make the UWB and mm-Wave communication technologies ideal for high throughput and short distance wireless personal area networks (WPANs). To ensure global compatibility and interference-free transmission with the existing narrowband technologies, the IEEE 802.15 working committee has developed several WPAN standards. Among them, six most popular standards, IEEE 802.15.1 for bluetooth technology, IEEE 802.15.2 for coexistence of WPANs, IEEE 802.15.3 for high-rate WPANs, IEEE 802.15.4 for low-rate WPANs, IEEE 802.15.5 for mesh networking and IEEE 802.15.6 for body area networks (BANs) technologies are shown in Fig. 1.1. In addition to this, the committee has also introduced the IEEE 802.15.3a standard for high-rate indoor UWB communication system, IEEE 802.15.3c standard for mm-Wave indoor communication system at 60 GHz band and IEEE 802.15.4a for low-rate UWB communication system.

In this thesis, we focus on the high-rate WPAN (IEEE 802.15.3a and IEEE 802.15.3c) standards and low-rate WPAN (IEEE 802.15.4a) standard to derive the characteristic function based computable BER formulae for the UWB and mm-Wave wireless communications systems with various networks, such as multiple-input-multiple-output (MIMO), two-hop relaying and transmit antenna selection with maximal ratio combining (TAS/MRC) scheme. Besides, we present the impacts of Rake receiver and channel parameters on the BER of the investigating systems.

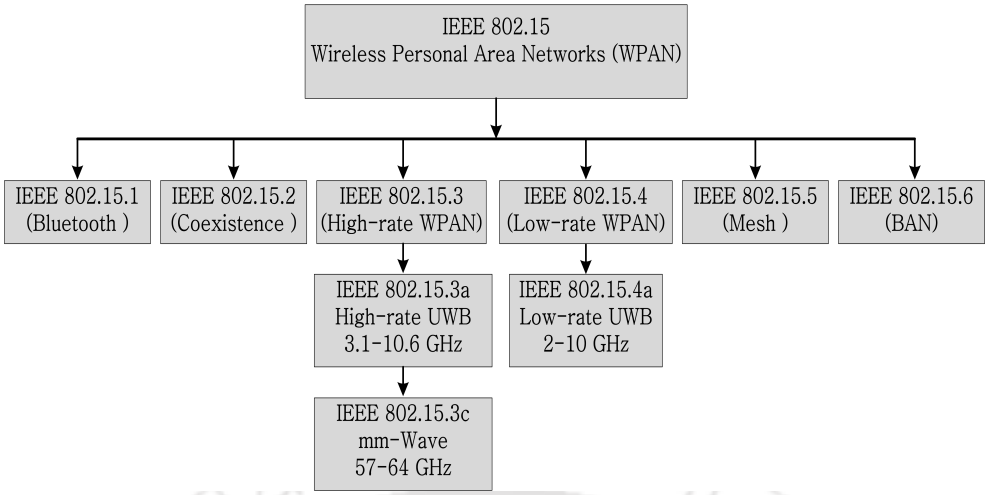

Figure 1.1: Organization of IEEE 802.15 working group

1.2 Ultra-Wideband Communication System

Impulse radio ultra-wideband (UWB) communication technology is a revolutionary, power-limited and carrier-free technology. It offers high-data-rate transmission, low-cost implementation, spectrum sharing and fading-robust communications. The term UWB was first used by the U.S. department of defence in the late 1980's, originally developed for highly secure military communications and radar applications. The first UWB signals were generated in experiments by Hertz in 1887, in which he generated sparks and radiated them using the wide-band pulse loaded dipoles. In 1901, G. Marconi performed an experiment, in which he transmitted the Morse-Code sequences across the Atlantic Ocean using the spark gap radio transmitters [1–3]. Although UWB has experienced, approximately, 40 years of technological developments, in the noteworthy milestone, a substantial change occurred in February 2002, when Federal Communications Commission (FCC) allocated the 3.1-10.6 GHz frequency spectrum for UWB technology under strict power emission limits. Similarly, in December 2004, European Union and in subsequent years, other countries adopted the similar approaches towards regularization of the UWB technology [4, 5]. According to the FCC Part 15 regulations, power constraint on the UWB signals (-41.3 dBm/MHz) allowed the UWB devices to share the 7.5 GHz wide frequency spectrum and interference-free transmissions with the others existing narrowband technologies

as shown in Fig. 1.2.

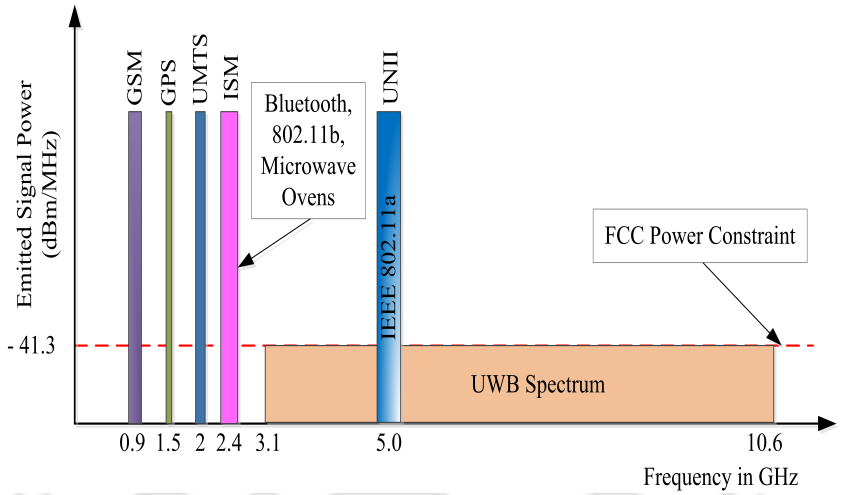

Figure 1.2: Spectral allocation and power emission limits of different radio systems

According to the Defence Advanced Research Projects Agency (DARPA) definition [6, 7], signals with a fractional bandwidth more than 25% or -10 dB bandwidth larger than 500 MHz are UWB signals. Mathematically, fractional bandwidth is defined as

$$B_f = \frac{2(f_H - f_L)}{f_H + f_L} \tag{1.1}$$

where f_H and f_L are the higher and lower frequencies bounds, respectively, of the -10 dB peak emission point. UWB can be characterized with ultra-short duration pulses which has excellent immunity to interference or multipath effects or fading problems. This type of transmission does not require the additional carrier modulation. Therefore, the technique is known as an impulse radio (IR) UWB. Some of the pulses, which are commonly used in UWB transmission are Gaussian pulse and its derivatives, Hermite pulse, Legendre pulse, Prolate pulse and etc. The nature of the above mentioned pulses together with the wide frequency spectrum of UWB technology offer several benefits. Some of the key benefits are listed below [8].

(i) Ability to share frequency spectrum

(ii) Large channel capacity

(iii) Ability to work with low signal to noise ratios

(iv) Multipath immunity and resistance to jamming

(v) Low probability of interception and malicious detection

(vi) Low-cost transceiver implementation

(vii) Superior penetration property

The parametric comparisons between the UWB and other narrow band technologies are given in Table 1.1.

Table 1.1: Parameter specifications for UWB and other narrow band technologies

PARAMETERS	TECHNOLOGIES			
	WLAN 802.11a	**BLUETOOTH**	**WLAN 802.11b**	**UWB**
Data Rate (Mbps)	54	1	11	100
Distances (m)	50	10	100	10
Spatial Capacity (Kbps/m2)	6.9	3.2	0.35	318.3
Spectral Capacity (bps/Hz)	2.7	0.012	0.1317	0.0133
Bandwidth (GHz)	0.02	0.0833	0.0835	7.5

In January 2003, the International Telecommunication Union (ITU) formed two task groups (TG) within IEEE 802.15 WPAN working group to investigate all the technical and compatibility issues of UWB technology [9, 10]:

(i) TG3a (IEEE 802.15.3a) for high data-rate UWB application

(ii) TG4a (IEEE 802.15.4a) for low data-rate UWB application

1.2.1 IEEE 802.15.3a WPAN standard

The aim of TG3a is to develop an alternate physical (PHY) layer for high-data-rate and short distance UWB communication. Originally, 25 proposals were presented in the first meeting of TG3a which was held in March 2003. Based on voting procedure and common consensus, some proposals have been eliminated. Later in the subsequent meetings (held in May 2003, July 2003 and September 2003), the total number of proposals were further reduced and finally, in September 2003, only two proposals were retained. One is called as Multiband Orthogonal Frequency Division Multiplexing (MB-OFDM) and the other is Direct Sequence UWB (DS-UWB). Since September 2003, TG3a encountered difficulty to further merge these two proposals or none of the two proposals have reached the 75% of the required votes. As a result, a motion to disband TG3a was adopted in 19 January 2006 [11, 12].

1.2.2 IEEE 802.15.4a WPAN standard

The main objective of TG4a of developing an alternative PHY layer for low-data-rate and long range UWB communication systems, was officially set up in March 2004. Unlike IEEE 802.15.3a standard, TG4a has successfully merged formal 26 proposals into one proposal and released a draft standard in April 2006 with 83.6% affirmation ratio [13–15].

The propagation characteristics and channel impulse response of the IEEE 802.15.3a and the IEEE 802.15.4a standards will be discussed in the subsequent chapters.

1.3 Millimeter-Wave Communication at 60 GHz Band

Millimeter-wave (mm-Wave) frequencies often refer to the frequency range from 30-300GHz, the wavelength of which is between 10-1mm, which means they are longer than infrared waves or X-rays but shorter than radio waves or microwaves. Frequency spectrum of mm-Wave band is depicted in Fig. 1.3. In this thesis, we will focus primarily on 60 GHz frequency band because it has enormous bandwidth. But it has strong oxygen absorption characteristics. Some key benefits that make mm-Wave communication at 60 GHz more attractive are [16–20]:

(i) *Unlicensed operation:* Companies do not have to buy a license from FCC, allowing them

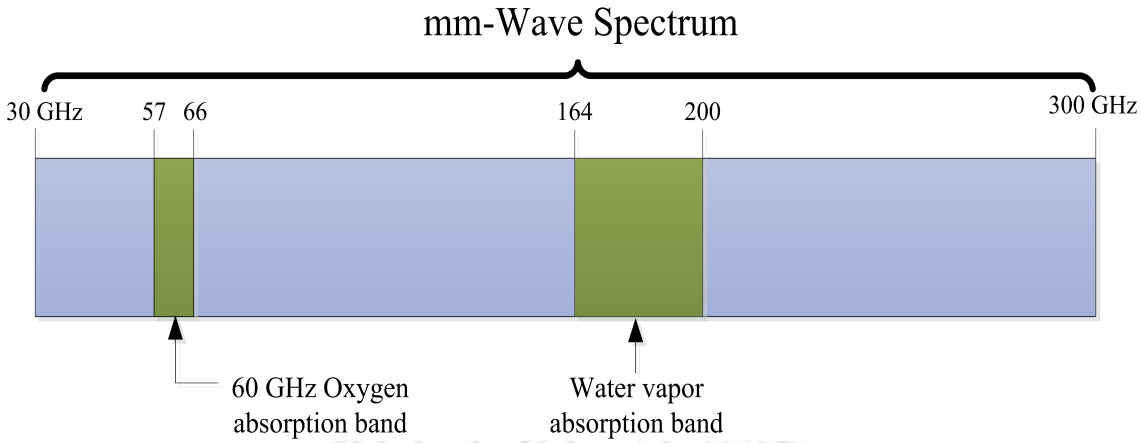

Figure 1.3: Millimeter wave spectrum

to deliver low cost and high performance wireless products.

(ii) *Huge channel bandwidth:* Most geographical regions provide 7 GHz bandwidth in the 60 GHz band.

(iii) *High security and excellent immunity to interference:* Oxygen absorption, a unique propagation characteristics of 60 GHz band provides an excellent mechanism to combat interference and ensures high security. Due to the absorption of electromagnetic energy by oxygen molecules, radiated signals cannot travel far beyond the intended receiver station.

(iv) *Narrow beam and frequency reuse:* Narrow beams of mm-Wave links allow for deployment of multiple independent links in close proximity and frequency can be reused due to the higher attenuation in free space at mm frequencies.

Unutilized 60 GHz band has allowed regulatory authorities around the world to create this (57-66 GHz) huge frequency spectrum for the unlicensed use. Region-wise spectrum allocation for mm-Wave band is illustrated in Fig. 1.4. In 2000, the Ministry of Public Management, Home Affairs, Post and Telecommunication (MPHPT) of Japan published 60 GHz regulations. In the year 2004, FCC of United States of America (USA) introduced the regulations in the 57-64 GHz band for the unlicensed use. The European Conference of Postal and Telecommunication

Administration (CEPT) and Ministry of Information and Communication (MIC), Korea established the regulations of the 60 GHz band in 2006. Australian Communications and Media Authority (ACMA) and the other regulatory authorities followed the international trend and released the 60 GHz regulations as well [21–23].

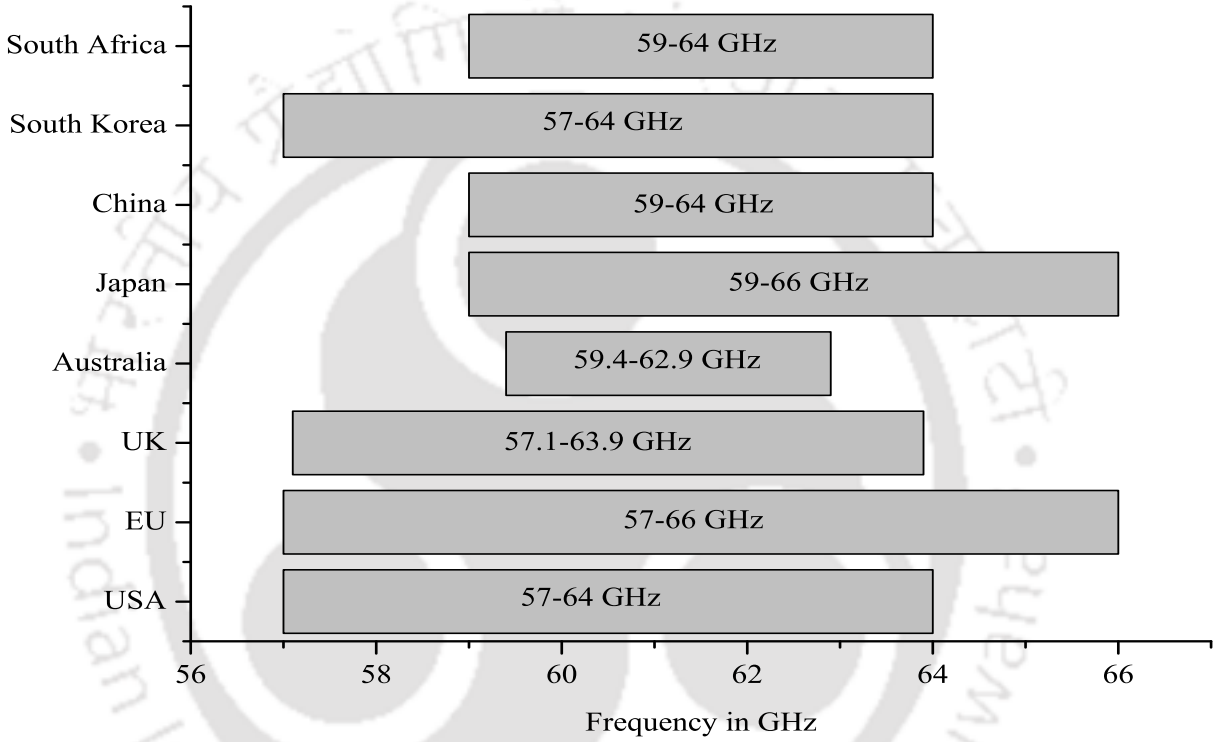

Figure 1.4: Unlicensed 60-GHz frequency allocations in selected geographical regions

After the regulations for the unlicensed operation in the 57-64 GHz band, several standards in 60 GHz wireless networks have been established by the several groups of international organizations [24–26]. The proposed standards are IEEE 802.15.3c, IEEE 802.11ad, European Computer Manufacturers Association (ECMA) 387, WiGig and Wireless HD. The IEEE 802.15.3c standard has been developed by the IEEE 802.15 Task Group (TG3c), which offers the alternative PHY for the high data rate wireless personal area network (WPAN) at 60 GHz

band, while the IEEE 802.11ad standard has been introduced by the IEEE 802 forum. Similarly, the ECMA 387 standard has been published by ECMA, while the specifications and the wireless interface for the WiGig and Wireless HD standards at 60 GHz have been published by the consortium of companies. In this thesis, we have adopted the IEEE 802.15.3c standard to analyse the performance of mm-Wave system. The propagation characteristics of the IEEE 802.15.3c standard and its parametric specifications will be covered in Chapter 6. Major area of applications of the mm-Wave wireless (MMW) technology are many, including telecommunications, military & defence, security services and medical & healthcare.

The mm-Wave communication at 60 GHz band is considered as one of the potential technology of 5G. The 5G technology is predicted to emerge in the coming years and the market is likely to witness its adoption significantly. Therefore, the Government of India (GOI) has particularly planned to provide necessary environment to the research community and industries so that country can play a leading role among the global community to design and finalize the 5G standards and frameworks. On September 26, 2017, the GOI announced that it has set up a 5G India 2020 forum comprising secretaries, industries, experts and academia (Professors from various IITs and other institutes). With this emphasis, the telecom gear maker Nokia is collaborating with the telecom giants including Bharti Airtel and state-run BSNL to prepare a roadmap for the development of a 5G network in the country. The company, which has already got the 5G IoT (Internet of Things) lab in Bangalore, will jointly conduct 5G demonstration and development. Ericsson and IIT Delhi have signed an MOU to jointly roll out a 5G program and will set up a center of excellence with 5G testbed. Huawei, one of the leading telecom and networking company highlighted its efforts in ensuring the rollout of a 5G network in the country on the platform India Congress 2017 organized in New Delhi. Imagination Technologies, a British based in technology company is already proving the WiFI chip module and other networking services on the IEEE 802.11ad WLAN standard which is very much similar to the IEEE 802.15.3c WPAN standard at 60 GHz band. Apart from this, several R&D centers and

faculties from IISc, IITM, IITD and other institutes in the country are working on mm-Wave communication at 60 GHz band.

1.4 Literature Review

The extensive literature related to the different performance evaluation parameters such as BER or symbol error rate (SER) and channel capacity of the short distance IEEE 802.15 WPAN communication systems, particularly, the UWB and the mm-Wave wireless communication systems have been reviewed. The review comprises of the literature of a TAS/MRC scheme, MIMO and cooperative networks associated with the UWB system presented in the various research articles. Furthermore, the existing literature related to an approximate model of the lognormal random variables (RVs) by other RVs have been reviewed. Summary of some of the reviewed literature relevant to the present research work has been presented in the subsequent paragraphs.

The error performance of the UWB wireless communication system over an IEEE 802.15.3a channel model has been analyzed and reported in [27–29]. The proposed solutions have been based on approximate model of a sum of independent lognormal RVs either by an another log-normal RV using Wilkinson's method [27] or by some other random distributions i.e., Pearson type IV distribution [28, 29]. In [30–32], the authors have investigated the performance for UWB wireless communications. In the investigations, the authors either did not consider the clustering phenomena or shadowing effect as in the IEEE 802.15.3a channel model. These two effects can not be ignored while investigating the performance of UWB system. In [33], the signal-to-interference-plus noise-ratio (SINR) of direct sequence UWB system in generalized S-V channels based on the theory of renewal process is analyzed. The analysis did not consider the shadowing effect. In [34], the authors have evaluated the pairwise error probability and out-age probability of MB-OFDM systems in the IEEE 802.15.3a channel model, but have ignored the effect of lognormal shadowing. In [35], the authors have derived the formulae for the char-acteristic function of the sum of gains arriving in a given time window, where multipath arrival

times and gains are specified by the IEEE 802.15.3a UWB channel model. In the derivation, the authors have considered the Gauss-Hermite and Gauss-Lengendre quadratures to find the approximate solutions of mathematically intractable integrals. The derived formulae are used to compute the PDF and CDF by numerically inverting the characteristic function. Using these formulae, the authors in [36], have derived the computable BER expression for binary signals in the IEEE 802.15.3a UWB channel model with a coherent Rake receiver. The derived computable BER formula is faster in computation and more accurate than the reported results, but it has failed to converge at high values of SNR. Because of the intractable mathematical expressions of lognormal distribution, the authors in [37] urged that lognormal distribution can be modeled by a Gamma distribution. Based on the theoretical and experimental results of shadowing phenomena, the authors in [38, 39] have shown that a Gamma distribution can be a good approximation to the lognormal distribution. In the approximation, the authors have equated the first two moments of both distributions and estimated the parameters of the Gamma approximation. From the results, it is evident that suggested approximation method is applicable in the relevant range ($\sigma \leq 9$dB) and the estimated Gamma distribution fits only the lower tails of the lognormal distribution. Literature in [40, 41] have demonstrated that a Mixture of Gamma (MG) distribution has great potential and can accurately approximate the composite shadowing/fading channel models, lognormal distribution and many other existing small-scale fading channels. In [42–45], the authors have computed the parameters of the estimated Gamma or Mixture of Gamma distributions by using Moments matching and Expectation-Maximization (EM) algorithms and observed that 2-step EM algorithm is more efficient and accurate than the moment matching method.

TAS technique was first introduced in 1973 [46]. This technique has drawn great attention and after combining with MRC diversity, the TAS/MRC scheme has been proposed in [47]. The advantages and initial results of the TAS/MRC scheme with various wireless systems encouraged researchers to explore the possibility of incorporation of TAS/MRC into the UWB com-

munication systems [48, 49]. The analysis reported in [50–52] demonstrates that TAS/MRC based wireless systems provide better SNR gains and BER performance than the space time block codes (STBCs) systems. In [53, 54], the MIMO technique has been applied to the UWB system for various wireless indoor channels. It has shown the improvement in the information rate and the robustness of the performance. The authors in [53], have employed a zero-forcing (ZF) scheme to separate N parallel transmitted data stream and then applied to a Rake receiver to combine the ZF paths carrying information. In [54], the authors have experimentally characterized the performance of the UWB system for spectral and polar antenna arrays. Apart from numerous benefits, a MIMO network poses higher hardware cost and calculation complexity. To address these issues, TAS scheme has emerged as a popular scheme. The performance of TAS scheme based MIMO-UWB systems has been investigated in [55]. The system has exploited spatial multiplexing and in order to cope the long delay spread of UWB channel, time reversal technique has been adopted. Most of the analyses of TAS scheme based UWB-MIMO systems have considered the simplified UWB channel model and also did not provide the BER formula, which presents opportunities for further investigations.

To discuss the shortcomings of conventional point-to-point communications, new class of methods of wireless communications called cooperative communication has been proposed in [56]. The core idea of the cooperative communication was introduced by Cover and El Gamal in 1979 [57], which enables the single antenna mobile to share their antenna and provide an additional new independent path to transmits the source information to the destination. Cooperative communications have been broadly categorized into user based cooperative diversity and relay based cooperative diversity [58–60]. Here, we focus on the relay based cooperative communication. Based on the relay protocols, many cooperative strategies have been suggested and reported in [61, 62]. Some of the popular relay protocols are Amplify and Forward (AF), Decode and Forward (DF), Selective relay, Coded cooperative and Compressed and Forward. The existing literature reported in [63, 64] have analyzed the performance of various relay pro-

tocols based two-hop wireless communication systems. The authors in [65], have first focused on the need of relaying UWB system and then investigated the performance. In the investigation, the authors have considered the simple-structured repeater as a relay, which can relay the pulse position modulation-UWB signal in the high-speed and delay-critical UWB communication environments. In [66, 67], the authors have presented the error performance of the DF and AF diversity schemes in the context of IR-UWB systems. The authors have also developed the coherent and non-coherent schemes that exploit the spatial diversity in a distributed manner among the different terminals of wireless networks. In [68], the authors have proposed an analytical model and have studied the performance of a cooperative link for time-hopping UWB system under the AF and DF relay models. The authors have considered the effect of multiuser interference while computing the outage probability and average bit error probability (BEP) of the system. To achieve a greater coverage of UWB technology, multihop relaying strategy has been suggested and an initial investigation over the IEEE 802.15.3a UWB channel is reported in [69]. In [70], the authors have provided the channel capacity of a hybrid relay scheme based UWB-MIMO systems.

Similar to the high-data-rate UWB system, performance of LR-UWB system over the IEEE 802.15.4a channel has been analyzed in [71, 72]. In [71], the authors have presented the simulation results of an LR-UWB system with a coherent Rake receiver. In [72], semi-analytical expressions for BEP and frame error rate for BPSK signals in the LR-UWB system have been derived. The formulation considered the coherent and non-coherent reception methods and performed the suboptimal multipath combining at the receiver. The BEP of cooperative TH-UWB systems with a DF relay protocol has been studied by considering realistic LR-UWB channel links specified in the IEEE 802.15.4a standard [73]. In [74, 75], the authors have developed the unified framework and have investigated the performance of a relay based MIMO network for the generalized fading scenario of Nakagami-*m* distributions, which is similar to the fading distribution specified in the IEEE 802.15.4a channel model. Most of the work in the literature

have analyzed the performance of the UWB relay based system for simplified UWB channel or narrowband Nakagami-*m* multipath fading channel. The investigation of TAS/MRC scheme at the direct (source to destination) as well as indirect (relay to destination) links of two hop UWB systems have not been presented in the literature.

The mm-Wave wireless communication system at 60 GHz has drawn a great attention due to its licence free utilization of 7.5 GHz wide frequency spectrum [76–78]. The SINR analysis of OFDM systems over the IEEE 802.15.3c channel at 60 GHz has been investigated in [79]. The derivation precisely captured the distinctive clustering phenomenon in the spatial-temporal domain. Simulation and semi-analytical analysis of mm-Wave communication at 60 GHz has been presented in [80, 81]. In [82], the authors have evaluated the error performance of mm-Wave system in the presence of human activity, which is an extension of the standard channel model proposed by the IEEE 802.15.3c channel. On the basis of measurement, the attenuation due to human blockage can be 20 dB or more, and hence, non- negligible. Performance analysis of low complexity precoding algorithms for large millimeter wave MIMO system has been presented in [83]. Upper bound on the error probability and ergodic channel capacity of the MIMO mm-Wave systems with hybrid beamforming have been derived in [84–89]. Performance evaluation of beamforming techniques for OFDM based 60 GHz millimeter-wave WPAN has been presented in [90]. The available literature has shown a predominant analysis of the channel capacity of beamforming based mm-Wave communication system.

1.5 Thesis Contribution

The major contributions of this thesis have been listed below.

I. Approximate model of a lognormal shadow fading

   (i) Present an approximate model of square of lognormal shadow fading distribution by the MG distributions and estimate its parameters using the moment matching with non-linear curve fitting method and Expectation-Maximization (EM) algorithm.

(ii) Evaluate Mean Square Error (MSE) between the estimated and exact distributions.

(iii) Generate the probability density function and cumulative distribution function plots of MG distributions for different number of mixing coefficients and compare it with that of actual lognormal shadow fading.

II. Performance analysis of UWB system over the IEEE 802.15.3a channel model

(i) Derive a characteristic function based computable BER formula of UWB wireless communication system over the IEEE 802.15.3a channel after approximating the square of a lognormal shadowing by MG distributions.

(ii) Compare the numerical results of the derived BER with the Monte-Carlo simulation results for different environments of the IEEE 802.15.3a channel.

III. Performance analysis of TAS/MRC based UWB-MIMO system

(i) Using the approximation of a lognormal shadow fading by the MG distributions by employing EM algorithm, we derive an expression of BER for the TAS/MRC based UWB-MIMO system over the IEEE 802.15.3a channel model.

(ii) The derived BER expression has been validated through extensive Monte-Carlo simulation results.

IV. TAS/MRC two hop relay based UWB system over the IEEE 802.15.3a channel model

(i) Evaluate the average BER of binary signals for TAS/MRC based UWB DF-relay system over the IEEE 802.15.3a channel.

(ii) Analytical results have been compared with the Monte-Carlo simulation results.

(iii) Discuss the impacts of various parameters of IEEE 802.15.3a channel on the performance of UWB system.

V. TAS/MRC based LR-UWB relay system over the IEEE 802.15.4a channel

(i) Compute the average BER of two hop LR-UWB DF-relay system over the IEEE 802.15.4a channel model with antenna selection at the source and relay terminals.

(ii) Derived expression has been validated by the Monte-Carlo simulation results for different environments of the IEEE 802.15.4a channel.

(iii) Compare our BER results for residential environments of LR-UWB system with the reported BER results for narrowband flat fading channels.

VI. BER analysis of the mm-Wave MIMO system for 60 GHz band

(i) Present the BER analysis of antenna beamforming based mm-Wave MIMO communication system over the IEEE 802.15.3c channel at 60 GHz.

(ii) The derived BER expression has been verified by the Monte-Carlo simulation results.

(iii) Examined the impacts of various parameters and Rake's fingers on the performance and suggest the sufficient number of Rake's finger to capture the maximum possible energy at the receiver.

1.6 Thesis Organization

This thesis is divided into seven chapters. A brief overview of content of each chapter has been given below.

In Chapter 2, an approximate model of lognormal shadow fading by the MG distributions using Moments matching method with non-linear curve fitting approach has been presented. We also examined the MSE to measure the exactness of the approximated distribution for different number of mixing coefficients of MG distributions. Using this approximation, a characteristic function based BER of UWB indoor communication system over the IEEE 802.15.3a channel has been derived. The numerical values of the derived BER is compared with the Monte-Carlo simulation results for different environments of the IEEE 802.15.3a channel model. Besides, we have also compared our results with the reported results.

Chapter 3 gives an overview of TAS/MRC scheme. Here, an approximation of the log-normal shadow fading by MG distributions using EM algorithm has been presented. Apart from this, an expression of BER for TAS/MRC scheme based UWB-MIMO system over the IEEE 802.15.3a channel has been derived. The analytical and Monte-Carlo simulation results of the investigated system for different number of antennas at the transmitter and the receiver side over different environments of the IEEE 802.15.3a channel has been presented. Besides, we have also discussed the impacts of intra and inter-cluster power decay factors of the IEEE 802.15.3a channel model on the BER of the UWB system.

Chapter 4 introduces the basic concepts of relay based cooperative communication and demonstrates the various cooperative strategies. The end-to-end BER analysis of TAS scheme decode and forward protocol employed UWB relay system over the IEEE 802.15.3a channel has been analyzed. Here, antenna selection has been performed at the source and relay terminals such that the selected transmitting antenna delivers the maximum signal to noise ratio (SNR) at the intended receiver. Additionally, we have examined the impacts of various parameters of the IEEE 802.15.3a channel on the BER and also suggested the sufficient number of Rake's fingers to capture the signal energy at the UWB receiver.

Chapter 5 deals with the LR-UWB wireless system. The channel impulse response and propagation characteristics for IEEE 802.15.4a standard has been discussed. We have evaluated the end-to-end BER of two hop UWB wireless systems similar to that of Chapter 4 over the IEEE 802.15.4a channel model. We have also examined the impact of fingers of Rake receiver and the parameters of the IEEE 802.15.4a channel on the performance of the investigating system. Additionally, we have also compared our results with the narrowband flat fading results.

Chapter 6 discusses the mm-Wave communication system at 60 GHz employing antenna beamforming. It presents the channel impulse response of the IEEE 802.15.3c channel model. An expression of BER for antenna beamforming based mm-Wave MIMO system at 60 GHz has been derived. The analysis includes the effect of Rake receiver's fingers and the impact of the

IEEE 802.15.3c channel's parameters on the BER.

Summary of the work presented in this thesis with conclusions and scope for future research have been provided in Chapter 7.

2

Performance Analysis of UWB Communication System over the IEEE 802.15.3a Channel

Contents

An analysis of the various performance measures of UWB systems is presented in [27–33, 36]. These analyses of UWB systems have either considered the simplified UWB channel models or an approximate model of the sum of lognormal RVs. Most of the reported analyses have not considered the clustering phenomena and the shadowing effect as in the IEEE 802.15.3a UWB channel model because lognormal distribution has no close-form formulae for its PDF and CDF which leads to intractable mathematical expression for BER expression. Furthermore, work presented in [37–42] have shown that various composite shadowing/fading channel models can be modeled by a Mixture of Gamma (MG) distributions and proved that MG distributions is closely fit these fading channel models.

In this chapter, we first present an approximate model of the lognormal shadow fading by the MG distributions. The parameters of the approximated distribution which matched the target distribution are estimated by using Moments matching method with non-linear curve fitting approach. Next we calculate the mean square error (MSE) between the exact and the estimated distributions for different number of mixing coefficients (N) and choose the value of N for the BER calculation, such that the MSE $\leq 10^{-3}$. With this approximation, we derive the characteristic function based computable BER formula of binary signals for UWB communication system over the IEEE 802.15.3a channel model. We use a coherent Rake receiver to capture the signal energy and consider the impact of fingers of the Rake receiver in the BER analysis. Further, we have utilized the Gauss-Hermite (GH) and Gauss-Legendre (GL) quadrature formulae to find the numerical solutions of mathematically intractable integrals. The derived analytical BER is validated with the Monte-Carlo simulation results and also compared these results with the reported results.

In the next section, we give a brief description of the IEEE 802.15.3a UWB channel model. Approximate model of lognormal shadowing by MG distributions using moment matching method is presented in section 2.2. In section 2.3, we derive the computable BER formula for UWB system over the IEEE 802.15.3a channel model. In section 2.4, we discuss the numerical

and simulation results and conclude the chapter with a brief summary in section 2.5.

2.1 IEEE 802.15.3a UWB Channel Model

TG3a standardization group has developed the IEEE 802.15.3a standard to provide an alternative PHY layer of the UWB wireless communication system. The IEEE 802.15.3a UWB channel model is different from the traditional narrowband wireless channel models because of the large bandwidth provided by the UWB system. The extremely large bandwidth gives rise to new effects in the channel model which are listed below.

- Only few multipath components falls within each resolvable delay bin. Therefore, Central limit theorem is not applicable.
- Multipath fading statistics in the UWB channels are lognormally distributed rather than Rayleigh distributed.
- The arrival processes of clusters and rays are modeled by the double stochastic Poisson processes. As a result, it is difficult to compute the signal energy received at the Rake receiver.

Mathematically, a channel impulse response of the IEEE 802.15.3a UWB channel is given by [11]

$$h(t) = X \sum_{m=0}^{M} \sum_{r=0}^{R} \alpha_{r,m} \delta \left(t - T_m - \tau_{r,m}\right) \tag{2.1}$$

where X represents the shadow fading and its distribution is modeled as a lognormal random variable, $\alpha_{r,m}$ denotes the multipath gain coefficients of r^{th} ray within the m^{th} cluster, T_m and $\tau_{r,m}$ are the arrival times of the m^{th} cluster and r^{th} ray of the m^{th} cluster, respectively. The process of times of arrival of cluster and ray are described by Poisson processes. Furthermore, the distribution of cluster inter-arrival time and ray inter-arrival time are exponential RVs, whose PDFs are given as follows.

$$f_{T_m}\left(T_m \setminus T_{m-1}\right) = \Lambda \, exp\left[-\Lambda(T_m - T_{m-1})\right], \quad m > 0 \tag{2.2}$$

$$f_{\tau_{r,m}}(\tau_{r,m} \setminus \tau_{(r-1),m}) = \lambda \, exp\left[-\lambda(\tau_{r,m} - \tau_{(r-1),m})\right], \quad r > 0 \tag{2.3}$$

where Λ and λ are the arrival rates of the cluster and ray, respectively. The propagation characteristics and power delay profile of a UWB channel are depicted in Fig 2.1. The multipath gain

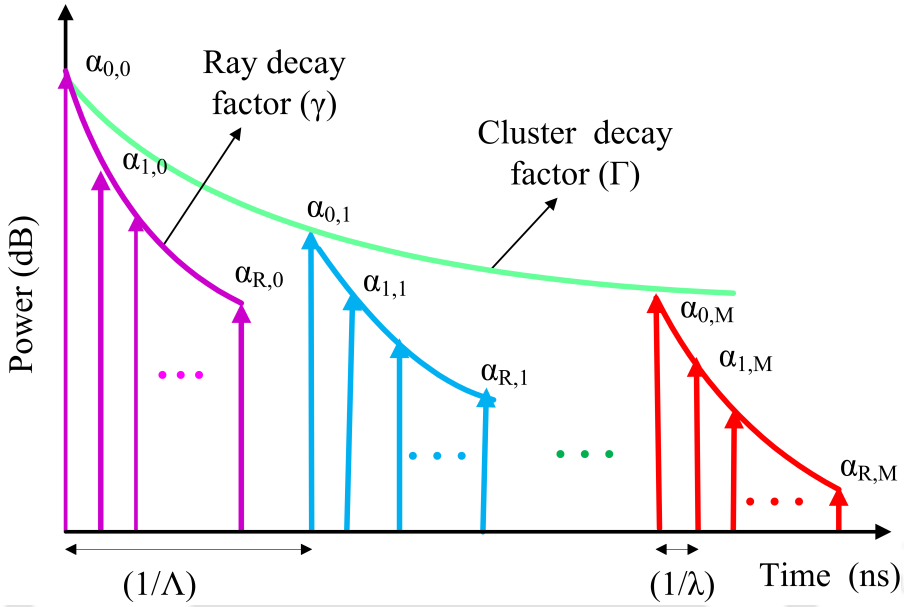

Figure 2.1: An illustration of power delay profile of the IEEE 802.15.3a UWB channel model

coefficients are defined as a product of small-scale ($\beta_{r,m}$) and large-scale (ξ_m) fading coefficients. The logarithm of this product is given by

$$20 \, log_{10}(\xi_m \beta_{r,m}) \sim \mathcal{N}\left(\mu_{r,m}, \sigma_1^2 + \sigma_2^2\right) \tag{2.4}$$

where σ_1 and σ_2 are the standard deviation for the cluster and ray, respectively. The behaviour of the average power delay profile is exponentially distributed, can be defined as

$$\mathbb{E}\left[\left|\xi_m \beta_{r,m}\right|^2\right] = \Omega_0 \exp\left(-\frac{T_m}{\Gamma} - \frac{\tau_{r,m}}{\gamma}\right) \tag{2.5}$$

where Ω_0 is the mean power of the first ray of the first cluster. From the equations (2.4) and (2.5), the mean, $\mu_{r,m}$ can be calculated as

$$\mu_{r,m} = \frac{10}{\ln(10)}\left[\ln(\Omega_0) - \frac{T_m}{\Gamma} - \frac{\tau_{r,m}}{\gamma} - \left(\frac{\ln(10)}{10}\right)^2 \left(\frac{\sigma_1^2 + \sigma_2^2}{2}\right)\right] \tag{2.6}$$

On the basis of experimental set-up, the IEEE 802.15.3a channel model (CM) is divided into the four categories, namely CM1, CM2, CM3, and CM4. CM1 describes a LOS (line-of-sight) scenario with a separation between a transmitter (Tx) and a receiver (Rx) of less than 4m. CM2 describes the same range, but for a non-LOS situation. CM3 describes a non-LOS scenario for distances between TX and RX of 4-10m. Scenario 4 finally describes an environment with strong delay dispersion, resulting in a delay spread of 25ns. From the experiment results, the numerical values of channel parameters are summarised in Table 2.1

Table 2.1: Parameter specifications of the IEEE 802.15.3a UWB channel

CHANNEL PARAMETERS	CM1	CM2	CM3	CM4
Cluster arrival rate (Λ) [1/ns]	0.0233	0.4	0.0667	0.0667
Ray arrival rate (λ) [1/ns]	2.5	0.5	2.1	2.1
Cluster decay factor (Γ) [dB]	7.1	5.5	14.0	24.0
Ray decay factor (γ) [dB]	4.3	6.7	7.9	12
Std. deviation for cluster (σ_1) [dB]	3.3941	3.3941	3.3941	3.3941
Std. deviation for ray (σ_2) [dB]	3.3941	3.3941	3.3941	3.3941
Std. deviation for shadowing (σ_X) [dB]	3	3	3	3

2.2 Approximate Model of Lognormal Shadowing

A variation of the received signal strength around the mean, due to the presence of a large object in the environment surrounding a transmitter and a receiver, is referred to as shadow fading and is usually modeled by the lognormal distribution.

2.2.1 Lognormal distribution

A lognormal distribution $\left\{X \sim \ln\mathcal{N}\left(\mu, \sigma^2\right)\right\}$, is the probability distribution of a random variable whose logarithm is normally distributed i.e., $\ln(X) \sim \mathcal{N}\left(\mu, \sigma^2\right)$. The probability density function, $f_X(x)$ and r^{th} moment, μ_{ln}^r of the lognormal distribution are defined as, respectively

$$f_X(x) = \frac{1}{\sqrt{2\pi}\sigma\, x} \exp\left(\frac{[\ln(x) - \mu]^2}{2\sigma^2}\right) \tag{2.7}$$

and

$$\mu_{\ln}^r = \exp\left(r\mu + \frac{r^2\sigma^2}{2}\right) \tag{2.8}$$

The main drawback of a lognormal distribution is its intractable mathematical expressions, thereby making the performance evaluation of communication systems over such channels very challenging [40]. Therefore, in this chapter the PDF of lognormal shadowing distribution is substituted by its MG distributions.

2.2.2 Mixture of Gamma (MG) distributions

Mixture of Gamma distributions is a linearly weighted sum of Gamma distributions. It offers a closed form expression of Moment Generating function (MGF), which is useful in the calculation of average BER. The PDF, $f_X(x)$ and MGF, $\eta_{MG}(s)$ of MG distribution are given respectively as,

$$f_X(x) = \sum_{n=1}^{N} w_n \, \mathcal{G}(x/k_n, \beta_n), \quad x > 0 \tag{2.9}$$

and,

$$\eta_{MG}(s) = \sum_{n=1}^{N} w_n \left(1 - \frac{s}{\beta_n}\right)^{-k_n} \tag{2.10}$$

where $\mathcal{G}(x_t/k_n, \beta_n) = \frac{\beta_n^{k_n}}{\Gamma(k_n)} x^{k_n - 1} e^{-\beta_n x}$ is the standard Gamma distribution with shape parameter (k_n) and scale parameter (β_n), $\Gamma(.)$ is the Gamma function and N is the number of mixing coefficients of MG distributions. The mixture coefficients, w_n satisfy $w_n > 0$ and $\sum_{n=1}^{N} w_n = 1$.

2.2.3 Parameter estimation

In this subsection, the parameters of MG approximation are estimated by using the Moment matching method with non-linear curve fitting approach. The estimation is performed in the four steps such that it matches the lognormal distribution, which are explained below.

(i) In the first step, we equate the first and second moments of Gamma and lognormal distributions and compute the shape and scale parameters as follows.

$$k = \frac{1}{e^{\sigma^2} - 1} \tag{2.11}$$

and

$$\beta = \frac{1}{\left(e^{\sigma^2} - 1\right)\left(e^{\mu + \frac{\sigma^2}{2}}\right)} \tag{2.12}$$

From [37, 38], it is evident that for $\sigma \leq 9$dB, the above estimated Gamma approximation closely fits the lower trails of the targeted distribution.

(ii) In the second step, we choose the value of N and divide the upper trail of the target distribution into $N-1$ partitions.

(iii) In third step, the estimation of $(N-1)$ Gamma components is performed by using non-linear curve fitting approach, such that single Gamma approximation match the single partition of the targeted distribution.

(iv) In the last step, by applying hit and trial method, we estimate, w_n for each Gamma approximation so that the resultant MG distributions can closely fit the targeted lognormal distribution.

In order to measure the exactness of the estimated distribution, we calculate the MSE between the PDFs of the exact and the estimated distributions and it is defined as

$$\text{MSE} = \mathbb{E}\left[\left(f_{Exact}(x) - f_{Est.}(x)\right)^2\right] \tag{2.13}$$

where, $f_{Exact}(x)$ and $f_{Est.}(x)$ are analogous to PDFs of lognormal distribution and its MG approximation.

2.3 BER Analysis

In this section, we derive the characteristic function based computable BER formula of binary signals with a coherent Rake receiver for the IEEE 802.15.3a UWB channel model, where a square of lognormal shadow fading is substituted by the MG distributions. Conditional error probability (CEP) of the binary signals for coherent Rake receiver is given by [91]

$$p_e(\gamma) = Q\left(\sqrt{(1-\rho_r)\,\gamma}\right) \tag{2.14}$$

where $\gamma = (E_b/N_0)\,\mathcal{E}$, is the received SNR, E_b represents the energy per bit, N_0 denotes the noise power spectral density (PSD) and $\mathcal{E}$ is the total signal energy received by the Rake receiver for

the IEEE 802.15.3a channel and ρ_r = 0 for orthogonal binary signals and ρ_r = -1 for antipodal binary signals. The average BER of binary signals with the coherent Rake receiver can be calculated by averaging the CEP over the pdf $f_{\mathcal{E}}(x)$, can be expressed as

$$p_e = \int_{-\infty}^{\infty} Q\left(\sqrt{(1-\rho_r)\frac{E_b}{N_0}x}\right) f_{\mathcal{E}}(x)\,dx \tag{2.15}$$

where $f_{\mathcal{E}}(x)$ is the PDF of the received signal energy ($\mathcal{E}$) in the IEEE 802.15.3a channel.

2.3.1 PDF of the received signal energy in the IEEE 802.15.3a channel

In the UWB system or multipath environments, the total transmitted signal energy is dispersed over the multipath components (rays/clusters). Due to the narrow time bin, these multipath components can be resolved separately which provide higher order of diversity gain. To attain this gain and collect the signal energy carried by rays, we used the $L-$ fingers of a coherent Rake receiver. Assuming, T_c as the chip duration between the two consecutive fingers, the approximate energy captured by a Rake receiver within the [0, LT_c] time window can be calculated as

$$\begin{aligned}\mathcal{E} &\triangleq X^2 \sum_{0\leqslant T_m+\tau_{r,m}\leqslant LT_c} \left|\alpha_{r,m}\right|^2 \\ &\triangleq X^2\left(\alpha_{0,0}^2 + \tilde{\phi}_{r,0} + \tilde{\phi}_{\otimes}\right)\end{aligned} \tag{2.16}$$

where X^2 is the square of lognormal shadowing, $\tilde{\phi}_{r,0}$ is the sum of squared path gains of first cluster excluding $\alpha_{0,0}^2$ and $\tilde{\phi}_{\otimes}$ is the sum of squared path gains in the remaining clusters. Note that, $\mathcal{E}_0 = \alpha_{0,0}^2 + \tilde{\phi}_{r,0} + \tilde{\phi}_{\otimes}$ and X^2 are statistically independent then the PDF of $\mathcal{E}$ can be obtained as

$$f_{\mathcal{E}}(x) = \int_{-\infty}^{\infty} \frac{1}{|y|} f_{X^2}\left(\frac{x}{y}\right) f_{\mathcal{E}_0}(y)\,dy \tag{2.17}$$

where $f_{X^2}(.)$ and $f_{\mathcal{E}_0}(.)$ represent the PDFs of X^2 and $\mathcal{E}_0$, respectively.

2.3.1.1 PDF of the received energy without shadow fading

Assuming, $\alpha_{0,0}^2$, $\tilde{\phi}_{r,0}$ and $\tilde{\phi}_{\otimes}$ are statistically independent to each other then the characteristic function, $\psi_{\mathcal{E}_0}(\nu)$ can be calculated as [35]

$$\psi_{\mathcal{E}_0}(\nu) = \mathcal{L}_{0,0}(\nu)\ \mathrm{e}^{-\lambda\tilde{\psi}_\nu(0,L)}\ \mathrm{e}^{-\Lambda\tilde{J}(\nu,L)} \tag{2.18}$$

where $\mathcal{L}_{T,t}(\nu)$ represents the characteristic function of the square of single path coefficient in the IEEE 802.15.3a channel with ray arrival time at $t = T + \tau$. Here, T and τ are the arrival times of the cluster and ray, respectively. The functions $\mathrm{e}^{-\lambda\tilde{\psi}_\nu(T,L)}$ and $\mathrm{e}^{-\Lambda\tilde{J}(\nu,L)}$ are the characteristic functions of a short noise random variable related to the Poisson processes of arrival rates λ and Λ, respectively. From the equations (2.6) and (2.7), the $\mathcal{L}_{T,t}(\nu)$ is calculated as

$$\mathcal{L}_{T,t}(\nu) = \int_{-\infty}^{\infty} e^{j\nu x} \frac{10}{\sqrt{2\pi}\,\sigma\, x \ln(10)} \exp\left[-\frac{1}{2\sigma^2}(10\log_{10}(x) - \mu_{T,t})^2\right] dx \tag{2.19}$$

where $\sigma = \sqrt{\sigma_1^2 + \sigma_2^2}$. This integral is mathematically intractable. It can be solved numerically by using Gauss-Hermite (GH) quadrature. Using this quadrature and after some simplifications, the Hermite solution of $\mathcal{L}_{T,t}(\nu)$ is given as

$$\mathcal{L}_{T,t}(\nu) = \frac{1}{\sqrt{\pi}} \sum_{i=1}^{N^H} w_i^H \exp\left(j\nu 10^{\frac{\sqrt{2}\sigma\left(x_i^H\right)+\mu_{T,t}}{10}}\right) \tag{2.20}$$

where $\left\{w_i^H,\ x_i^H,\ N^H\right\}$ are the weights, i^{th} roots and number of nodes of GH quadrature, respectively. Accordingly, the functions $\tilde{\psi}_\nu(T,L)$ and $\tilde{J}(\nu,L)$ are defined as follows

$$\tilde{\psi}_\nu(T,L) = \int_{T}^{LT_c} \left[1 - \mathcal{L}_{T,t}(\nu)\right] dt, \quad \text{for } T \leqslant LT_c \tag{2.21}$$

and

$$\tilde{J}(\nu,L) = \int_{0}^{LT_c} \left[1 - \mathcal{L}_{T,T}(\nu)\, e^{-\lambda\tilde{\psi}_\nu(T,L)}\right] dT \tag{2.22}$$

Since the range of above integrals are finite, the integrals can be computed using Gauss-Legendre (GL) formula. Then the above expressions can be written as

$$\tilde{\psi}_{\nu}(T,L) = \frac{LT_c - T}{2} \sum_{j_1=1}^{N^L} w_{j_1}^L \left[1 - \mathcal{L}_{T,t}(\nu)\right]\Big|_{t=\frac{LT_c-T}{2}x_{j_1}^L + \frac{LT_c+T}{2}} \tag{2.23}$$

and

$$\tilde{J}(\nu,L) = \frac{LT_c}{2} \sum_{j_2=1}^{N^L} w_{j_2}^L \left[1 - \mathcal{L}_{T,T}(\nu)\, e^{-\lambda\tilde{\psi}_{\nu}(T,L)}\right]\Big|_{T=\frac{LT_c}{2}\left(x_{j_2}^L+1\right)} \tag{2.24}$$

where $\left\{w_j^L, x_j^L, N^L\right\}$ represent the weights, j^{th} roots and number of nodes of GL quadrature, respectively. From the equations (2.18), (2.20), (2.23) and (2.24), the characteristic function $\psi_{\mathcal{E}_0}(\nu)$ is given as

$$\begin{aligned}\psi_{\mathcal{E}_0}(\nu) = \frac{1}{\sqrt{\pi}} \sum_{i=1}^{N^H} w_i^H \exp\left(j\nu 10^{\left(\frac{\sqrt{2}\sigma x+\mu_{0,0}}{10}\right)}\right) \exp\left(-\frac{\lambda LT_c}{2} \sum_{j_1=1}^{N^L} w_{j_1}^L \left[1 - \mathcal{L}_{0,t}(\nu)\right]\Big|_{t=\frac{LT_c}{2}\left(x_{j_1}^L+1\right)}\right) \\ \times \exp\left(-\frac{\Lambda LT_c}{2} \sum_{j_2=1}^{N^L} w_{j_2}^L \left[1 - \mathcal{L}_{T,T}(\nu)\, e^{-\lambda\tilde{\psi}_{\nu}(T,L)}\right]\Big|_{T=\frac{LT_c}{2}\left(x_{j_2}^L+1\right)}\right)\end{aligned} \tag{2.25}$$

The PDF of $\mathcal{E}_0$ is calculated as $f_{\mathcal{E}_0}(x) = \frac{1}{2\pi}\int_{-\infty}^{\infty} \psi_{\mathcal{E}_0}(\nu)\, e^{-j\nu x} d\nu$. Using GH quadrature, the $f_{\mathcal{E}_0}(x)$ can be expressed as

$$f_{\mathcal{E}_0}(x) = \frac{1}{2\pi} \sum_{i_1=1}^{N^H} w_{i_1}^H\, \psi_{\mathcal{E}_0}(\nu) \exp\left(-jx\nu + \nu^2\right)\Big|_{\nu=x_{i_1}^H} \tag{2.26}$$

From the equations (2.15), (2.17) and (2.26), the BER of the UWB systems is obtained as

$$p_e = \frac{1}{2\pi} \sum_{i_2=1}^{N^H} \sum_{i_1=1}^{N^H} \frac{w_{i_2}^H w_{i_1}^H}{|y|}\, \psi_{\mathcal{E}_0}(\nu)\, \mathrm{e}^{\left(y^2+\nu^2-j\nu y\right)} \int_0^{\infty} Q\left(\sqrt{(1-\rho_r)\frac{E_b}{N_0}x}\right) f_{X^2}\left(\frac{x}{y}\right) dx\Big|_{y=x_{i_2}^H, \nu=x_{i_1}^H} \tag{2.27}$$

According to [92], Q-function is approximated as $Q(x) = \frac{1}{12}e^{-x^2/2} + \frac{1}{4}e^{-2x^2/3}$ and considering the MG approximation, the final BER expression of a UWB system for the IEEE 802.15.3a channel

model can be expressed in term of MGF of MG distributions, is given by

$$p_e = \frac{1}{8\pi^{3/2}} \sum_{i_2=1}^{N^H} \sum_{i_1=1}^{N^H} \frac{w_{i_2}^H w_{i_1}^H y}{|y|} \psi_{\mathcal{E}_0}(\nu)\, \mathrm{e}^{(-j\nu y+\nu^2+y^2)} \left[\frac{1}{3}\eta_{MG}\left(-\frac{\Xi_0 y}{2}\right) + \eta_{MG}\left(-\frac{2\Xi_0 y}{3}\right)\right]\Bigg|_{y=x_{i_2}^H, \nu=x_{i_1}^H} \tag{2.28}$$

where $\Xi_0 = \frac{(1-\rho_r)E_b}{N_0}$.

2.4 Numerical Results and Discussion

To have a better understanding, this section is divided into two parts. In the first part, we consider the approximate model of a square of lognormal shadowing by the MG distributions and show the PDF and CDF plots of both distributions. Additionally, we calculate the MSE to measure the exactness of the approximate distribution. The second part presents the simulation and analytical BER of the UWB systems over the IEEE 802.15.3a channel and compares these results with the reported results.

As suggested, we consider the lognormal shadow fading, with zero mean and 3 dB standard deviation i.e., $X \sim ln\mathcal{N}(0, 3\text{dB})$. Hence the square of a lognormal shadowing is $X^2 \sim ln\mathcal{N}(0, 6\text{dB})$. The parameters of its MG distributions for $N = 1$, 3 and 5 are found out as in subsection 2.2.3 and are given in Table 2.2. In Fig. 2.2 and Fig. 2.3, we show the PDFs and

Table 2.2: Estimated MG distributions parameters

NUMBER OF MIXING COEFFICIENTS (N)	SHAPE PARAMETER (k_n)	SCALE PARAMETER (β_n)	MIXTURE COEFFICIENTS (w_n)
N=1	1.6353	0.7763	1
N=3	3.5977	0.2406	0.68
	1.6353	0.7763	0.17
	16.5165	0.1397	0.15
N=5	3.5977	0.2406	0.65
	1.6353	0.7763	0.15
	13.9	0.1164	0.1
	21.2589	0.1164	0.079
	47.5872	0.0776	0.021

CDFs of the square of lognormal shadowing with its MG appropriation for the estimated parameters, which are given in Table 2.2. From Fig. 2.2, it is clear that lower tails of the exact

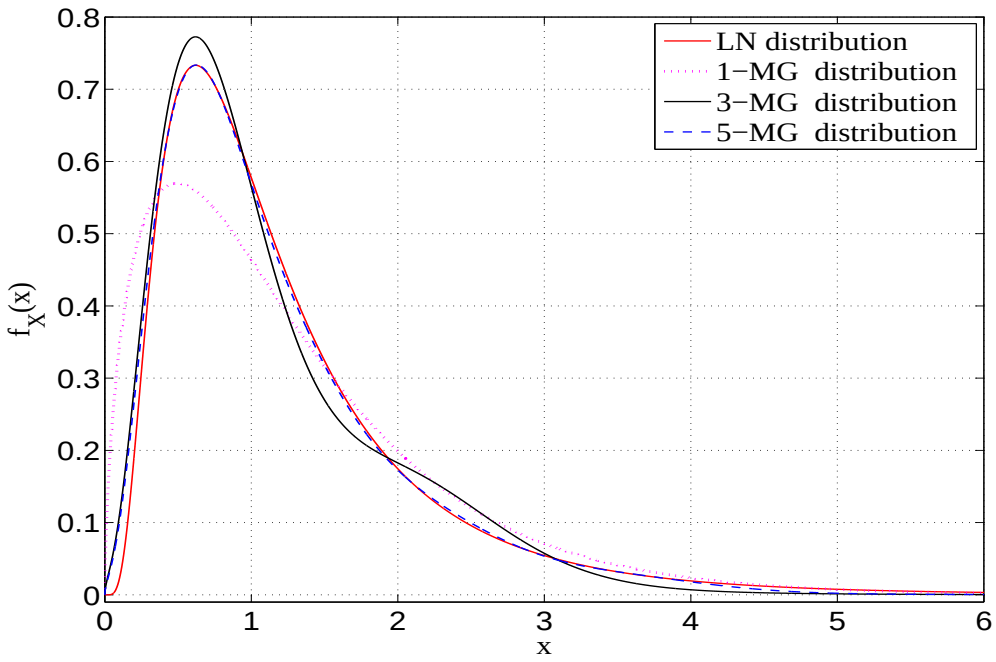

Figure 2.2: PDFs of square of lognormal shadowing and its MG distributions for N = 1, 3 and 5

distribution (in red) and its MG approximation for $N = 1$ (in magenta) fit closely as reported in [38]. It can be observed that the PDFs of MG distributions for N =3 and 5 fit the lower tails as well upper tails of the desired distribution and its exactness is improved with the increase in the order of mixing coefficients (N). Similar conclusion can be also drawn for CDF results shown in Fig 2.3. From the results, it is clear that 5-MG distributions (blue dashed) is a close fit for the square of lognormal shadowing.

Fig. 2.4 shows the MSE for different number of mixing coefficients of MG approximation. We observe that MSE decreases with increase in N and at N=5, MSE≈ 0.001. Note that lesser MSE implies MG approximation is a close fit for the desired distribution, consequently a good match of the analytical BER with the simulation results. From equation (2.28), it is obvious that accuracy, complexity and computational time increase with the increase in N. Therefore, we choose $N = 5$, for our further BER calculations.

For the second part of this section, we set $N^H = N^L = 40$, $\rho_r = 0$, $T_c = 1$ ns, $N = 5$,

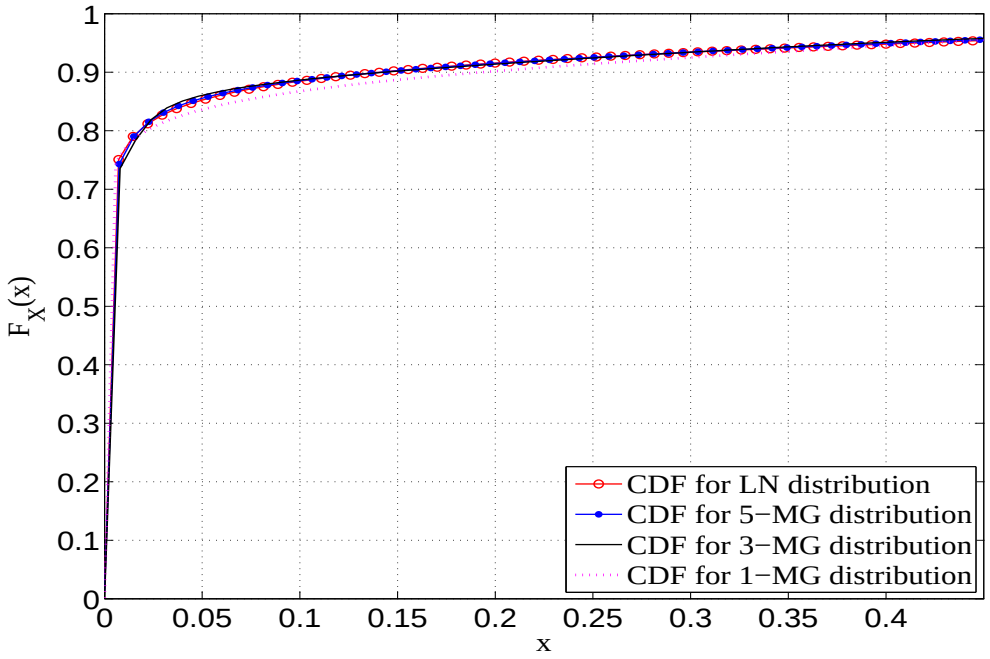

Figure 2.3: CDFs of square of lognormal shadowing and its MG distributions for N = 1, 3 and 5

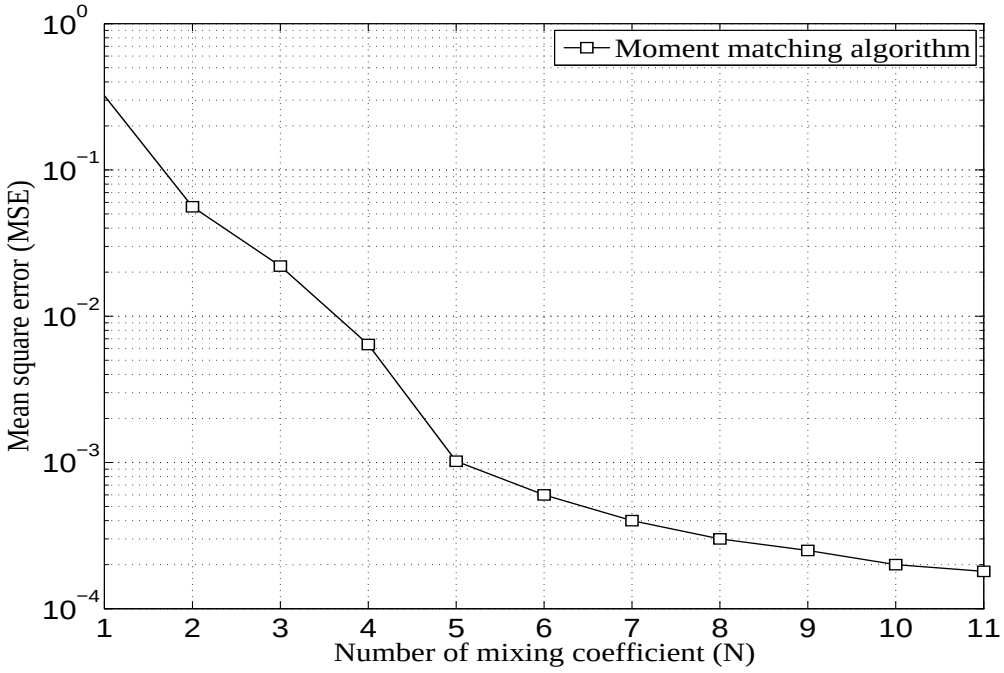

Figure 2.4: MSE vs number of mixing coefficients (N) of MG distributions

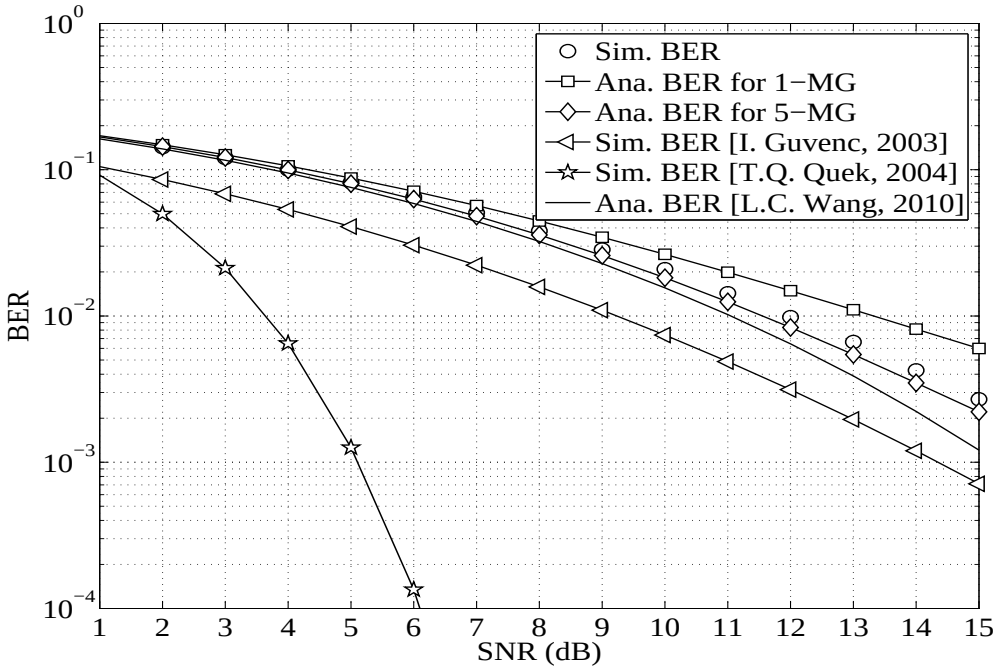

Figure 2.5: Simulation and analytical BER curves of the UWB systems over the IEEE 802.15.3a channel (CM1)

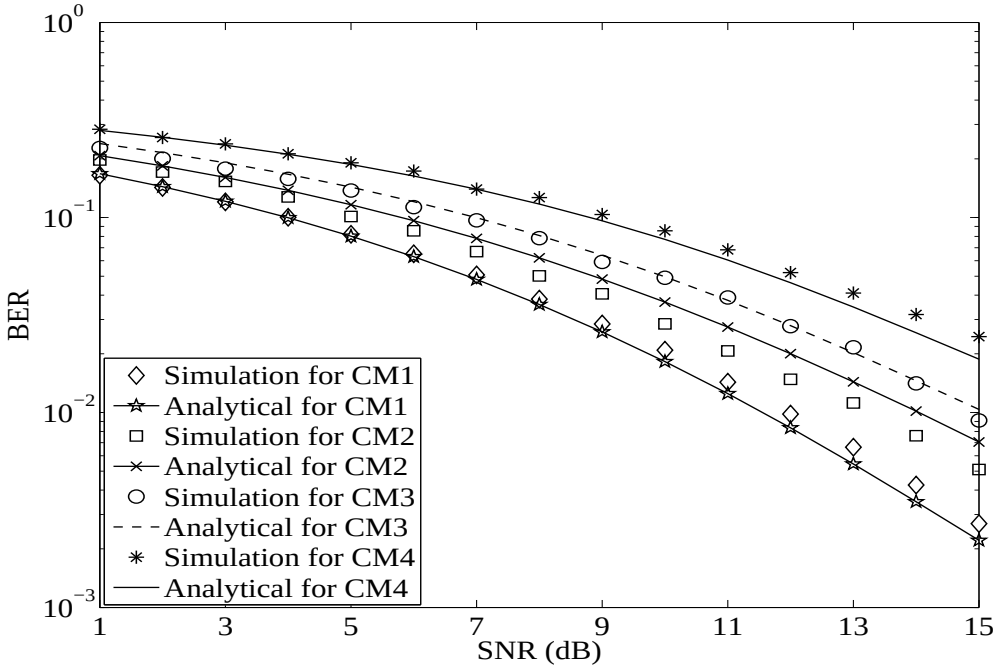

Figure 2.6: Simulation and analytical BERs of the UWB system for 5-MG distributions

$L = 10$ and number of bits to 100000. Fig. 2.5 shows the simulated and analytical BER of the UWB systems over the IEEE 802.15.3a channel (CM1) and compares with the BERs reported in [30, 31, 36]. The figure shows that reported simulated BERs are lower than our results. This is because, reported analyses did not consider the impacts of clustering phenomena and shadowing effect which are encountered by the UWB signals and can not be ignored, while evaluating the performance of UWB systems. It is also observed that, the derived BER for 5-MG distributions closely matches with the simulation results. In Fig. 2.6, the derived analytical BER (2.28) is verified by simulations for all four channel environments of the IEEE 802.15.3a UWB channel model. Results show that analytical BER is a good match with the simulations. Nevertheless, there are some discrepancies between the simulation and analytical results. The explanations for these discrepancies lie in the adoption of the GH and GL numerical formulae for evaluations of the numerical solution of the mathematically intractable integrals involved and the approximation involved to calculate the signal energy captured by the coherent L-fingers of Rake receiver.

2.5 Summary

In this chapter, we have discussed the approximate model of the square of lognormal shadowing by the MG distribution by using Moments matching method with non-linear curve fitting approach and calculate the MSE to measure the exactness of the estimated distribution. We have also shown the PDF and CDF plots of square of lognormal shadowing and its MG approximation for $N = 1$, 3 and 5. According to these results, we have seen that only lower tails of the 1-MG approximation match with the targeted distribution while the 5-MG approximation fits very closely. Additionally, MSE has improved from 0.321 (for 1-MG) to 0.00102 (for 5-MG). Furthermore, by considering MG distributions, we have derived the computable BER formula of binary signals for UWB systems over the IEEE 802.15.3a channel model. In the analysis, we have incorporated the impacts of Rake receiver on the performance of UWB system and utilized the Gaussian quadrature formulae to find the numerical solutions of mathematically

intractable integrals. Moreover, we have compared the numerical results of the derived BER with the Monte-Carlo simulations and with the reported BER results. It has been observed that the analytical BER for 5-MG approximation is a good match with the simulation results, which validates the accuracy of the derived BER and justifies the approximations and assumptions taken during the analysis. It is important to note that, derived BER expression is applicable for all four channel models of the IEEE 802.15.3a channel.

Note that our computable BER formula is faster and have good agreement with the simulation than the reported results. It can save a significant amount of computer simulation time. For instance, our computer (Intel(R) Core (TM)i5-3470 CPU with 4Gigabytes of RAM) takes 25 minutes to calculate the analytical BER in Fig. 2.5 whereas the same computation took 95 minutes for BER calculation reported in [36]. Note that, the Monte-Carlo simulation for the BER of the investigated system took around 33 hours. However, the disadvantage of a non-linear curve fitting approach is that it needs rigorous hit and trial method to arrive at the optimal values of the parameters of MG distributions.

3

Performance Analysis of TAS/MRC based UWB-MIMO Communication System

Contents

3.1 Introduction

In the year 2002, FCC allocated the 3.1- 10.6 GHz frequency spectrum for unlicensed utilization of the UWB technology. In this regulation, the commission has imposed restriction on the maximum allowable transmission power for the UWB signal in order to minimize the interference to the other narrowband technologies existing in the same frequency spectrum. This power constraint limits the transmission data-rate and coverage area of the UWB technology. To address this limitation, researchers have incorporated the MIMO network into the UWB system and have investigated the various performance measures. Some of these analyses are available in [47–55]. However, these analyses have not considered the appropriate UWB channel model. The MIMO network emerges as one of the most potential technology in the modern wireless communication systems. It can effectively enhance the system performance without increasing the bandwidth and the transmitting power. However it requires multiple RF chains, which are typically very expensive and introduce design and hardware complexities. In order to overcome this problem, the TAS scheme provides a good trade-off among the cost, complexity and the performance of the systems. It can achieve full diversity gain with a less complex hardware implementation. To the best of our knowledge, none of the reported works have evaluated the error performance of the TAS/MRC based UWB-MIMO system over the IEEE 802.15.3a channel model.

In this chapter, we approximate the square of lognormal shadowing by the MG distributions and estimate its parameters by using the Expectation-Maximization (EM) algorithm. Considering this approximation, we derive the numerically evaluated BER expression for the TAS/MRC based UWB-MIMO system over the IEEE 802.15.3a channel. We perform antenna selection at the transmitter and utilize the MRC diversity scheme at the receiver to combine all the received signals. We plot the PDF and the CDF of the MG distributions for the different number of mixing coefficients (N) and calculate the MSE to examine the exactness of the MG approximation. Additionally, we present the Monte-Carlo simulations to validate our results and discuss the

impacts of inter-cluster power decay factor (Γ) and intra-cluster power decay factor (γ) of the IEEE 802.15.3a channel on the BER.

In the next section, we describe the system model. We present the parameter estimation by using EM algorithm in section 3.3. We derive the numerical expression for BER of the investigated UWB systems in section 3.4. In section 3.5, we present the analytical and simulation results and summarize the inferences of the chapter in section 3.6.

3.2 System Model

TAS based MIMO system comprising of N_t antennas at this transmitter and N_r antennas at the receiver is depicted in Fig. 3.1. We perform the TAS/MRC scheme assuming full channel

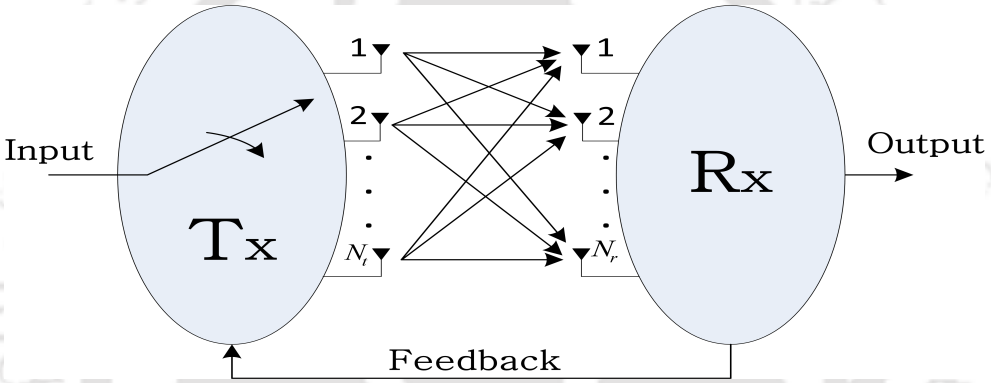

Figure 3.1: System model of TAS-MIMO systems

state information (CSI) is available at the transmitter and is is also assumed that only one transmitting antenna is active at a time for the transmission. Let us define, x to be the transmitted signal then the received signal vector, ($\mathbf{y}$) can be expressed as

$$\mathbf{y} = \mathbf{h}_u x + \mathbf{n} \tag{3.1}$$

where $\boldsymbol{y} \in \mathbb{C}^{N_r}$, $\boldsymbol{h}_u \in \mathbb{C}^{N_r}$ is the impulse response vector of the IEEE 802.15.3a channel for the u^{th} transmitting antenna and $\boldsymbol{n} \in \mathbb{C}^{N_r}$ is the additive white Gaussian noise (AWGN) vector with each noise component having power N_0. The TAS/MRC scheme with its decision criteria and parameter estimation of the MG distributions by the EM algorithm are discussed below.

3.2.1 Transmit antenna selection with maximal ratio combining (TAS/MRC) scheme

Transmit antenna selection (TAS) is an effective technique to address the challenges, like the hardware and the design complexities encountered while incorporating the MIMO network. In general, TAS uses a subset of the total transmitting antennas for the transmission; mathematically it is denoted as TAS/MRC $(N_t, p; N_r)$. It means among the N_t transmitting antennas, p antennas are selected for the transmission whereas at the receiver all the N_r antennas are active for the reception and one may combine the received signals by N_r antennas utilizing the MRC scheme. In this thesis, the antenna selection is performed such that the selected antenna delivers the maximum instantaneous SNR at the receiver. The receiver sends the information (I) of the resulting instantaneous SNR to the transmitter through the feedback link as shown in Fig. 3.1. Mathematically, the decision information (I) is given by

$$I = \underset{1 \leqslant u \leqslant N_t}{\arg\max} \left\{ C_u = \sum_{v=1}^{N_r} \left| h_{v,u} \right|^2 \right\} \tag{3.2}$$

where $h_{v,u}$ is the impulse response of the IEEE 802.15.3a channel between the u^{th} transmitting antenna and the v^{th} receiving antenna for $u \in \{1, 2, ..., N_t\}$ and $v \in \{1, 2, ..., N_r\}$. Under the assumption of perfect CSI available at the transmitter, C_u is sorted in the ascending order of magnitude, such as $C_{(1)} \leqslant C_{(2)} \leqslant, ..., \leqslant C_{(u)}$. According to this order statistics, it is assumed that the u^{th} transmitting antenna delivers the maximum instantaneous SNR, hence it is selected for the transmission. The PDF of the u^{th} selected antenna can be computed as [93]

$$f_{C_{(u)}}(x) = N_t \left\{ F_{C_u}(x) \right\}^{(N_t - 1)} f_{C_u}(x) \tag{3.3}$$

where $f_{C_u}(.)$ and $F_{C_u}(.)$ are the PDF and the CDF of the received signal energy (C_u) for MRC system .

3.3 Parameter Estimation by Expectation Maximization (EM) Algorithm

Expectation-Maximization (EM) algorithm is an iterative method for finding the maximum-likelihood estimate of an underlying distribution from a given sample. Essentially, the EM

algorithm implements two steps iteratively until convergence.

(i) *Expectation step (E-step):* The expectancy of the complete log-likelihood function is calculated with respect to the observed information and current estimate of the model parameters.

$$Q\left(\Theta, \Theta^{(i)}\right) = \mathbb{E}\left[\log L\left(\Theta/\mathbf{x}, \mathbf{r}\right)\Big/\mathbf{x}, \Theta^{(i)}\right] \tag{3.4}$$

(ii) *Maximisation step (M-step):* Maximised the output of the E-step with respect to the unknown parameters. Output of $(i+1)$ iterations, after execution of M-step, is given by

$$\Theta^{(i+1)} = \arg\max_{\Theta} \left\{Q\left(\Theta, \Theta^{(i)}\right)\right. \tag{3.5}$$

Let us consider $\mathbf{x} = \{x_1, x_2, ..x_L\}$ be a given sample data set of a square of lognormal shadowing and $\Theta = \{\theta_1, \theta_2, ..., \theta_N\}$ is the set of unknown parameters of the MG distributions, where $\theta_n = \{w_n, k_n, \beta_n\}$. To find the optimum values of the unknown parameters, the log-likelihood (LLH) function is defined as

$$\log L\left(\Theta/\mathbf{x}\right) = \sum_{t=1}^{L} \log\left(\sum_{n=1}^{N} w_n \, \mathcal{G}\left(x_t/k_n, \beta_n\right)\right) \tag{3.6}$$

It is very difficult to compute the logarithm of sums by traditional maximum likelihood methods. Therefore, a data augmentation step is necessary to find a tractable solution. It is assumed that sample data set, $\mathbf{x}$ is incomplete and i.i.d. distributed. Let us introduce a set of second random variables, $\mathbf{r} = \{r\}_{t=1}^{L}$ associated with $\mathbf{x} = \{x\}_{t=1}^{L}$ such that $P\left(r_t = n/x_t, \Theta\right)$, which represents the probability of x_t to be drawn from the n^{th} Gamma distribution and $P\left(r_t = n\right) = w_n$. Now the LLH of the augmented data is given by

$$\log L\left(\Theta/\mathbf{x}, \mathbf{r}\right) = \sum_{t=1}^{L} \log\left\{w_{r_t} \, \mathcal{G}\left(x_t/k_{r_t}, \beta_{r_t}\right)\right\} \tag{3.7}$$

Expanding E-step gives

$$Q\left(\Theta,\Theta^{(i)}\right)=\sum_{t=1}^{L}\sum_{n=1}^{N}\left\{\left[\log\left(w_n\right)+\log\left(\mathcal{G}\left(x_t/k_n,\beta_n\right)\right)\right]P\left(r_t=n\middle/x_t,\Theta^{(i)}\right)\right\} \tag{3.8}$$

Using the Bayes' rule, $P\left(r_t=n\middle/x_t,\Theta^{(i)}\right)$ can be calculated as

$$P\left(r_t=n\middle/x_t,\Theta^{(i)}\right)=\frac{w_n\,\mathcal{G}\left(x_t\middle/k_n^{(t)},\beta_n^{(t)}\right)}{\sum_{j=1}^{N}w_j\,\mathcal{G}\left(x_t\middle/k_j^{(t)},\beta_j^{(t)}\right)} \tag{3.9}$$

Solving $\frac{\partial Q\left(\Theta,\Theta^{(i)}\right)}{\partial\Theta}=0$, yields

$$w_n^{(i+1)}=\frac{1}{L}\sum_{t=1}^{L}P\left(r_t=n\middle/x_t,\Theta^{(i)}\right), \tag{3.10}$$

$$\beta_n^{(i+1)}=\frac{k_n^{(t)}\sum_{t=1}^{L}P\left(r_t=n\middle/x_t,\Theta^{(i)}\right)}{\sum_{t=1}^{L}x_tP\left(r_t=n\middle/x_t,\Theta^{(i)}\right)} \tag{3.11}$$

and

$$k_n^{(i+1)}=k_n^{(i)}+\frac{a^{(i)}}{L}\sum_{t=1}^{L}\left\{\log\left(x_t\right)+\log\left(\beta_n^{(i)}\right)-\psi\left(k_n^{(i)}\right)\right\}P\left(r_t=n\middle/x_t,\Theta^{(i)}\right) \tag{3.12}$$

where $a^{(i)}\in(0,1)$ represents the step size and $\psi(z)=\frac{\partial\log(\Gamma(z))}{\partial z}$ is the polygamma function. Since $\psi(z)$ has no explicit expression, it has to be estimated numerically. According to [43], $\psi(z)\approx\log(x-0.5)+\frac{1}{24\log(x-0.5)^2}$ when $x\geq 2$.

3.4 Performance Analysis

Considering the MG distributions by using EM algorithm, we derive an expression of BER for the TAS/MRC based UWB-MIMO communication system. From the equations (2.15) and (3.3), average BER of the investigated UWB system with a coherent Rake receiver can be obtained as

$$p_e=N_t\int_0^{\infty}Q\left(\sqrt{(1-\rho_r)\frac{E_b}{N_0}x}\right)\left\{F_{C_u}(x)\right\}^{(N_t-1)}f_{C_u}(x)\,dx \tag{3.13}$$

3.4.1 PDF and CDF of the received signal energy for the MRC system

From (3.2), let us define $\mathcal{E}_{u,v} = \left|h_{v,u}\right|^2$, to be the energy captured by the coherent Rake receiver for $u-v$ channel link in the IEEE 802.15.3a channel model. The PDF, $f_{\mathcal{E}}(x)$ has already been presented in the section 2.3.1. Under the assumption of i.i.d. channel link, characteristic function of C_u can be expressed as

$$\Psi_{C_u}(\vartheta) = \prod_{v=1}^{N_r} \psi_{\mathcal{E}_{u,v}}(\vartheta) \tag{3.14}$$

where $\psi_{\mathcal{E}_{u,v}}(.)$ is the characteristic function $\mathcal{E}_{u,v}$ and can be calculated as $\psi_{\mathcal{E}}(\vartheta) = \int_{-\infty}^{\infty} e^{j\vartheta x} f_{\mathcal{E}}(x)\, dx$. Using Gauss-Hermite Quadrature and equation (2.17), the PDF of C_u can be expressed as

$$f_{C_u}(x) = \frac{1}{2\pi} \sum_{i=1}^{N^H} w_i^H \left(\prod_{v=1}^{N_r} \sum_{i_1=1}^{N^H} \sum_{i_2=2}^{N^H} \frac{w_{i_1}^H w_{i_2}^H}{|z|} f_{X^2}^{u,v}\left(\frac{y}{z}\right) f_{\mathcal{E}_0}^{u,v}(z)\, e^{\left[j\vartheta y + y^2 + z^2\right]}\Big|_{\substack{y=x_{i_1}^H \\ z=x_{i_2}^H}} \right) e^{\left[-j\vartheta x + \vartheta^2\right]}\Big|_{\vartheta = x_i^H} \tag{3.15}$$

Now using the Gauss-Legendre quadrature, the CDF $F_{C_u}(x)$ can be calculated as

$$F_{C_u}(x) = \frac{x}{2} \sum_{j_1=1}^{N^L} w_{j_1}^L f_{C_u}\left(\frac{x}{2}\left(x_{j_1}^L + 1\right)\right) \tag{3.16}$$

Combining the equations (3.13), (3.15) and (3.16) and using the Gauss-Laguerre quadrature, the final BER for TAS/MRC based UWB-MIMO systems over the IEEE 802.15.3a channel model is given as

$$p_e = \frac{N_t}{(2\pi)^{N_t}} \sum_{s=1}^{S^L} \left\{ w_s^L Q\left(\sqrt{(1-\rho_r)\frac{E_b}{N_0} x} \right) \left[\frac{x}{2} \sum_{j_1=1}^{N^L} \sum_{i=1}^{N^H} w_{j_1}^L w_i^H\, \Psi_{C_u}(\vartheta)\, e^{\left[\frac{-j\vartheta x}{2}\left(x_{j_1}^L+1\right)+\vartheta^2\right]}\Big|_{\vartheta = x_i^H} \right]^{(N_t-1)} \right.$$
$$\left. \times \left(\sum_{i=1}^{N^H} w_i^H\, \Psi_{C_u}(\vartheta)\, e^{\left[-j\vartheta x + \vartheta^2\right]}\Big|_{\vartheta = x_i^H} \right) \exp(x) \right\} \Big|_{x = x_s^L} \tag{3.17}$$

where $\left\{w_s^L, x_s^L, S^L\right\}$ represent the weights, s-roots and number of nodes of the Gauss-Laguerre quadrature, respectively.

3.5 Results and Discussion

We present an approximate model of a square of lognormal shadowing by the MG distributions using the EM algorithm. In order to estimate the parameters of the MG distributions for $X^2 \sim ln\mathcal{N}(0, 6\text{dB})$, we first initialize the parameters and then update these parameters after execution of each iteration of the EM algorithm such that it increases the likelihood function, $L(\Theta/\mathbf{x}, \mathbf{r})$. The initial and updated parameters after execution of 20 iterations are given in Table3.1. The PDF and the CDF plots of square of lognormal shadowing and its MG distribu-

Table 3.1: Initial and updated parameters of MG approximations for $N = 1$, 3 and 5

NO. OF MIXING COEFFICIENTS (N)	PARAMETERS OF MG DISTRIBUTIONS					
	INITIAL			UPDATED		
	k_n^0	β_n^0	w_n^0	$k_n^{(i+1)}$	$\beta_n^{(i+1)}$	$w_n^{(i+1)}$
$N = 1$	0.5	7	1	4.5942	3.6211	1
$N = 3$	25	6	0.65	4.9918	6.8299	0.5654
	7	0.3	0.25	0.69993	4.1868	0.3781
	19	4	0.1	9	2.2728	0.0565
$N = 5$	5	2	0.35	4.9968	2.9530	0.2832
	7	3	0.15	6.9993	6.2683	0.1732
	9	4	0.2	8.999	10.6092	0.2003
	2	0.5	0.2	1.9818	0.8950	0.1551
	7	7	0.1	6.9957	15.1586	0.1882

tions for above estimated parameters are shown in Fig. 3.2. It is clearly seen that an accuracy of the MG approximation improves with the increase in Gamma components and 5-MG approximation closely fits the square of a lognormal shadowing distribution. Fig. 3.3 exhibits the MSE for different number of mixing coefficients and noticed that adding more Gamma components gradually reduced the MSE, in other words the exactness of the MG approximations is improved but at the cost of increasing complexity. From the results, we found that the EM algorithm outperforms the Moments matching with non-linear curve fitting approach.

For simulation and analytical results, we set $N^H = N^L = S^L = 40$, $\rho_r = 0$, $T_c = 1$ ns and $L = 10$. Considering the 5-MG approximations, the simulation and analytical BER of TAS/MRC based UWB-MIMO systems over the IEEE 802.15.3a CM1 channel model for different num-

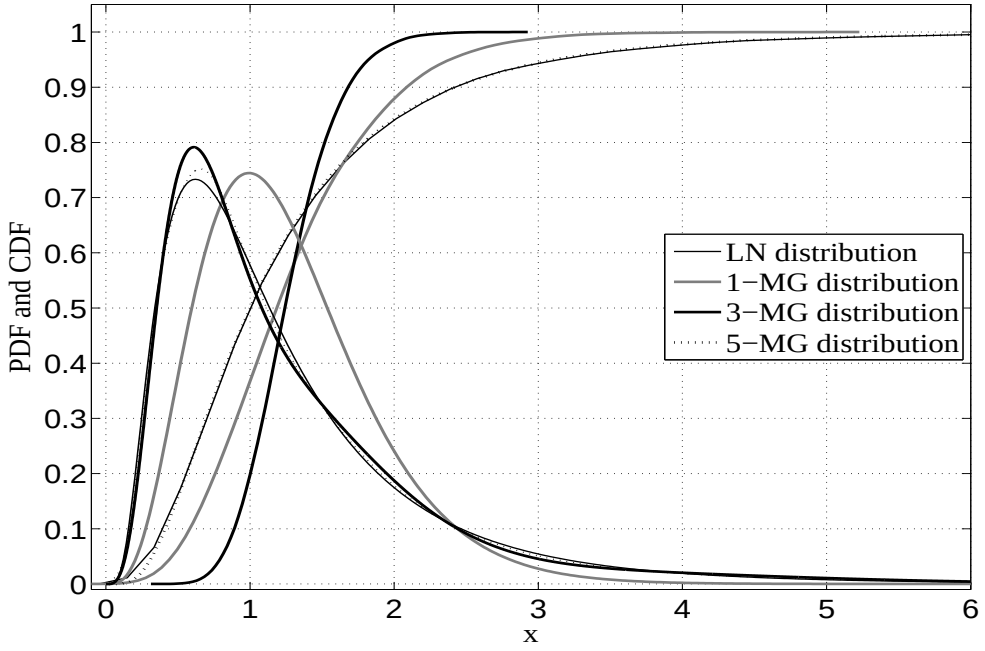

Figure 3.2: PDF and CDF plots of square of lognormal shadowing and its MG distributions for N = 1, 3 and 5

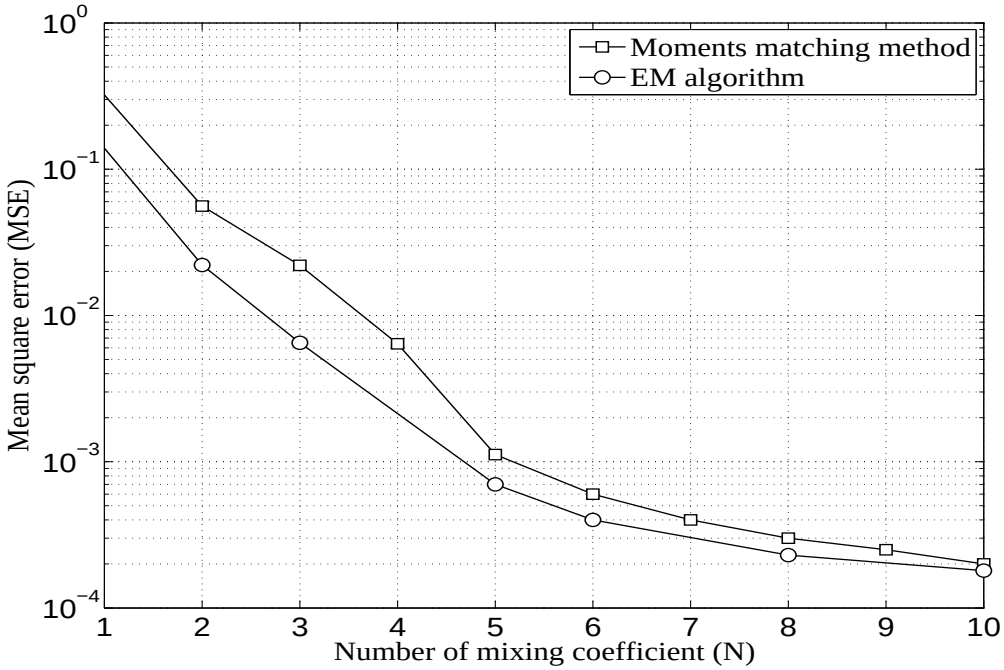

Figure 3.3: MSE vs number of mixing coefficients of MG distributions

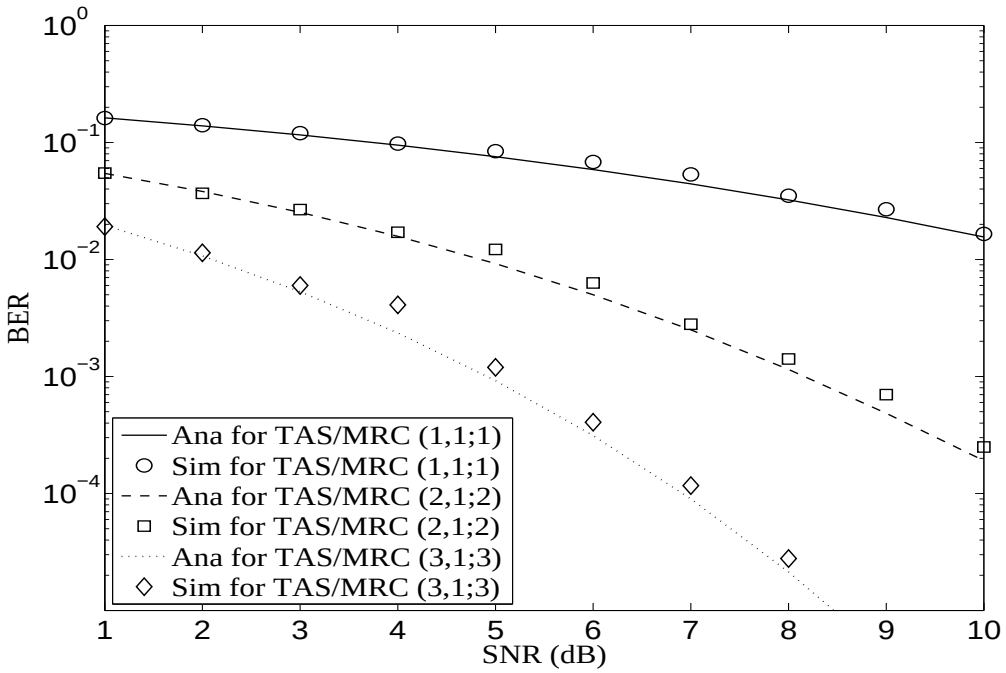

Figure 3.4: Simulation and analytical BERs of the TAS/MRC (N_t, 1; N_r) based UWB systems over the IEEE 802.15.3a CM1 (Ana→ analytical & Sim → Simulation)

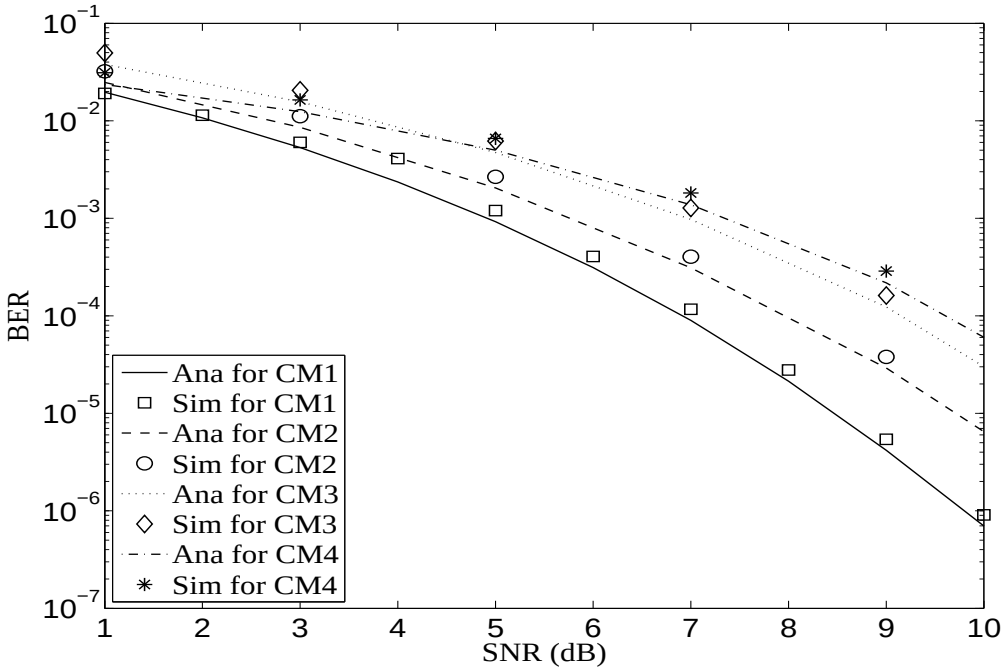

Figure 3.5: Simulation and analytical BERs of TAS/MRC (3,1;3) based UWB-MIMO systems over the IEEE 802.15.3a channel model (CM1~4)

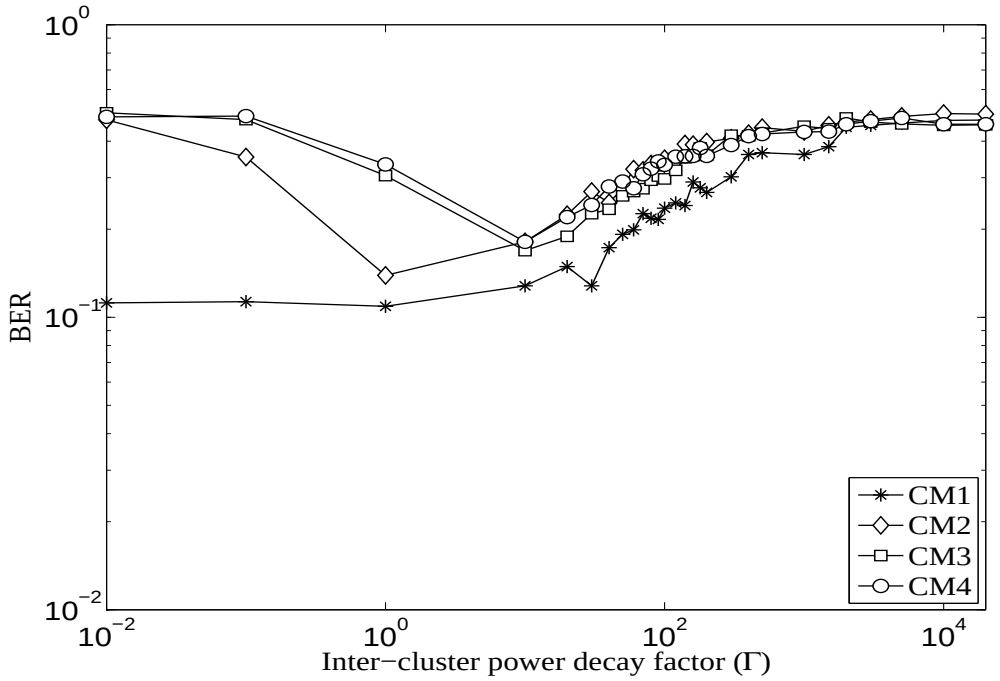

Figure 3.6: BER vs inter-cluster power decay factor (Γ) for SISO-UWB system at SNR=3dB

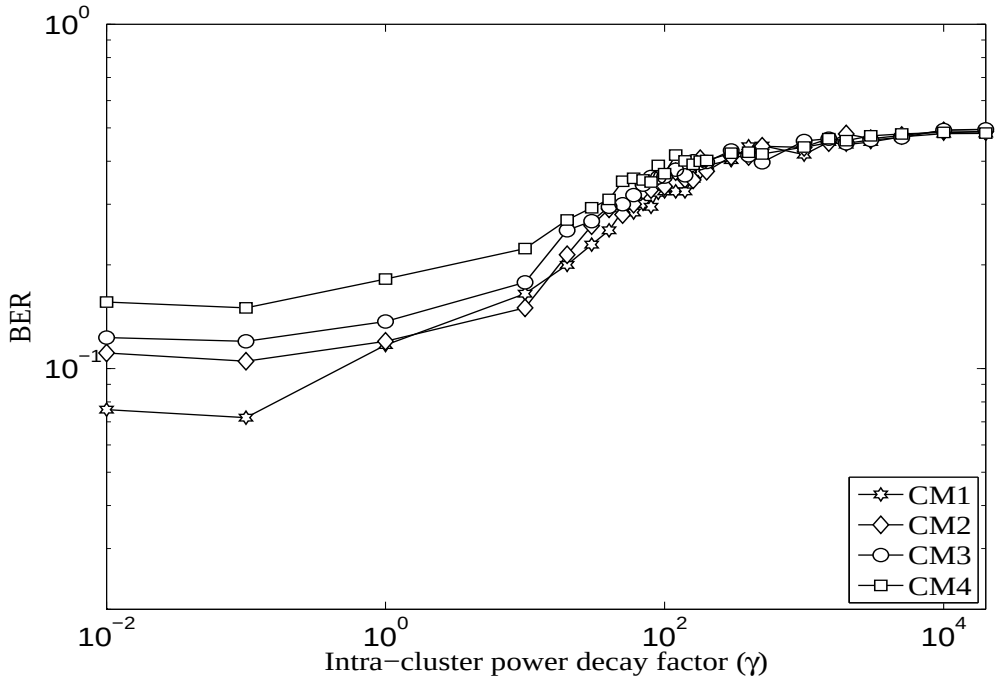

Figure 3.7: BER vs intra-cluster power decay factor (γ) for SISO-UWB system at SNR=3dB

ber of antennas at the transmitter and the receiver are shown in Fig. 3.4. It is observed that, when N_t or N_r increases, BER improves. This is because, we get the diversity gain due to the multiple antennas employed in the MIMO network. Similarly, Fig. 3.5 shows the simulated and analytical BERs for TAS/MRC (3,1;3) based UWB systems over all four channel environments of the IEEE 802.15.3a channel model. From the results, it is observed that the derived results shows a reasonably close match with the simulation results.

Fig. 3.6 and Fig. 3.7 demonstrate the impacts of inter-cluster and intra-cluster power decay factors on the BER of the SISO-UWB systems over the IEEE 802.15.3a channel model at SNR = 3dB. In the Fig. 3.6, when Γ increases, BER curves first decrease and then increase and for the very large values of Γ, BER curves become flat. This phenomenon can be explained as follows. From the IEEE 802.15.3a channel power delay profile given in equation (2.5), the average energy of MPCs depends on Ω_0 and the exponential term. When Γ is small, the exponential term dominates and energy captured by the Rake receiver increases with an increase in Γ there by BER decreases. When Γ is large, the term $\Omega_0 = \left(\frac{1}{(1+\Gamma\Lambda)(1+\lambda\gamma)}\right)$ starts dominating and therefore BER curve shows increasing trends. But at the very large value of Γ, the total received energy at the receiver is almost constant hence there is no variation in the BER curves. A similar explanation can be put forth for Fig. 3.7.

3.6 Summary

This chapter describes the approximation of a square of lognormal shadowing by the MG distributions and estimates its parameters by utilising the EM algorithm. For the estimated parameters, we demonstrated the PDF and CDF plots for different values of mixing coefficients of the MG distributions. Additionally, we have calculated the MSE to measure the exactness of the MG approximation and found that adding more Gamma components gradually improves the exactness of the MG approximation at the cost of higher complexity. It is also observed that the estimation using the EM algorithm is more efficient and accurate than the Moment matching methods. Moreover, we derived the numerical expression of BER of binary signals

for TAS/MRC based UWB-MIMO communication system over the IEEE 802.15.3a channel model. The simulation results for the different environments of IEEE 802.15.3a channel model with various antenna configurations are presented to validate the accuracy of the derived BER expression. The results show that the performance of the TAS/MRC system improves without any additional hardware and design complexities posed by the MIMO networks. The derived analytical results showed reasonably close agreement with the simulation results. Apart from this, we examined the impacts of inter and intra cluster power decay factors on the BER.

4

BER Analysis of TAS/MRC Based UWB Relay System over the IEEE 802.15.3a Channel

Contents

4.1 Introduction

To address the limitations of conventional point to point wireless networks and to extend the coverage area of the wireless communication systems, a new class of diversity methods called Cooperative communication (CC) has been introduced. The core idea behind the implementation of the CC is to harness the benefits of an additional relay (R) terminal. In the CC, source (S) terminal transmits the information to the destination (D) through multiple nodes (or relays). In this way, the destination receives the transmitted data with multiple copies that are generally affected by different and statistically independent fading paths. The destination then combines all the received signals to obtain the diversity gain. Depending on the type of signal processing performed at relays, the cooperative diversity schemes can be classified as Amplify-and-Forward (AF), Decode-and-Forward (DF), Estimate-and-Forward, etc. The two cooperative schemes that are extensively studied in the literature are the AF and the DF. With AF, relays receive noisy versions of the source data, amplify and re-transmit to the destination. Whereas in the DF, relays decode the source data, re-encode and re-transmit to the destination. In [63–70], the authors have investigated the channel capacity and the error performance of single and multi-antenna UWB relay systems using the AF and the DF protocols for conventional narrowband fading channels.

Based on the analysis of the TAS/MRC based UWB-MIMO wireless system investigated in Chapter 3, an end to end error performance for the DF-relaying UWB-MIMO system over the IEEE 802.15.3a channel model with antenna selection scheme at the source and the relay terminals is derived. Here, the antenna selection is performed such that the selected antenna delivers the maximum receive SNR at the destination. The derived analytical expression of BER is validated with the results of an extensive Monte-Carlo simulation. Furthermore, the impacts of inter-cluster arrival rate (Λ), standard deviation of shadow fading (σ_X) and the Rake's fingers (L) on the BER is investigated.

Chapter 4 is organized as follows. The system model is described in section 4.2. The

derivation of end to end BER expression of the investigated two-hop UWB DF-relay system is derived in section 4.3. In section 4.4 the simulation and analytical results are shown and the chapter is summarized in section 4.5.

4.2 System Model

We consider the TAS/MRC based two hop MIMO system and it is depicted in Fig. 4.1, in which $\{S, R\}$ terminals employ N_t number of transmitting antennas and $\{R, D\}$ terminals employ N_r number of receiving antennas. In this system TAS scheme is performed in the source to destination ($S \rightarrow D$) and the relay to destination ($R \rightarrow D$) links in such a manner that it maximizes the total received SNR at the destination terminal. In the source to relay ($S \rightarrow R$) link, source terminal does not perform the TAS scheme and it uses the same transmitting antenna which has been selected in the ($S \rightarrow D$) link.

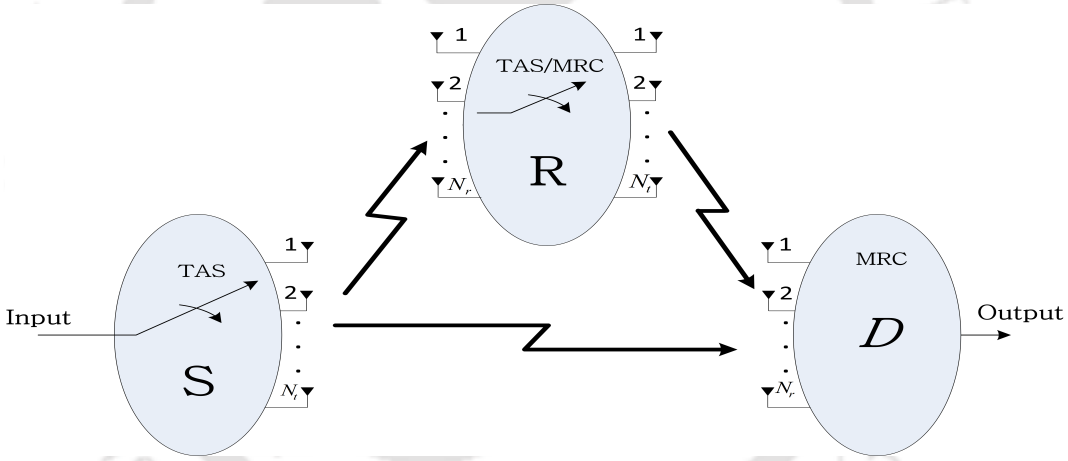

Figure 4.1: System model of TAS/MRC based two hop MIMO system

In the two hop DF-relay wireless communication systems, transmission is performed in two time slots. In the first time slot, source broadcasts the information to the destination and the relay terminals. In the second time slot, the relay initiates the transmission to the destination terminal only if it can correctly decode the broadcasted information of the source in the first time slot. Let x to be the transmitted symbol and p_1 and p_2 to be the transmitted powers at the source and the relay terminals, respectively. The received signal vectors in the ($S \rightarrow D$), ($S \rightarrow R$) and

($R \rightarrow D$) links can be written as follows.

$$\mathbf{y}^{(SD)} = \sqrt{p_1}\mathbf{h}_{(u)}^{(SD)}x + \mathbf{n}^{(SD)}, \tag{4.1}$$

$$\mathbf{y}^{(SR)} = \sqrt{p_1}\mathbf{h}_{u}^{(SR)}x + \mathbf{n}^{(SR)} \tag{4.2}$$

and

$$\mathbf{y}^{(RD)} = \sqrt{p_2}\mathbf{h}_{(u)}^{(RD)}x + \mathbf{n}^{(RD)} \tag{4.3}$$

where $\boldsymbol{y} \in \mathbb{C}^{N_r}$ and $\boldsymbol{h} \in \mathbb{C}^{N_r}$ are vectors of the received signal and the impulse response of the IEEE 802.15.3a channel, respectively and $\boldsymbol{n} \in \mathbb{C}^{N_r}$ is the AWGN noise vector. The superscripts and subscripts represent the corresponding channel links and the transmit antenna indexing, respectively.

4.3 Performance Analysis

In this section, we compute the end to end BER for the TAS/MRC based UWB-MIMO relay system with a coherent Rake receiver, where relay is configured to perform the DF coperative strategy. The end to end CEP for the DF-relay wireless system can be expressed as [60]

$$p_e(\gamma) = p_e(\gamma_{(SR)})\, p_e(\gamma_{(SD)}) + p_e(\gamma_{(SRD)})\,[1 - p_e(\gamma_{(SR)})] \tag{4.4}$$

where $\gamma_{(ab)}$ is the received SNR in the $a \rightarrow b$ channel link and $p_e(.)$ is the CEP for the binary signals with a coherent Rake receiver and is defined in equation (2.14). Assuming all the channel links are i.i.d., the average end to end BER of the investigated UWB systems can be calculated as

$$p_e = p_e^{(SR)} p_e^{(SD)} + p_e^{(SRD)}\left[1 - p_e^{(SR)}\right] \tag{4.5}$$

where $p_e{}^{(ab)} = \int_{-\infty}^{\infty} p_e(\gamma_{(ab)})\ f_{\gamma_{(ab)}}(\gamma)\ d\gamma$.

4.3.1 Average BER for the source to relay link

In the source to relay ($S \rightarrow R$) link, source terminal uses the same transmitting antenna which has been selected in the ($S \rightarrow D$) link and relay utilizes the MRC scheme to combine all

the N_r received signals arrived at the relay. Now after performing MRC, the instantaneous SNR at the relay terminal can be computed as

$$\begin{aligned}\gamma_{(SR)} &= \frac{p_1}{N_0}\sum_{v=1}^{N_r}\mathcal{E}_{u,v}^{(SR)} \\ &= \frac{p_1}{N_0}C_u^{(SR)}\end{aligned} \tag{4.6}$$

where $\mathcal{E}_{u,v}^{(SR)}$ is the energy captured by the Rake receiver at the v^{th} antenna of the relay terminal and is calculated as in (2.16). From the equations (2.15) and (3.15) and using the Gauss-Laguerre formula, the average BER for ($S \rightarrow R$) link can be computed as

$$p_e{}^{(SR)} = \frac{1}{2\pi}\sum_{s=1}^{S^L}\sum_{i=1}^{N^H} w_s^L\, w_i^H\, \Psi_{C_u}^{(SR)}(\vartheta)\, Q\left(\sqrt{(1-\rho_r)\frac{p_1}{N_0}x}\right) e^{\left[\vartheta^2+(1-j\vartheta)x\right]}\Big|_{\substack{\vartheta=x_i^H \\ x=x_s^L}} \tag{4.7}$$

4.3.2 Average BER for the source to destination link

In the source to destination ($S \rightarrow D$) link, it is assumed that a source terminal selects the u^{th} transmitting antenna after performing the TAS/MRC scheme such that it maximizes the instantaneous SNR at the destination. The total received SNR after applying MRC in the ($S \rightarrow D$) link is obtained as

$$\begin{aligned}\gamma_{(SD)} &= \frac{p_1}{N_0}\underset{1\leqslant u\leqslant N_t}{\arg\max}\left\{C_u^{(SD)}\right\} \\ &= \frac{p_1}{N_0}C_{(u)}^{(SD)}\end{aligned} \tag{4.8}$$

From the equation (3.17), the average BER for the ($S \rightarrow D$) link can be evaluated as

$$\begin{aligned}p_e^{(SD)} = \frac{N_t}{(2\pi)^{N_t}}\sum_{s=1}^{S^L}\Bigg\{ & w_s^L Q\left(\sqrt{(1-\rho_r)\frac{p_1}{N_0}x}\right)\left(\sum_{i=1}^{N^H} w_i^H\, \Psi_{C_u}^{(SD)}(\vartheta)\, e^{\left[-j\vartheta x+\vartheta^2\right]}\Big|_{\vartheta=x_i^H}\right)e^{x} \\ & \times\left[\frac{x}{2}\sum_{j_1=1}^{N^L}\sum_{i=1}^{N^H} w_{j_1}^L w_i^H\, \Psi_{C_u}^{(SD)}(\vartheta)\, e^{\left[\frac{-j\vartheta x}{2}\left(x_{j_1}^L+1\right)+\vartheta^2\right]}\Big|_{\vartheta=x_i^H}\right]^{(N_t-1)}\Bigg\}\Bigg|_{x=x_s^L}\end{aligned} \tag{4.9}$$

4.3.3 Average BER for the source to relay to destination link

In the source to relay to destination ($S \rightarrow R \rightarrow D$) link, a destination receives signals from the source and relay terminals when a relay decodes the broadcasted information correctly in the first time slot and performs the MRC diversity scheme to combine the received signals. The total instantaneous SNR at the destination after performing MRC can be formulated as

$$\gamma_{(SRD)} = \frac{p_1}{N_0} C_{(u)}^{(SD)} + \frac{p_2}{N_0} C_{(u)}^{(RD)} \tag{4.10}$$

Assuming $p_1 = p_2$ and $(S \rightarrow D)$, $(R \rightarrow D)$ links are i.i.d, then the received SNR in $(S \rightarrow R \rightarrow D)$ link is calculated as $\gamma_{(SRD)} \triangleq \gamma_{(SD)}$ with the substitution of $2N_r$ in place of N_r. Hence, the average probability of error in this link can be calculated as

$$p_e^{(SRD)} \triangleq p_e^{(SD)}\Big|_{N_r=2N_r,\ \gamma_{(SD)}=\gamma_{(SRD)}} \tag{4.11}$$

Combining the equations (4.5), (4.7), (4.9) and (4.11), the final average BER expression for TAS/MRC based UWB DF-relay system over the IEEE 802.15.3a channel can be obtained by

$$\begin{aligned}\tilde{p}_e(\gamma) = N_t \Bigg\{ & \left(\sum_{s=1}^{S^L} w_s^L Q\left(\sqrt{(1-\rho_r)\frac{p_1}{N_0} x_s^L} \right) e^{\left(x_s^L\right)} \left[F_{C_u}^{(SD)}\left(x_s^L\right) \right]^{(N_t-1)} f_{C_u}^{(SD)}\left(x_s^L\right) \right) \\ & \times \frac{1}{2\pi} \left(\sum_{s=1}^{S^L} \sum_{i=1}^{N^H} w_s^L\, w_i^H\, \Psi_{C_u}^{(SR)}(\vartheta)\, Q\left(\sqrt{(1-\rho_r)\frac{p_1}{N_0} x_s^L} \right) e^{\left[\vartheta^2 + (1-j\vartheta)x_s^L\right]} \Big|_{\vartheta = x_i^H} \right) \\ & + \left[1 - \frac{1}{2\pi} \left(\sum_{s=1}^{S^L} \sum_{i=1}^{N^H} w_s^L\, w_i^H\, \Psi_{C_u}^{(SR)}(\vartheta)\, Q\left(\sqrt{(1-\rho_r)\frac{p_1}{N_0} x_s^L} \right) e^{\left[\vartheta^2 + (1-j\vartheta)x_s^L\right]} \Big|_{\vartheta = x_i^H} \right) \right] \\ & \times \left(\sum_{s=1}^{S^L} w_s^L Q\left(\sqrt{(1-\rho_r)\frac{p_1}{N_0} x_s^L} \right) e^{\left(x_s^L\right)} \left[F_{C_u}^{(SD)}\left(x_s^L\right) \right]^{(N_t-1)} f_{C_u}^{(SD)}\left(x_s^L\right) \Big|_{N_r=2N_r, \gamma_{(SD)}=\gamma_{(SRD)}} \right) \Bigg\}\end{aligned} \tag{4.12}$$

where $f_{C_u}(.)$, $F_{C_u}(.)$ and $\Psi_{C_u}(.)$ have been presented in section 3.4.1.

4.4 Numerical Results and Discussion

In this section, we present the simulation and the analytical BER results of TAS/MRC based UWB DF-relay system over the IEEE 802.15.3a channel and examine the impacts of various channel parameters on the performance. Fig. 4.2 shows the simulated and the analytical BERs of the TAS/MRC $(N_t, 1; N_r)$ based UWB DF-relay system and compare these results with the BER of a conventional (without relay and single antenna link) UWB system over the IEEE 802.15.3a channel model (CM1). As expected, the DF-relaying UWB system has lesser BER than the conventional UWB system. Additionally, the BER of the DF-relaying UWB system improves with an increase in the number of antennas at the transmitter and at the receiver. An improvement in the BER is because of the diversity gain achieved by employing the cooperative technique and MIMO network into the conventional UWB systems. The TAS/MRC (4,1;4) based DF-relaying UWB system has lesser BER than the BER of the TAS/MRC (2,1;2) or TAS/MRC (3,1;3) based DF-relaying UWB systems. Similarly, Fig. 4.3 shows the simulation and the analytical BER of TAS/MRC (3,1;3) based DF-relaying UWB system over the IEEE 802.15.3a channel model (CM1~4). The results show that the derived analytical BER is in good match with the simulation results, which validates the accuracy of the derived expression.

Fig. 4.4 shows the effect of shadow-fading with the standard deviation σ_X = 3 dB and σ_X = 6 dB on the BER of the conventional and investigated UWB systems over the IEEE 802.15.3a channel model (CM1). It is observed that, BER at σ_X = 3 dB is lesser than the BER at σ_X = 6 dB. Hence, the impact of shadow fading in the analysis of UWB system over the IEEE 802.15.3a channel model can not be ignored. Furthermore, the impact of Rake's fingers on the BER of the of the TAS/MRC (3,1;3) based DF-relaying and the conventional UWB systems over the IEEE 802.15.3a channel (CM1~4) at SNR = 5 dB is shown in Fig. 4.5. In general, as L increases, the BER decreases, because of the increase in the amount of signal energy received by the Rake receiver. But for large values of L, BER curves become flat. A possible reason is that, with an increase in the number of fingers beyond certain values of L, the increments in the signal energy

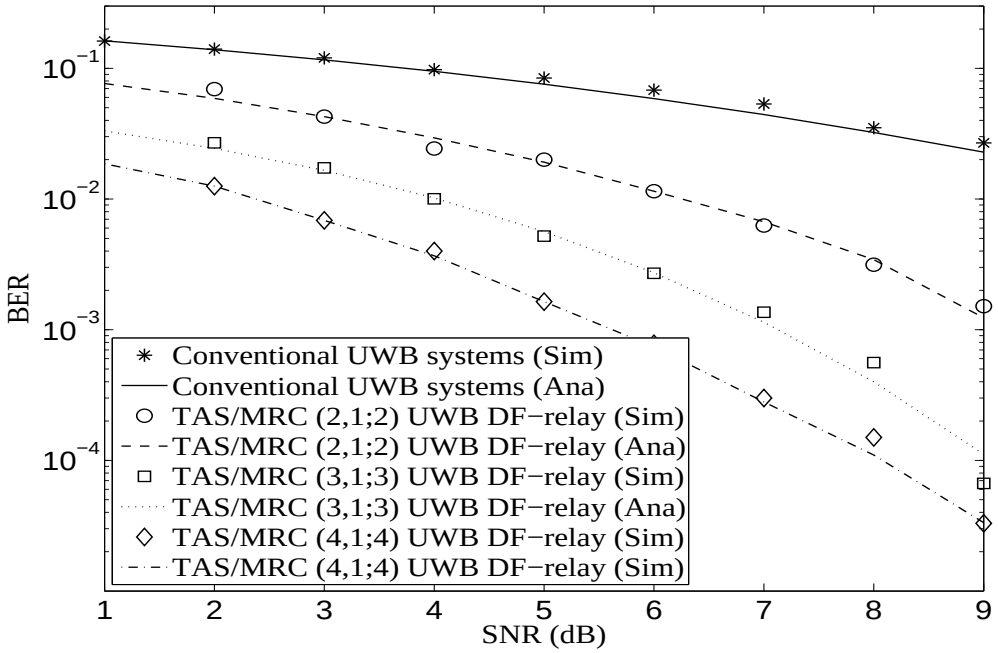

Figure 4.2: BERs of the conventional UWB and TAS/MRC $(N_t, 1; N_r)$ based UWB DF-relay system over the IEEE 802.15.3a channel (CM1)

becomes very small. Moreover, BER of conventional UWB system beyond $L = 70$ has almost same values for all four channel models. A similar inference is also drawn from the BER of TAS/MRC (3,1;3) based DF-relaying UWB system for $L \geq 90$.

Fig. 4.6 shows the BER of conventional UWB systems over the IEEE 802.15.3a channel (CM2) for various values of inter-cluster arrival rate (Λ). We observe that when Λ increases, the BER decreases. This is because increase in Λ signifies the arrival of increased number of clusters within the same $[0, LT_c]$ time interval and the Rake receiver can now collect more signal energy, thereby improving the BER.

4.5 Summary

In this chapter, we derived the BER expression for the TAS/MRC based DF-relaying UWB system over the IEEE 802.15.3a channel model. Additionally, we presented the Monte-Carlo simulation and the analytical BER results for the DF-relaying UWB systems for the different number of antenna configurations in the TAS/MRC scheme and compared these results with the

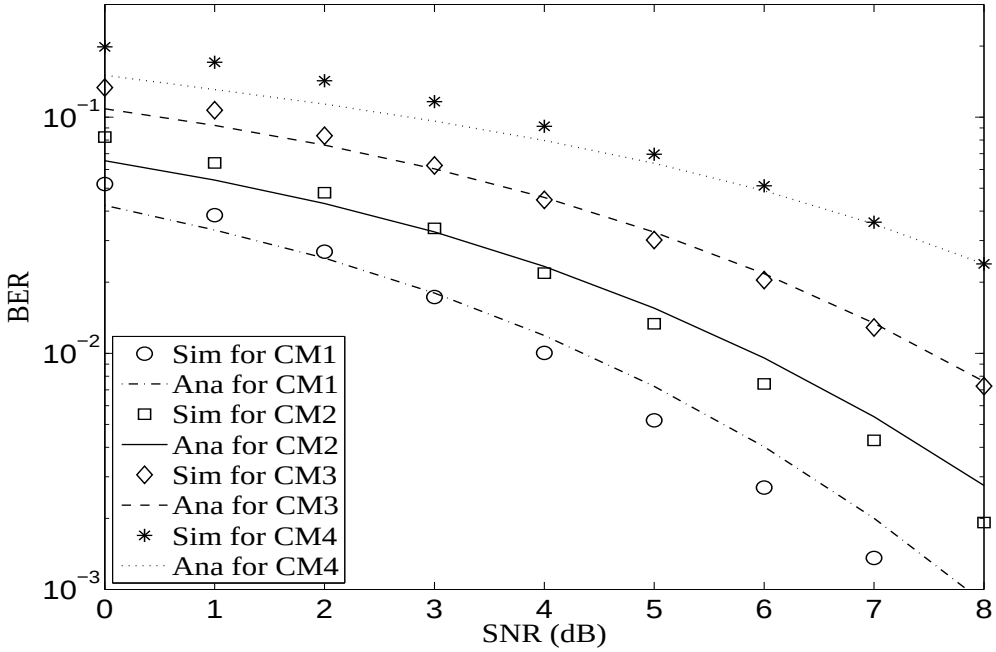

Figure 4.3: Simulation and analytical BER of TAS/MRC $(3, 1; 3)$ based UWB DF-relay system

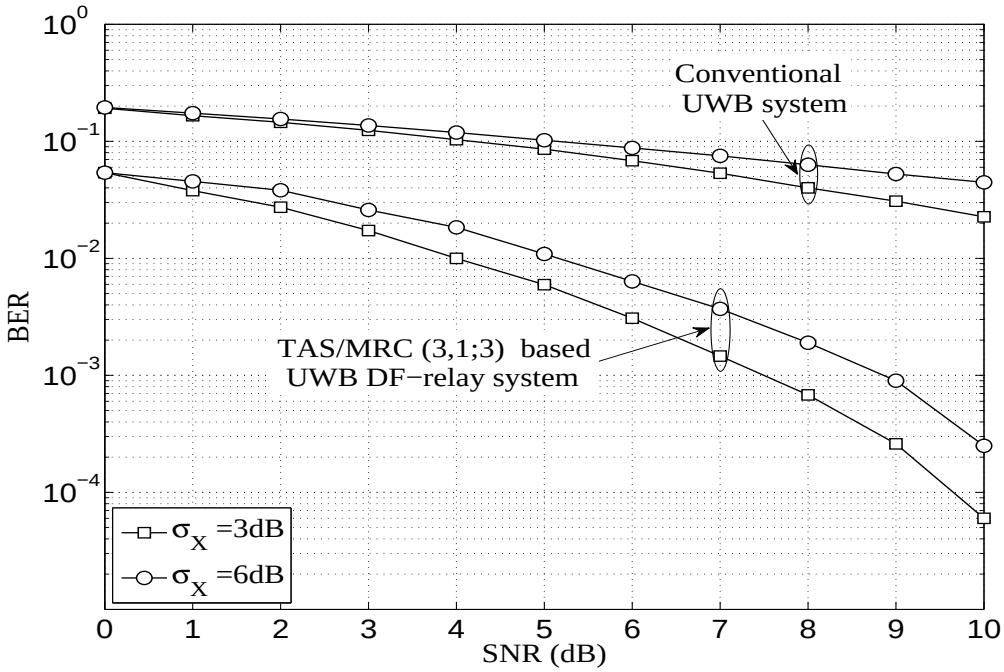

Figure 4.4: Effect of standard deviation of shadow fading (σ_X = 3dB and 6dB) on the BER of UWB system over the IEEE 802.15.3a (CM1)

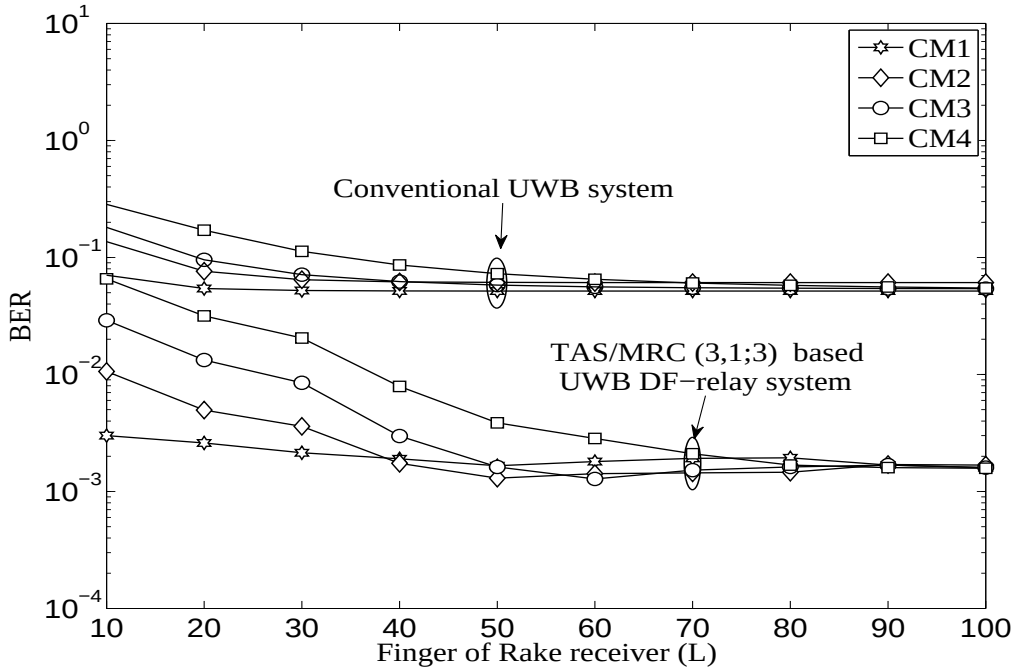

Figure 4.5: BER vs Rake fingers (L) for the IEEE 802.15.3a (CM1) for SNR= 5 dB

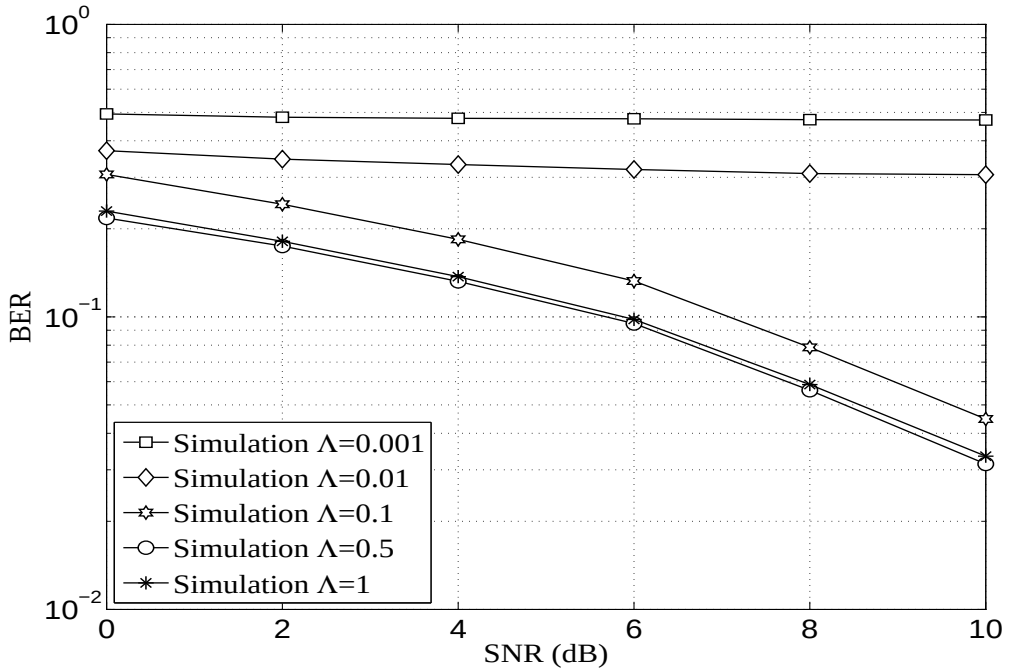

Figure 4.6: BER of conventional UWB system for different values of inter-cluster arrival rate (Λ) in the IEEE 802.15.3a (CM2)

BER of the conventional UWB system. From the extensive Monte-Carlo simulation results, it is found that the DF-relaying UWB system has lesser BER than the conventional UWB system and it improves with an increase in the number of antennas in the TAS/MRC scheme. The presented results show that the derived analytical BER is a good match with the simulation results for the IEEE 802.15.3a channel models (CM1~4). Furthermore, we investigated the effects of σ_X, Λ and L on the BER of the DF-relaying and conventional UWB systems. We would also like to emphasize that the presented analytical method can be applied to the other multipath channel models with any fading distribution.

5

BER Analysis of TAS/MRC Based LR-UWB Relay System over the IEEE 802.15.4a Channel

Contents

5.1 Introduction

IEEE 802.15 WPAN working group has categorized the UWB technology into high-data-rate and low-data-rate UWB (LR-UWB) technologies and has recommended the IEEE 802.15.3a and the IEEE 802.15.4a channel standards for the implementation of these two UWB systems, respectively. In the previous chapters, we dealt with the high-data-rate UWB system and derived the BER of various diverse UWB networks and discussed the effects of various parameters of the IEEE 802.15.3a channel model on the performance. In this chapter, we study the propagation characteristics and the power delay profile of the IEEE 802.15.4a channel and compute the average BER for the DF-relaying LR-UWB system with TAS scheme at the source and the relay terminals. Additionally, we examine the impacts of various parameters of the IEEE 802.15.4a channel on the BER and suggest the sufficient number of Rake's finger required to capture the signal energy for various environments of the IEEE 802.15.4a channel model. Furthermore, we demonstrate the Monte-Carlo simulation and the numerical results of the derived BER expression and compare these results with the reported BER for the narrowband flat fading channels.

Several research findings on the performance evaluation of the IEEE 802.15.4a channel in various scenarios have been reported in the literature. Initial work on the error performance analysis of LR-UWB system over the IEEE 802.15.4a channel model have been reported in [71, 72, 94]. In [73, 74], the authors have analyzed the error performance of two hop LR-UWB systems over the simplified UWB channel or narrowband flat fading channels. In [75], the authors have investigated the BER of the cooperative communication over the $\kappa - \mu$ fading channel ($\kappa - \mu$ is a generalized narrowband flat fading model which accommodates most of the known fading models such as Rayleigh distribution for $\kappa \to 0$ & $\mu = 1$ Nakagami-m distribution for $\kappa \to 0$ & $\mu = m$ and so on).

The remainder of this chapter is organized as follows. In the next section, we describe the system and channel model. We derive an expression of BER for the TAS/MRC based DF-

relaying LR-UWB system in section 5.3. In section 5.4, we present the analytical and the simulation results and summarize the outcomes of the chapter in section 5.5.

5.2 System and Channel Model

We consider a LR-UWB relay system with the antenna selection at the source and the relay terminals as shown in Fig. 4.1. In the system, relay is configured to perform the DF cooperative strategy and the antenna selection is carried out such that the selected transmitting antenna is delivers the maximum received SNR at the destination. A brief description of the system model and the mathematical expressions of received signals vectors are already given in section 4.2. In this chapter, channel impulse response for each channel link is modeled as IEEE 802.15.4a standard, which is suitable for the LR-UWB applications. The propagation characteristics and the power delay profile of the IEEE 802.15.4a channel is defined below.

5.2.1 IEEE 802.15.4a channel model

TG4a has developed the IEEE 802.15.4a standard for implementation of the LR-UWB system covering frequency range 2-10 GHz. Mathematically, an impulse response of the IEEE 802.15.4a channel from the u^{th} transmitter to the v^{th} receiver can be expressed as [13]

$$h_{(u,v)}(t) = \sum_{m=0}^{M} \sum_{r=0}^{R} \alpha_{r,m}^{(u,v)} \exp\left(j\phi_{r,m}^{(u,v)}\right) \delta\left(t - T_m^{(u,v)} - \tau_{r,m}^{(u,v)}\right) \tag{5.1}$$

where $\alpha_{r,m}$ is the multipath gain coefficient (MPC) of the r^{th} ray within the m^{th} cluster, T_m and $\tau_{r,m}$ are the cluster and ray arrival times, respectively. The phase $\phi_{r,m}$ is uniformly distributed in the range $[0, 2\pi]$, R and M represent the number of rays within the cluster and the number of clusters, respectively. According to TG4a report, α is Nakagami-m distributed, where parameter- m is modeled as a lognormally distributed random variable, whose logarithm has a mean ($\mu_m(\tau) = m_0 - k_m\tau$) and a standard deviation $\left(\sigma_m(\tau) = \hat{m}_0 - \hat{k}_m\tau\right)$. The parameters $\{m_0, k_m\}$ and $\left\{\hat{m}_0,\ \hat{k}_m\right\}$ are the mean factors and the variance factors for parameter-m, respectively. For the first component of each cluster, the Nakagami factor m is modeled differently and it is defined as $m = \tilde{m}_0$, where $\tilde{m}_0$ is the Nakagami-m factor for strong components. The

distribution of cluster arrival time is modeled as the Poisson process and it is defined in 2.2. While the distribution of ray arrival time is modeled as the mixtures of two Poisson processes. If λ_1 and λ_2 are the ray arrival rates, then the distribution of ray arrival time is given by

$$f\left(\tau_{r,m}/\tau_{(r-1),m}\right) = \beta\lambda_1 e^{\left(-\lambda_1\left[\tau_{r,m}-\tau_{(r-1),m}\right]\right)} + (1-\beta)\,\lambda_2 e^{\left(-\lambda_2\left[\tau_{r,m}-\tau_{(r-1),m}\right]\right)}, \quad r > 0 \tag{5.2}$$

where β is the mixture probability. Now an average arrival rate, λ is obtained as

$$\begin{aligned}\lambda &= \frac{1}{\mathbb{E}\left[\text{ Average arrival time}\right]} \\ &= \frac{\lambda_1\lambda_2}{(1-\beta)\,\lambda_1 + \beta\lambda_2}\end{aligned} \tag{5.3}$$

In the IEEE 802.15.4a channel, the power delay profile within the cluster is exponential and it is defined as

$$\mathbb{E}\left[\left|\alpha_{r,m}\right|^2\right] = \frac{\Omega_m}{\gamma_m}\exp\left(-\frac{\tau_{r,m}}{\gamma_m}\right) \tag{5.4}$$

where Ω_m is the integrated energy of m^{th} cluster and γ_m represents the intra-cluster decay time constant, depends linearly on the arrival time of the cluster and it is defined as

$$\gamma_m \propto k_\gamma T_m + \gamma_0 \tag{5.5}$$

where k_γ and γ_0 are the intra-cluster decay time constant parameters. The shape of average power delay profile for NLOS path of the office and the industrial environments is given by

$$\mathbb{E}\left[\left|\alpha_{r,1}\right|^2\right] = \left(1-\chi e^{\left[-\tau_{r,m}/\gamma_{rise}\right]}\right)e^{\left[-\tau_{r,m}/\gamma_1\right]}\left(\frac{\gamma_1+\gamma_{\text{rise}}}{\gamma_1}\right)\left(\frac{\Omega_1}{\gamma_1+\gamma_{\text{rise}}\,(1-\chi)}\right) \tag{5.6}$$

where the parameter χ describes the attenuation of the first component, the parameter γ_{rise} determines how fast the PDP increases to its local maximum, and γ_1 determines the decay at later times. Assuming $M_{cluster}$ to be a normally distributed random variable with zero mean and $\sigma_{cluster}$ standard deviation, the integrated energy of m^{th} cluster over the cluster shadowing can be expressed as

$$10\log\left(\Omega_m\right) = 10\log\left(\exp\left(-\frac{T_m}{\Gamma}\right)\right) + M_{cluster} \tag{5.7}$$

Assuming $\Omega = \mathbb{E}\left[\left|\alpha_{r,m}\right|^2\right]$ and from the equations (5.4), (5.7) after substituting $T_m = T$, $\tau_{r,m} = T - \tau$, and we have

$$\Omega = \frac{1}{\gamma_m} \exp\left(-\frac{T}{\Gamma} - \frac{T-\tau}{\gamma_m}\right) \tag{5.8}$$

On the basis of practical measurements, the IEEE 802.15.4a channel model is categorized into five different environments viz, Residential, Indoor Office, Outdoor, Open Outdoor and Industrial environments. Every channel environment is further classified according to the LOS and NLOS paths. The measured values and parametric specifications of the IEEE 802.15.4a channel parameters for various environments are given in the Appendix B.

5.3 Performance Analysis

In this section, we derive an expression of BER for binary signals in the TAS/MRC based DF-relaying LR-UWB MIMO system over the IEEE 802.15.4a channel model. The derivation of BER over the IEEE 802.15.4a channel is similar to the derivation over the IEEE 802.15.3a channel presented in Chapter 4, the main difference is in the computation of characteristic function of energy captured by a Rake receiver in the IEEE 802.15.4a channel.

5.3.1 Characteristic function of the received signal energy for the MRC system

Let $\tilde{\mathcal{E}}_{u,v}$ be the energy captured by a Rake receiver in the $(u-v)^{th}$ channel link for the LR-UWB system. Similar to the IEEE 802.15.3a standard, $\tilde{\mathcal{E}}_{u,v}$ in the $[0,\ LT_c]$ time window can be computed as

$$\tilde{\mathcal{E}}_{u,v} \triangleq \sum_{0<T_m+\tau_{r,m}\leqslant LT_c} \left|\alpha_{r,m}^{u,v}\right|^2 \tag{5.9}$$

For brevity, we omit the antenna index. From the equations (2.16) and (2.18), a characteristic function, $\psi_{\tilde{\mathcal{E}}}(\vartheta)$ can be defined as

$$\psi_{\tilde{\mathcal{E}}}(\vartheta) = \mathcal{L}_{0,0}(\vartheta)\ \mathrm{e}^{-\lambda\tilde{\psi}_{\vartheta}(0,L)}\ \mathrm{e}^{-\Lambda\tilde{J}(\vartheta,L)} \tag{5.10}$$

For the IEEE 802.15.4a UWB channel $\alpha_{T,\tau}$ is a random variable having Nakagami-m distribution, then the distribution $\alpha_{T,\tau}^2$ is modeled as a Gamma distribution. Hence the characteristic

function, $\mathcal{L}_{T,\tau}(\vartheta)$ can be calculated as

$$\mathcal{L}_{T,\tau}(\vartheta) = \left(1 - \frac{i\vartheta\Omega}{m}\right)^{-m} \tag{5.11}$$

where Ω represents the average energy of $\alpha_{r,m}$ is defined in equation (5.8) and $m = \exp\left(m_0 + \frac{\hat{m}^2}{2}\right)$. Combining the equations (2.22), (2.24), (3.14) (5.10) and (5.11), the characteristic function of the received signal energy (C_u) is obtained as

$$\begin{aligned}\Psi_{C_u}(\vartheta) = &\left(1 - \frac{i\vartheta}{\gamma_0 e^{\left(m_0+\frac{\hat{m}^2}{2}\right)}}\right)^{-N_r \exp\left(m_0+\frac{\hat{m}^2}{2}\right)} e^{\left(-\frac{N_r \lambda L T_c}{2} \sum_{j=1}^{N^L} w_j^L \left[1-\mathcal{L}_{o,\tau}(\vartheta)\right]\Big|_{\tau=\frac{LT_c}{2}\left(x_j^L+1\right)}\right)} \\ &\times e^{\left(-\frac{N_r \lambda L T_c}{2} \sum_{j_1=1}^{N^L} w_{j_1}^L \left[1-\mathcal{L}_{T,T}(\vartheta) e^{\left[-\lambda \tilde{\psi}_\vartheta(T,L)\right]}\right]\Big|_{T=\frac{LT_c}{2}\left(x_{j_1}^L+1\right)}\right)}\end{aligned} \tag{5.12}$$

The final BER expression of the TAS/MRC based DF-relaying LR-UWB system over the IEEE 802.15.4a channel can be obtained by substituting the result of $\Psi_{C_u}(\vartheta)$ in the equation (4.12).

5.4 Numerical Results and Discussion

In this section, we present the Monte-Carlo simulation and the analytical results of binary signals for the TAS/MRC based DF-relaying LR-UWB system. Fig. 5.1 shows the comparison of BER conventional (without relay) and TAS/MRC (3,1;3) based DF-relaying UWB systems over the IEEE 802.15.3a and the IEEE 802.15.4a channel models (CM1). As expected, the BER over the IEEE 802.15.3a channel is lower than the IEEE 802.15.4a channel. This is because, the IEEE 802.15.3a channel standard has been developed for short distance UWB communication and consequently in a given time-window, more MPCs arrive at the Rake receiver than in the IEEE 802.15.4a channel standard.

The effect of L on the BER of TAS/MRC (3,1;3) based DF-relaying LR-UWB system over various environments of the IEEE 802.15.4a channel at SNR= 5dB is shown in Fig. 5.2. Initially, as L increases, the BER decreases because more signals energy is captured by the Rake receiver. But beyond certain values of L ($L \geqslant 15$ for CM1~2 and $L \geqslant 25$ for CM3~6), the BER curves become flat. This is because, beyond a certain L, the contribution to the total signal en-

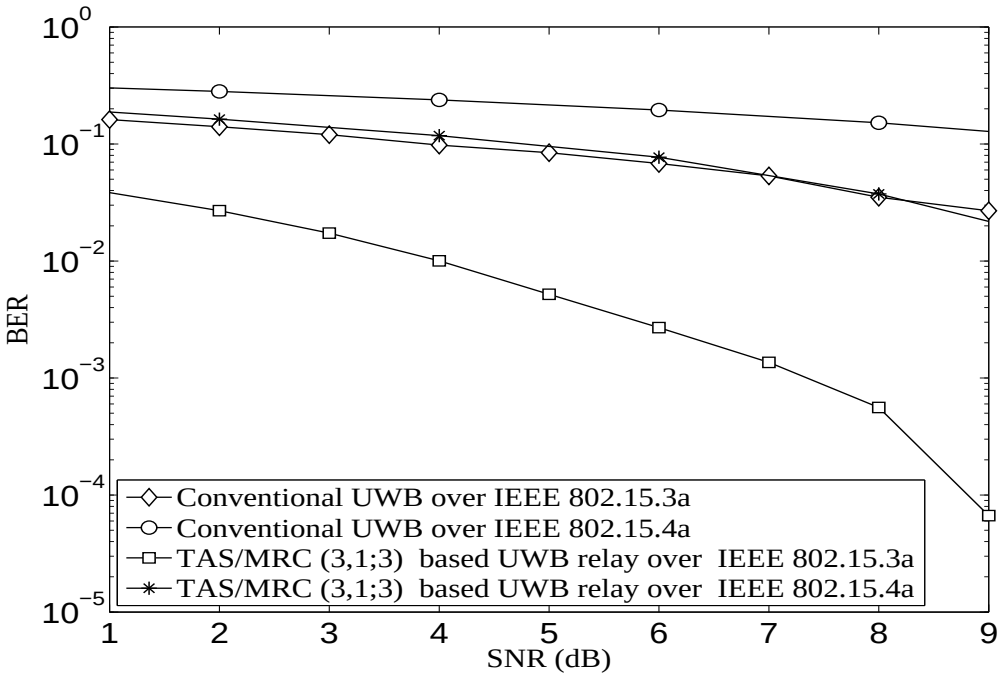

Figure 5.1: BER for conventional and TAS/MRC (3, 1; 3) based UWB DF-relay system over the IEEE 802.15.3a and the IEEE 802.15.4a channel model (CM1)

ergy captured by the Rake receiver is only marginal with increasing L. Therefore, BER curves become almost flat. For further simulations and the numerical calculations, we choose $L = 25$ for all channel models so that performance can be compared fairly in all cases.

Fig. 5.3 shows the effect of number of antennas on the BER of the TAS/MRC $(N_t, 1; N_r)$ based DF-relaying UWB communication over the IEEE 802.15.4a channel (CM1). The UWB relay system has lesser BER than the conventional UWB system and BER also improves with an increase in the number of antennas in the TAS scheme due to the diversity gain achieved by incorporating MIMO technology. Similarly, the simulation and analytical BER of binary signals for the TAS/MRC (3, 1; 3) based DF-relaying UWB system over different environments of the IEEE 802.15.4a channel (CM1~6) are shown in Fig. 5.4. The results show that the derived analytical result reasonably matches to the simulation results, which validate the accuracy of the derived BER expression.

Fig. 5.5 shows the simulated and analytical BERs of the UWB system (with and without

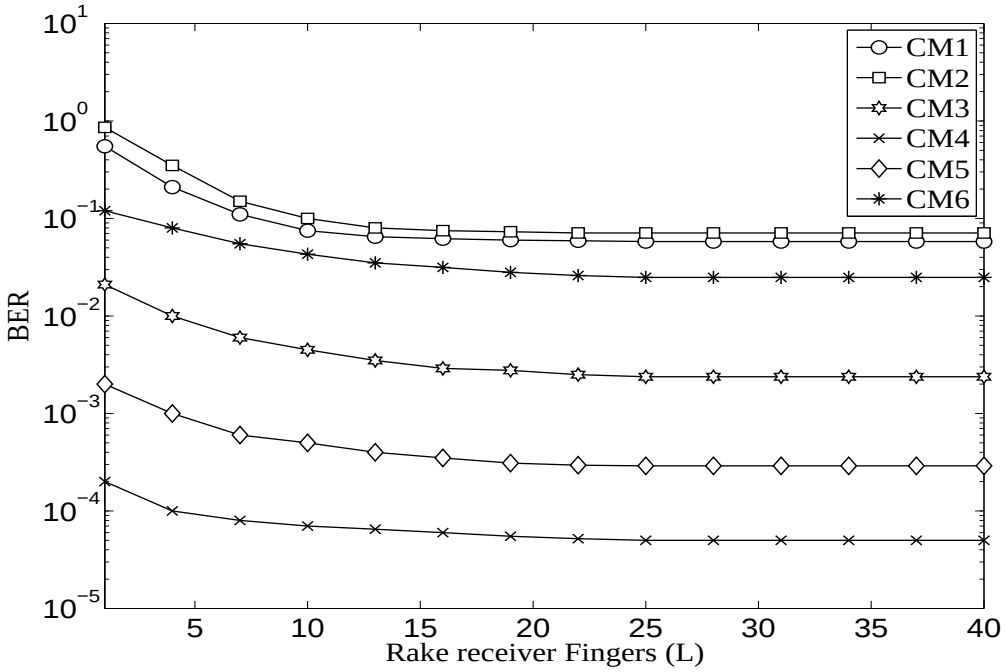

Figure 5.2: BER vs L for TAS/MRC $(3, 1; 3)$ based LR-UWB relay system for SNR=5dB

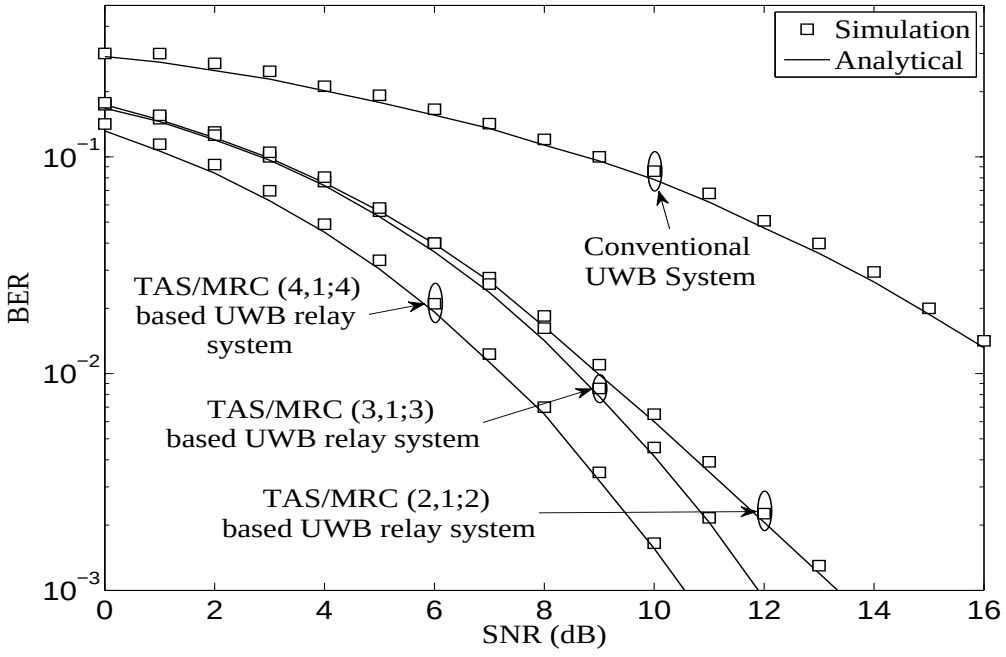

Figure 5.3: Simulation and analytical BER of the conventional and TAS/MRC $(N_t, 1; N_r)$ based UWB DF-relay system over the IEEE 802.15.4a channel (CM1)

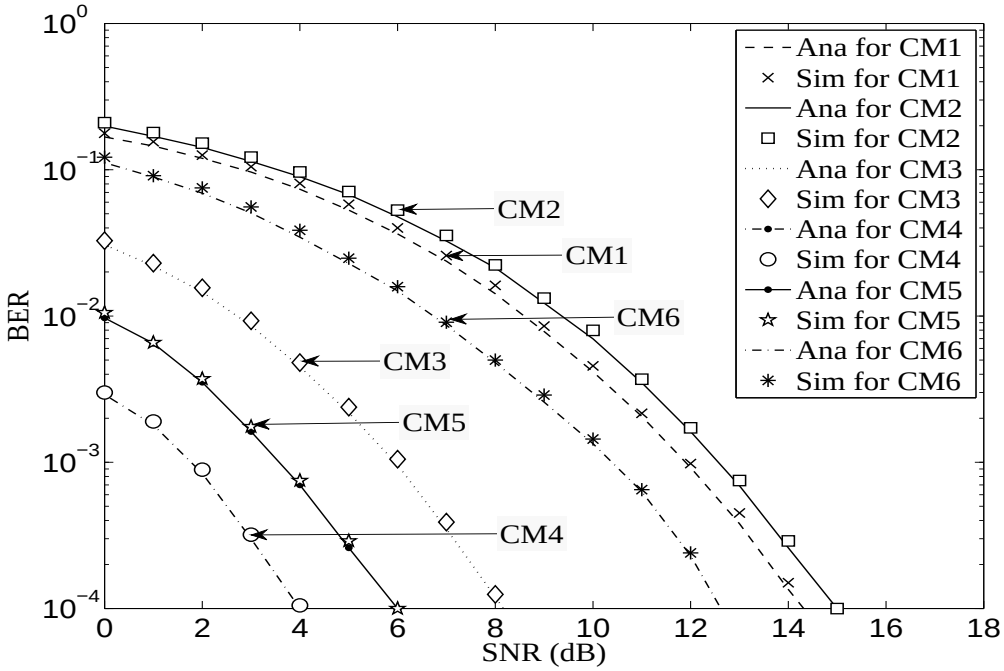

Figure 5.4: Simulation and analytical BER of the TAS/MRC (3, 1; 3) based UWB DF-relay system over the IEEE 802.15.4a channel (CM1~6)

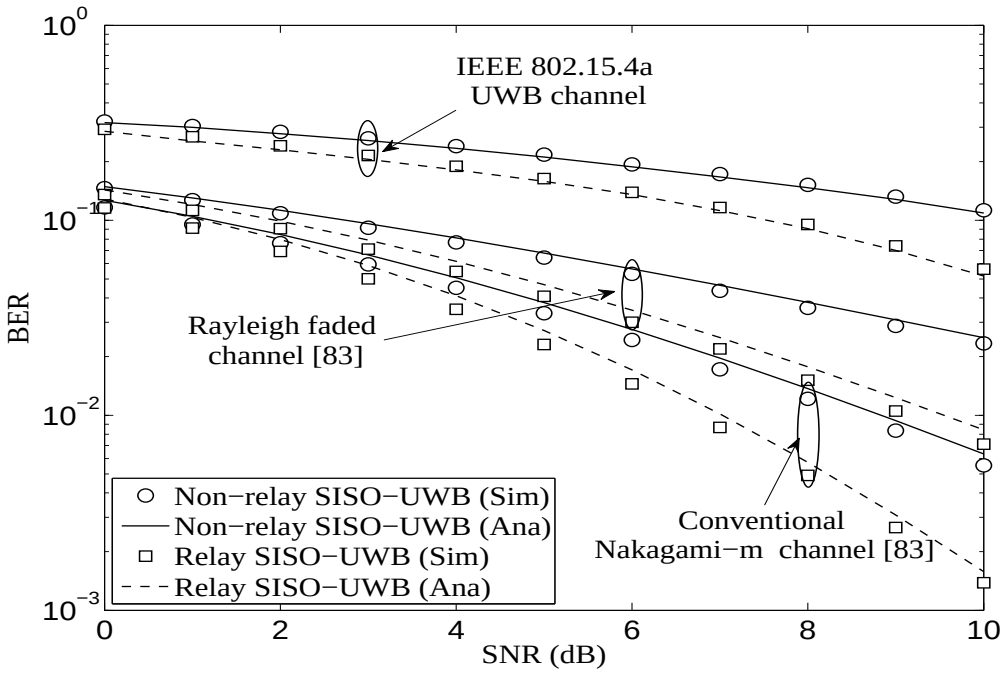

Figure 5.5: BER of conventional UWB system over the IEEE 802.15.4a channel (CM1) and narrowband Nakagami-*m* fading channel for *m*=1 and 2.0324

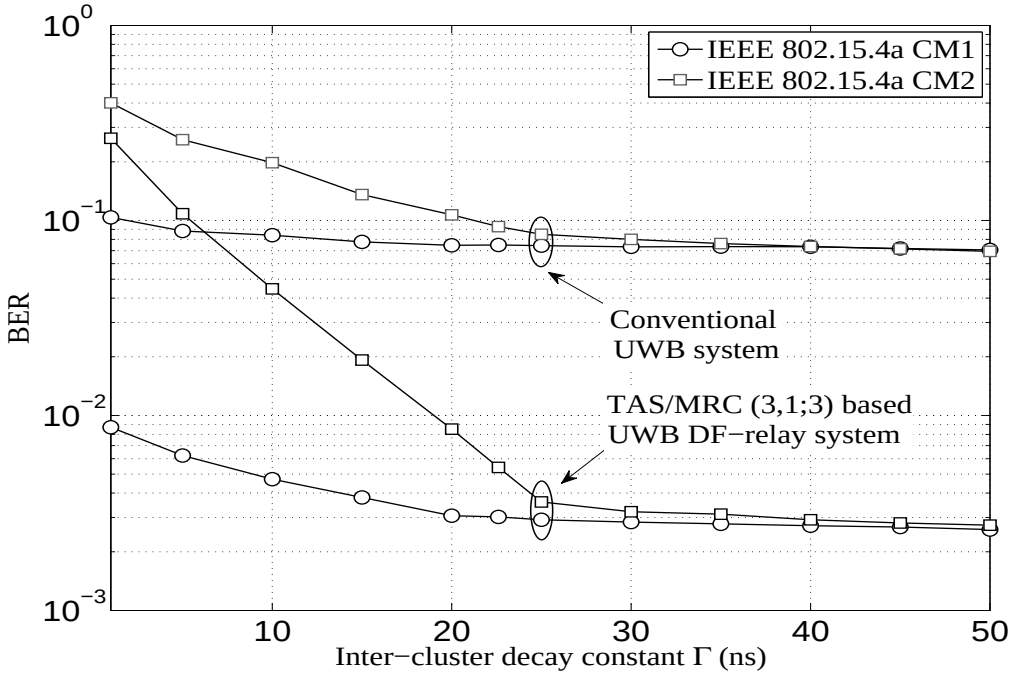

Figure 5.6: BER vs Γ for the IEEE 802.15.4a UWB channel (CM1~2) for SNR=10dB

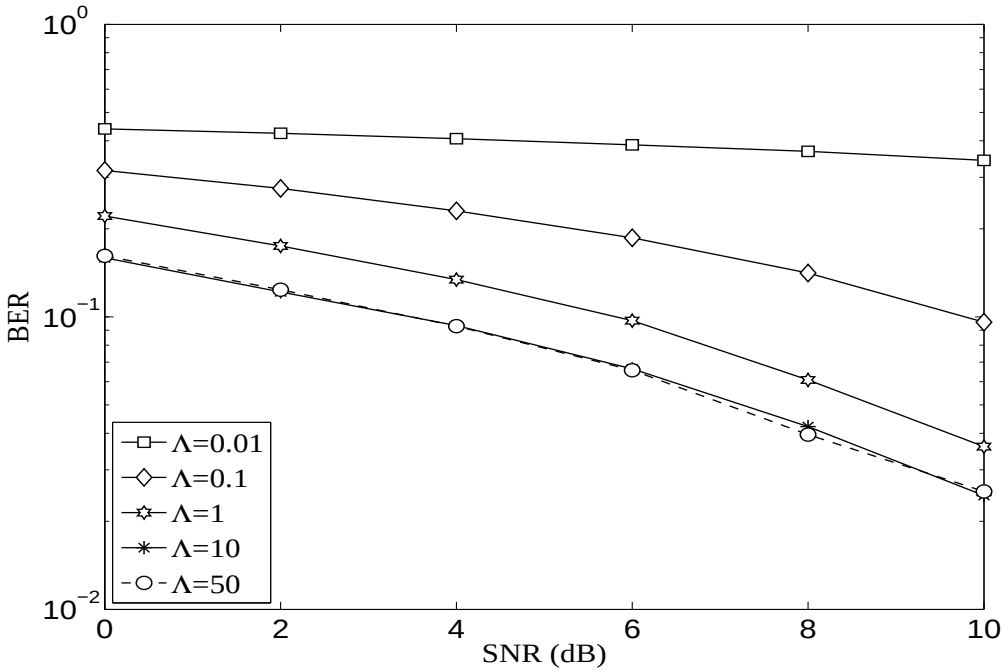

Figure 5.7: BER of conventional LR-UWB system over the IEEE 802.15.4a channel (CM2) for Λ = 0.01, 0.1, 1 10 and 50

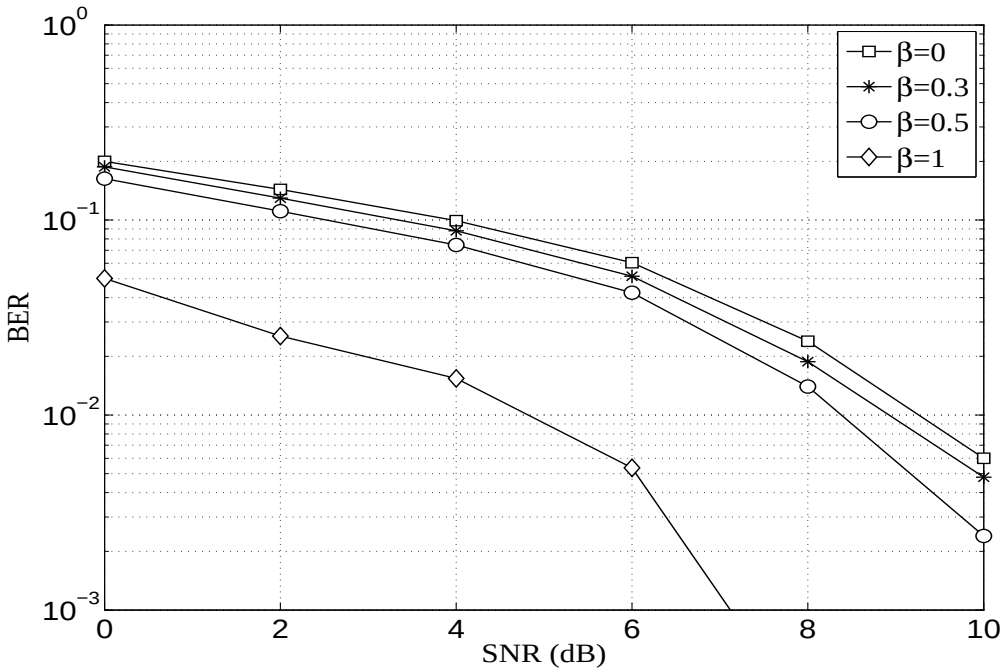

Figure 5.8: BER of TAS/MRC (3, 1; 3) based LR-UWB DF-relay system over the IEEE 802.15.4a channel (CM2) for different values of mixture probability

relay) over the IEEE 802.15.4a channel and narrowband Nakagami-*m* flat fading channel (*m* = 1, and 2.0324) for *L*=10. As expected, the narrowband Nakagami-*m* fading has lesser BER than the IEEE 802.15.4a channel model and BER for narrowband fading channels decreases with increasing the value of *m*.

Fig. 5.6 shows the effect of the inter-cluster decay constant (Γ) on the BER of the conventional and the TAS/MRC (3,1;3) DF-relaying UWB systems over the IEEE 802.15.4a channel (CM1~2), at SNR=10dB. It is observed that the BER of both UWB systems decreases with an increase in Γ. But after certain values of Γ (Γ= 22ns for CM1 & Γ= 26ns for CM2), the BER curves go flat. Initially, the integrated energy of the m^{th} cluster, (Ω_m) increases with an increase in Γ. As a result, the energy captured by the Rake receiver also keeps increasing. Later on, at Γ= 22ns for CM1 and Γ= 26 ns for CM2, most of the m^{th} cluster energy already gets integrated. Therefore, beyond these values of Γ, the BER curves become flat.

Fig. 5.7 shows the impact of inter-cluster arrival rate (Λ) on the BER of conventional UWB

system. We observe that when Λ increases, the BER decreases because more clusters arrive in the given time window and the Rake receiver collects more signal energy for the channel, hence improving the BER. Fig. 5.8 shows the effect of β on the BER of the investigated UWB system over the IEEE 802.15.4a channel (CM2). As β increases, the BER decreases. From equation (5.2), when β increases, the ray process has the higher probability to choose the arrival rate λ_1 rather than λ_2. For the IEEE 802.15.4a channel (CM2), $\lambda_1 = 1.77$ and $\lambda_2 = 0.15$. As we already know, the higher arrival rate means more signal energy captured by the Rake receiver thereby improving the BER.

5.5 Summary

In this chapter, we derived the computable BER formula of binary signals for the TAS/MRC based DF-relaying LR-UWB system over the IEEE 802.15.4a channel. Our numerical results showed that there is a significant improvement in the BER of the DF-relaying UWB system. We also showed the BERs of the low-data-rate UWB system for the various fading channels and compared these results with the BER of the conventional UWB system over the IEEE 802.15.4a channel. The results showed that the numerical values of the derived BER are in good match with the Monte-Carlo simulation results, which justify the approximations and assumptions taken in our analysis. We also found that the numerical computation of the derived BER is faster than the Monte-Carlo simulation. Furthermore, we investigated the impact of number of fingers of Rake receiver on the BER and suggested the sufficient number of L for various environments of the IEEE 802.15.4a channel model. Additionally, we have discussed the effects of various parameters in the IEEE 802.15.4a channel model on BER performance of the TAS/MRC based DF-relaying LR-UWB system.

6

Analysis of mm-Wave MIMO System over the IEEE 802.15.3c Channel at 60 GHz

Contents

6.1 Introduction

the licence-exempted wide frequency spectrum in the mm-Wave for indoor communications at 60 GHz band has shown enormous potential for bandwidth-hungry applications such as high definition video streaming, live gaming and so on. In the available literature [79–81, 83–85], the spectral efficiency, the outage channel capacity, and the average output SINR of the mm-Wave system with various antenna beamforming techniques have been reported. Beamforming is a signal processing technique used in the antenna arrays to compensate the high path loss phenomenon and obtain the reliable transmission quality at 60 GHz band. The main idea of beamforming is to control the phase of the signal fed to each transmitting antenna via a network of analog phase shifters. A large bandwidth and the stochastic nature of the IEEE 802.15.3c channel pose difficulties in the theoretical analysis of the mm-Wave communication at 60 GHz band. Simulation results and semi-analytical analysis of 60 GHz band have been reported in [82, 86, 90], but the BER analysis of mm-Wave system with the antenna beamforming has not been reported (to the best of the knowledge of the authors).

In this chapter, we derive an analytical expression of antenna beamforming based BER for the mm-Wave MIMO indoor communication system over the IEEE 802.15.3c channel model. The analysis includes the impact of a coherent Rake receiver on the BER and suggests the sufficient number of Rake fingers required to capture the maximum signal energy in the IEEE 802.15.3c channel environment. Additionally, we discuss the effect of the power decay factors and the arrival rates on the performance. We present the Monte-Carlo simulation and the analytical results and examine the accuracy of our BER expression.

This chapter is organised as follows. Section 6.2 describes the system and channel model. In Section 6.3, the BER analysis of MIMO mm-Wave system over the IEEE 802.15.3c channel model at 60 GHz is presented. In Section 6.4, the Monte-Carlo simulation results are provided and discussed. The chapter is summarised in Section 6.5.

6.2 System and Channel Model

In this section, the IEEE 802.15.3c channel model at 60 GHz band and the mm-Wave communication system with uniform antennas array (ULAs) are described in brief.

6.2.1 IEEE 802.15.3c channel model

IEEE 802.15.3c channel model is known as the modified Saleh- Valenzuela (SV) indoor channel model. It combines a LOS component using a two-path model with the NLOS reflective clusters of the S-V model. The channel model considers the spatial temporal phenomenon and the angle-of-arrival (AOA) information, which are widely used for describing the multipath propagation in the indoor communication system. Although the angle of departure (AOD) is not defined in the original IEEE 802.15.3c mm-Wave channel model [19], but it is necessary to examine the system performance with the antenna beamforming. Therefore, in this analysis we considers the modified version of the IEEE 802.15.3c channel, which has four parameters, including multipath gain coefficients, time of arrival (TOA), AOA and AOD. A impulse response of modified version of the IEEE 802.15.3c channel is given by

$$h(t,\theta,\phi) = \beta\delta(t)\,\delta(\theta)\,\delta(\phi) + \sum_{m=1}^{M}\sum_{r=1}^{R} \alpha_{r,m}\delta(t - T_m - \tau_{r,m})\delta(\theta - \theta_m - \omega_{r,m})\,\delta(\phi - \phi_m - \psi_{r,m}) \quad (6.1)$$

where β represents the gain coefficient of the LOS path, which are dependent on the antenna-heights, the antenna gains, the Tx-Rx separation and the path loss of the first impulse. θ_m and ϕ_m are the AOA and AOD of the m^{th} cluster, respectively. Similarly, $\omega_{r,m}$ and $\psi_{r,m}$ are the AOA and AOD for the r^{th} ray of the m^{th} cluster, respectively. Assuming AOD has the same statistics as that of the AOA, A graphical representation of the multipath propagation behaviour at 60 GHz band is shown in Fig. 6.1. The figure clearly shows that the MPCs (rays) arrived in the form of bunches (cluster) which are independent of each other. The number of cluster (M) is a

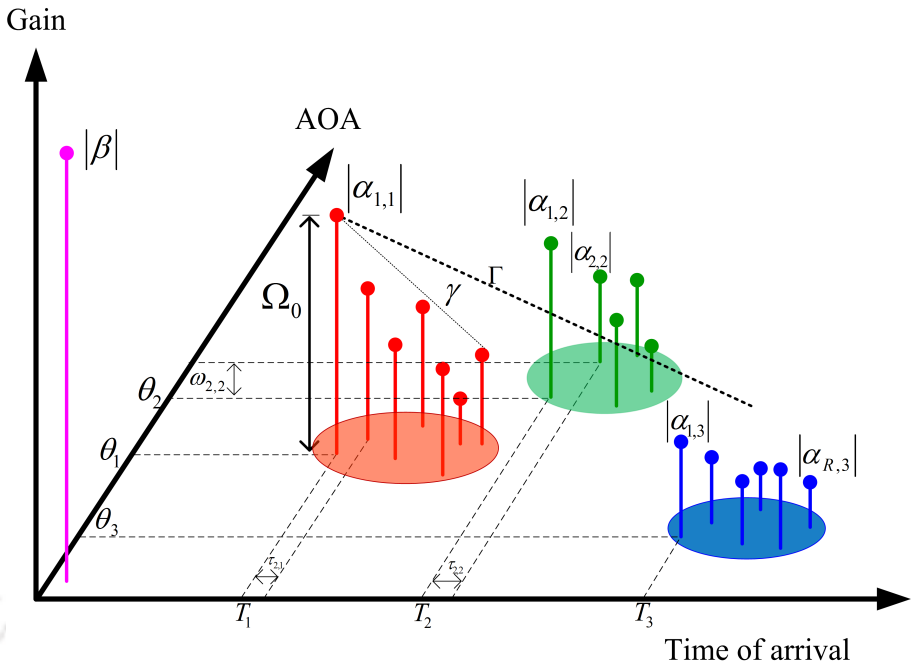

Figure 6.1: Graphical representation of the IEEE 802.15.3c channel model

random variable, whose probability mass function (pmf) is expressed as

$$f_M(m) = \begin{cases} \left(1+\bar{L}\right)e^{-\bar{L}}, & m = 1 \\ \bar{L}^m e^{-\bar{L}}/m! & m \geq 2 \\ 0, & \text{otherwise} \end{cases} \tag{6.2}$$

where $\bar{L} = \mathbb{E}[M]$. The distribution of the cluster and the ray time-of-arrival are modeled as Poison processes. In the angular domain, AOA of the LOS component, $\{\theta_{LOS}\}$, is assumed to be zero degree and a distribution of $\{\theta_m\}$, to be uniform random variables distributed over $[0,\ 2\pi]$. On the other hand, the distribution of $\{\omega_{r,m}\}$, is modeled as a zero mean Gaussian random variable with σ_ϕ standard deviation and is given as

$$f(\omega_{r,m}) = \frac{1}{\sqrt{2\pi}\sigma_\phi} \exp\left(-\omega_{r,m}^2/2\sigma_\phi^2\right) \tag{6.3}$$

The second order moment or average power of the complex multipath gain coefficient ($\alpha_{r,m}$) can be calculated as

$$\mathbb{E}\left[\left|\alpha_{r,m}\right|^2\right] = \Omega_0 \exp\left(-\frac{T_m}{\Gamma} - \frac{\tau_{r,m}}{\gamma} - \tilde{\kappa} I_{[\tilde{\kappa}\neq 0]}\right) \tag{6.4}$$

where $\tilde{\kappa}$ is the Rician factor and $I_{[A]}$ denotes the indicator function of an event $\{A\}$. On the basis of practical measurements, the IEEE P802.15 WPAN channel model subcommittee has categorized the 60 GHz indoor communication environment into five different categories viz, Residential, Office, Library, Desktop and Kiosk. These environments are further classified according to the LOS and NLOS scenarios. They are further sub-categorized based on the Half-Power Beam-Width (HPBW) of the transmit and receive antenna arrays. The parametric specifications and the measured data of the IEEE 802.15.3c channel parameters for different environment are given in the Appendix C.

6.2.2 System model

The ULAs based mm-Wave MIMO system, having N_t transmit and N_r receive antennas with the bank of coherent Rake receiver is shown in Fig. 6.2. Note that the mm-Wave communication

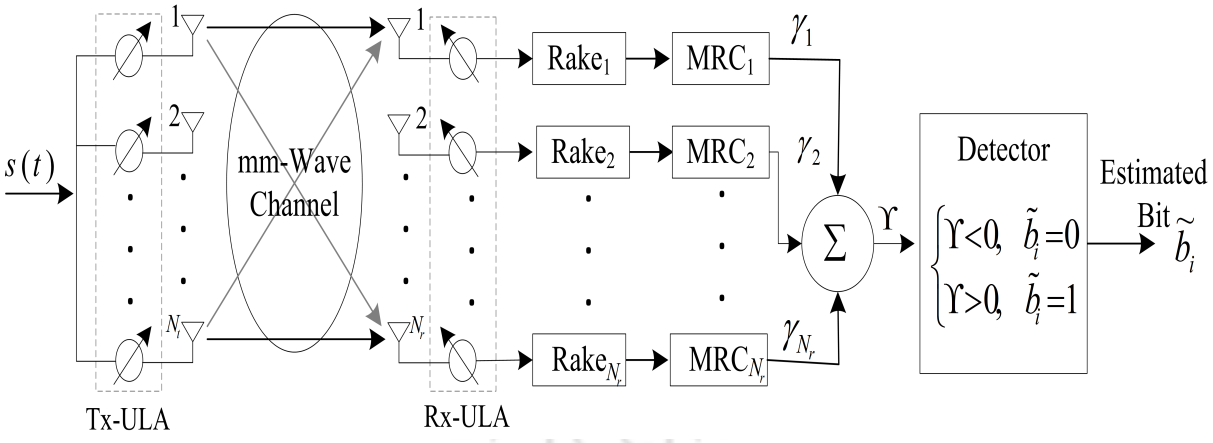

Figure 6.2: Block diagram of mm-Wave MIMO system model employing coherent Rake receivers

at 60 GHz exclusively support the rank one transmission i.e., all transmitting antennas are fed with the same symbol at one time instant. The mathematical expression of binary phase shift

keying (BPSK) modulated transmitted signal is given by

$$s(t) = \sqrt{E_b} \sum_{i=-\infty}^{\infty} b_i \, p(t - iT_s) \tag{6.5}$$

where $b_i \in \{\pm 1\}$ represents the i^{th} transmitted bit, $p(t)$ is the unit energy raised-cosine pulse of duration T_p and T_s is the symbol duration. We denote $R_g(.)$ as the normalized autocorrelation function of pulse $p(t)$ and assume that $R_g(\delta) \approx 0$, when $|\delta| \geq T_p$. It is also assumed that each transmitted symbol having only one pulse hence $T_s = T_p$. Considering the transmit and the receive antennas are perfectly aligned and statistically independent, the effective mm-Wave channel impulse response after considering the ULAs can be expressed as

$$\boldsymbol{h}(t) = \int_{-\pi}^{\pi} \int_{-\pi}^{\pi} \boldsymbol{h}(t, \theta, \phi) \, \vartheta(\theta) \, \zeta(\phi) \, d\theta d\phi \tag{6.6}$$

where $\boldsymbol{h}(t) \in \mathbb{C}^{N_r \times N_t}$ is the matrix of effective mm-Wave channel, $\vartheta(\theta)$ and $\zeta(\phi)$ represent the array response vector of ULAs at the transmitter and the receiver side, respectively, which satisfy $\|\vartheta(\theta)\|_2 = 1$ and $\|\zeta(\phi)\|_2 = 1$, are defined as

$$\vartheta(\theta) = \frac{1}{\sqrt{N_t}} \left[1, e^{\left(\frac{j2\pi d \sin(\theta)}{\lambda_c}\right)}, ..., e^{\left(\frac{j2\pi (N_t - 1) d \sin(\theta)}{\lambda_c}\right)}\right]^T \tag{6.7}$$

and

$$\zeta(\phi) = \frac{1}{\sqrt{N_r}} \left[1, e^{\left(\frac{j2\pi d \sin(\phi)}{\lambda_c}\right)}, ..., e^{\left(\frac{j2\pi (N_r - 1) d \sin(\phi)}{\lambda_c}\right)}\right]^T \tag{6.8}$$

where λ_c is the wavelength of the carrier frequency and $d = \lambda/2$ is the half wavelength spacing between the two consecutive antennas. Since, all the transmitting antennas are independent and transmit one symbol at a time, then the received signal at the v^{th} receiving antenna can be given as

$$r_v(t) = \sqrt{\frac{E_b}{N_t N_r}} \sum_{i=-\infty}^{\infty} \sum_{u=1}^{N_t} b_i \left\{ \beta_{(u,v)} p(t - iT_s) + \sum_{m=1}^{M} \sum_{r=0}^{R} \alpha_{r,m}^{(u,v)} p\left(t - \delta_{r,m}^{(u,v)} - iT_s\right) e^{\left(j \, \Theta_{r,m}^{(u,v)}\right)} \right\} + \eta_{(v)}(t) \tag{6.9}$$

where $\delta_{r,m}^{(u,v)} = T_m^{(u,v)} + \tau_{r,m}^{(u,v)}$, $\Theta_{r,m}^{(u,v)} = \frac{2\pi d}{\lambda_c}\left[(u-1)\sin\left(\theta_m^{(u,v)} + \omega_{r,m}^{(u,v)}\right) + (v-1)\sin\left(\phi_m^{(u,v)} + \psi_{r,m}^{(u,v)}\right)\right]$ and $\eta_{(v)}(t) \backsim \mathcal{N}\left(0, \frac{N_0 N_t}{N_r}\right)$.

6.3 BER Analysis

In this chapter, we derive a characteristic function based BER formula of antenna beamforming based mm-Wave MIMO communication system with the bank of coherent Rake receiver. In the analysis, it is assumed that a perfect CSI is available at the receiver and the Rake receiver correlates the received signal of the (i') symbol with a template signal as follows.

$$\phi(t) = \beta p(t - i'T_s) + \sum_{m'=1}^{M}\sum_{r'=0}^{R} \alpha_{r',m'}\, p(t - \delta_{r',m'} - i'T_s)\, e^{\left(j\Theta_{r',m'}\right)} \tag{6.10}$$

The output of the Rake receiver correlator can be calculated as $R_v = \int_{i'T_s}^{(i'+1)T_s} r_v(t)\,\phi_v^*(t)\,dt$, where $\phi_v^*(t)$ denotes the complex conjugate of the template signal. Under the assumption of perfect synchronization i.e., $(m = m')$ & $(r = r')$ and using the relation $R_g(\delta) = R_g(-\delta)$, the output of the correlator at v^{th} receive antenna can be evaluated as

$$R_v = \sqrt{\frac{E_b}{N_t N_r}} \sum_{i'=0}^{\infty}\sum_{u=1}^{N_t} b_{i'} \left(\beta_{u,v}^2 + \sum_{m=1}^{M}\sum_{r=0}^{R} 2\,\beta_{u,v}\,\alpha_{r,m}^{(u,v)}\, R_g\left(\delta_{r,m}^{(u,v)}\right)\cos\left(\Theta_{r,m}^{(u,v)}\right) + \sum_{m=1}^{M}\sum_{r=0}^{R}\left|\alpha_{r,m}^{(u,v)}\right|^2\right) + \tilde{\eta}_v(t) \tag{6.11}$$

where $\tilde{\eta}_v(t) = \int_{i'T_s}^{(i'+1)T_s} \eta_v(t)\,\phi^*(t)\,dt$, is the noise component. In order to remove the inter-pulse interference, it is assumed that $\delta_{r,m} \geq T_p$, hence $R_g(\delta_{r,m}) \approx 0$. Assuming all the receiving antennas are sufficiently far away to make them uncorrelated and have equal noise power, the total received instantaneous SNR (Υ) can be computed as

$$\Upsilon = \frac{E_b}{N_t^2 N_0} \sum_{v=1}^{N_r}\sum_{u=1}^{N_t}\left(\beta_{(u,v)}^2 + \sum_{m=1}^{M}\sum_{r=0}^{R}\left|\alpha_{r,m}^{(u,v)}\right|^2\right) \tag{6.12}$$

6.3.1 PDF of the total received instantaneous SNR

Let us define, $\mathcal{E}_{(u,v)} \triangleq \sum_{m=1}^{M}\sum_{r=0}^{R}\left|\alpha_{r,m}^{(u,v)}\right|^2$ be the energy carried by all the multipath rays excluding the LOS component in the $(u-v)^{th}$ channel link for 60 GHz band. Assuming i.i.d. channel links, the characteristic function, $\Psi_\Upsilon(\vartheta)$ of the total received instantaneous SNR can be com-

puted as

$$\Psi_{\Upsilon}(\vartheta) = \prod_{v=1}^{N_r}\prod_{u=1}^{N_t} \psi_{\mathcal{E}}^{(u,v)}\left(\frac{E_b}{N_t^2 N_0}\vartheta\right)\exp\left(\frac{jE_b\beta_{(u,v)}^2}{N_t^2 N_0}\vartheta\right) \tag{6.13}$$

where $\psi_{\mathcal{E}}^{(u,v)}(.)$ is the characteristic function of $\mathcal{E}_{(u,v)}$ in the IEEE 802.15.3c channel model. For simplicity, we omit the antenna indexing (u,v) in the calculation of $\psi_{\mathcal{E}}^{(u,v)}(\vartheta)$. It may be noted that the number of clusters (M) is a random variable in the IEEE 802.15.3c channel model. Using equation (6.2), the average received energy with respect to M can be computed as

$$\begin{aligned}\tilde{\mathcal{E}} &= \sum_{m=1}^{\infty}\left(\sum_{\ell=1}^{m}\sum_{r=0}^{R}\left|\alpha_{r,\ell}\right|^2\right) f_M(m) \\ &= \left(1+\bar{L}\right)e^{-\bar{L}}\tilde{\mathcal{E}}_1 + \sum_{m\geq 2}\tilde{\mathcal{E}}_m\left(\frac{\bar{L}^m e^{-\bar{L}}}{m!}\right)\end{aligned} \tag{6.14}$$

where $\tilde{\mathcal{E}}_1 = \sum_{r=0}^{R}\left|\alpha_{r,1}\right|^2$ and $\tilde{\mathcal{E}}_m = \sum_{\ell=2}^{m}\sum_{r=0}^{R}\left|\alpha_{r,\ell}\right|^2$ are the energies carried by the rays which arrived within the first cluster and the remaining clusters, respectively. In this analysis, we conjecture that, $\tilde{\mathcal{E}}_1$ is close to $\mathcal{E}_1$, sum of the squared path gains of the first cluster that fall within $[0, LT_c]$ time window. Similarly, $\tilde{\mathcal{E}}_m$ is close to $\mathcal{E}_m$, the sum of squared path gains of rays in the remaining clusters, which are defined as $\mathcal{E}_1 \triangleq \sum_{(r,1):0<(T_1+\tau_{r,1})\leqslant LT_c}\left|\alpha_{r,1}\right|^2$ and $\mathcal{E}_m \triangleq \sum_{(r,m):0<(T_m+\tau_{r,m})\leqslant LT_c}\left|\alpha_{r,m}\right|^2$. It is noted that $\mathcal{E}_1$ and $\mathcal{E}_m$ are assumed to be statistically independent to each other. From the equation (2.18), the characteristic function of $\tilde{\mathcal{E}}$ can be calculated as

$$\psi_{\tilde{\mathcal{E}}}(\vartheta) = \exp\left[-\lambda\tilde{\psi}_{\kappa_1}(0,L)\right]\left(\prod_{m\geqslant 2}\exp\left[-\Lambda\tilde{J}(\kappa_2,L)\right]\right) \tag{6.15}$$

where $\kappa_1 = \left(1+\bar{L}\right)e^{-\bar{L}}\vartheta$ and $\kappa_2 = \frac{\bar{L}^m e^{-\bar{L}}}{m!}\vartheta$. From the equations (2.26), (6.13) and (6.15), the hermite computation form for $f_{\Upsilon}(x)$ can be obtained by

$$f_{\Upsilon}(x) = \frac{1}{2\pi}\sum_{i=1}^{N^H} w_i^H\left(\prod_{v=1}^{N_r}\prod_{u=1}^{N_t}\mathrm{e}^{\left(\frac{jE_b\beta_{(u,v)}^2 x_i^H}{N_t^2 N_0}-\lambda\tilde{\psi}_{\tilde{\kappa}_1}^{(u,v)}(0,L)\right)}\prod_{m2}e^{\left(-\Lambda\tilde{J}_{(u,v)}(\tilde{\kappa}_2,L)\right)}\right)\mathrm{e}^{\left(-jxx_i^H+\left(x_i^H\right)^2\right)} \tag{6.16}$$

where $\tilde{\kappa}_1 = \frac{E_b\left(1+\bar{L}\right)e^{-\bar{L}}}{N_0 N_t^2}x_i^H$ and $\tilde{\kappa}_2 = \frac{E_b}{N_0 N_t^2}\frac{\bar{L}^m e^{-\bar{L}}}{m!}x_i^H$. Combining the equations (2.15) and (6.16) and using Gauss-Laguerre quadrature, the final BER expression for binary signal in the antenna

beamforming based mm-Wave MIMO system over the IEEE 802.15.3c channel model at 60 GHz band is given by

$$p_e = \frac{1}{2\pi}\sum_{s=1}^{S^L}\sum_{i=1}^{N^H}\left\{ w_s^L\, w_i^H \left(\prod_{v=1}^{N_r}\prod_{u=1}^{N_t} \exp\left(\frac{j\, E_b\, \beta_{(u,v)}^2\, x_i^H}{N_t^2 N_0} - \lambda\, \tilde{\psi}_{\tilde{\kappa}_1}^{(u,v)}(0,L) \right) \prod_{m2} e^{\left(-\Lambda \tilde{J}_{(u,v)}(\tilde{\kappa}_2,L)\right)} \right) \right. \\ \left. \times\, Q\left(\sqrt{(1-\rho_r)\, x} \right) \mathrm{e}^{\left[x\left(1-jx_i^H\right)+\left(x_i^H\right)^2 \right]} \Big|_{x=x_s^L} \right\} \tag{6.17}$$

6.4 Numerical Results and Discussion

This section presents the simulated and analytical BERs of the mm-Wave MIMO communication system for four different environments of the IEEE 802.15.3c channel- Residential LOS (CM1), Residential NLOS (CM2), Office LOS (CM3) and Desktop NLOS (CM8). For simulation and analysis, we set $M = 4$, the raised-cosine pulse of a roll-off factor $a = 0.8$, $T_p = 0.5$ns, $T_s = 0.5$ns, sampling time $T_{samp} = 0.01$ ns and central carrier frequency $f_c = 60$ GHz. Fig. 6.3 shows the effect of number of fingers of the Rake receiver on the BER of mm-Wave SISO communication system at SNR of 5dB. It is observed that the BER for different channel models become flat after certain values of L. These values are $L \geq 27$, $L \geq 27$, $L \geq 10$ and $L \geq 10$ for CM1.1, CM2.1, CM3.1 and CM 8.1, respectively. From this observation, it is inferred that, for CM1.1 the rays carry most of the energy fall within first 27ns, whereas for CM3.1, it falls within 10ns. Therefore, for further simulations, we choose $L = 27$, for all four channel models so that the performance can be fairly compared in all the cases.

Fig. 6.4 shows the simulated and analytical BERs of the mm-Wave SISO communication system over different environments of the IEEE 802.15.3c channel model. It is seen that the analytical results of our derived BER is a good match with the simulation results. However, there is the marginal difference between the analytical and the simulated BERs which are attributed to: (1) The use of the Gauss-Hermite and Gauss-Legendre formulae in the numerical integrations and (2) error in calculating the energy at the Rake receiver. From the equation (6.17), it is clear that the above-mentioned errors will scale up with an increase in the size of the antenna

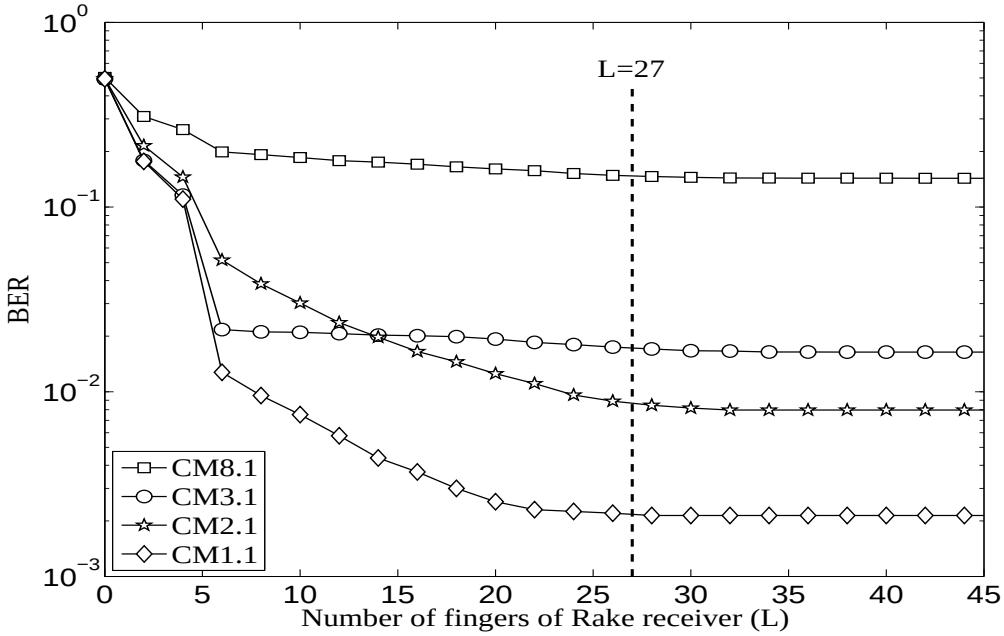

Figure 6.3: BER vs. *L* for various environments of the IEEE 802.15.3c channel model for SNR=5 dB

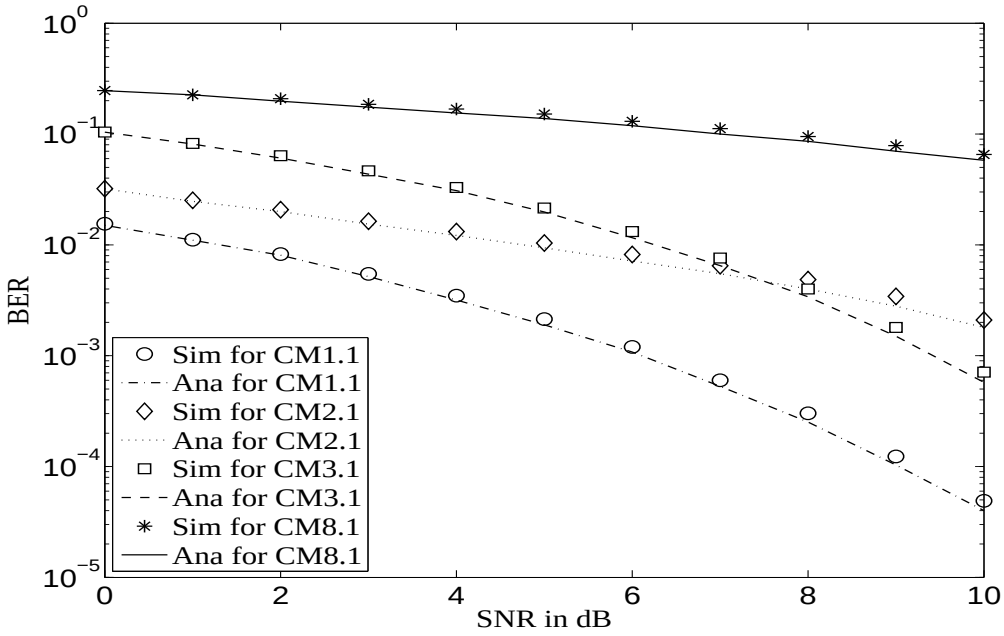

Figure 6.4: BER (simulation and analytical) of mm-Wave SISO communication for various environments of the IEEE 802.15.3c channel

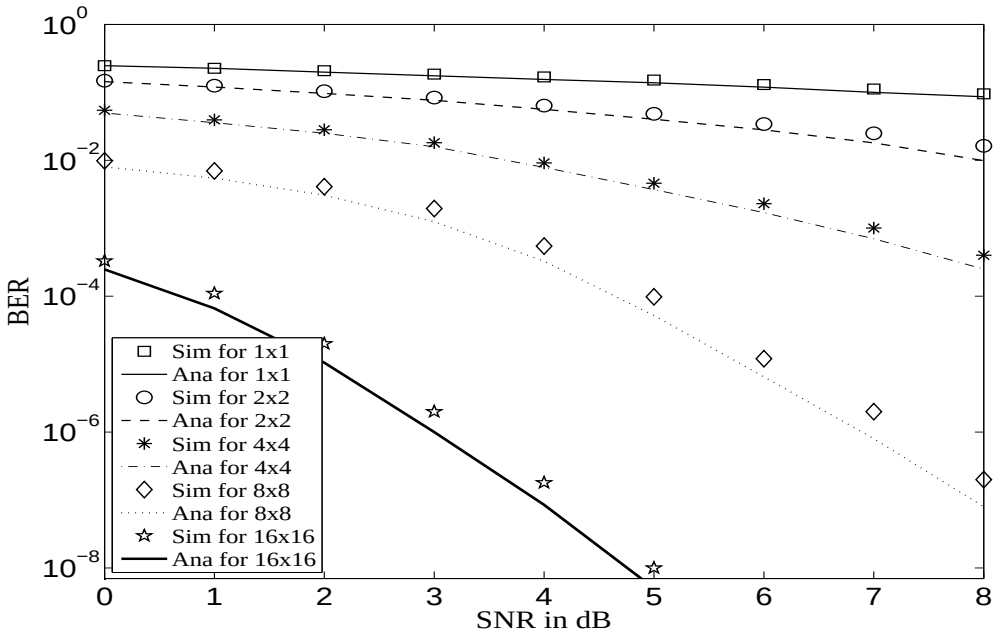

Figure 6.5: BER (simulation and analytical) for $N_t \times N_r$ mm-Wave MIMO system over the IEEE 802.15.3c channel (CM8.1)

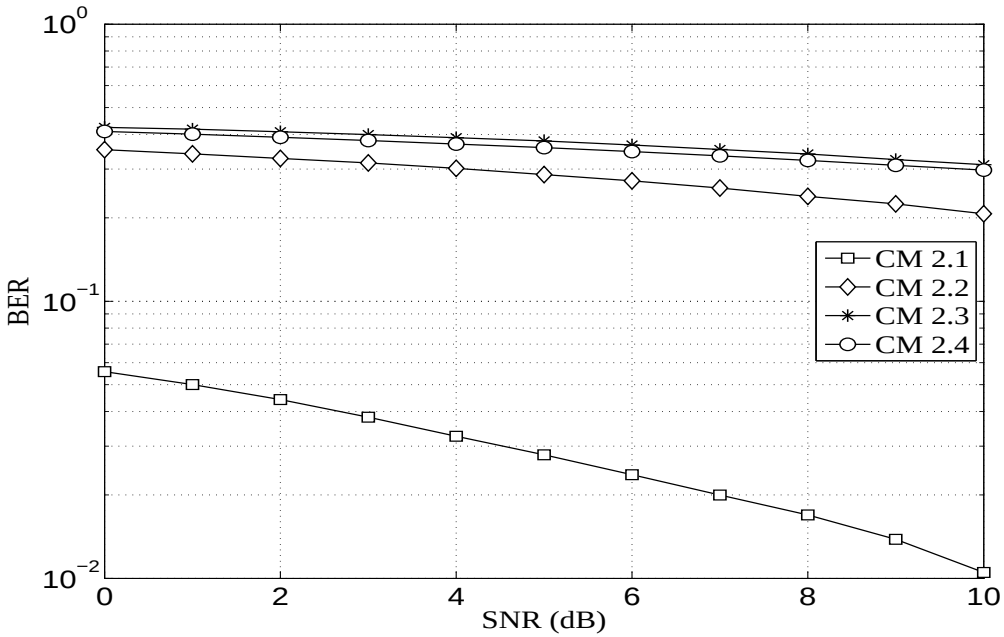

Figure 6.6: The effects of HPBW on the BER for all four sub-categories of the IEEE 802.15.3c channel (CM2)

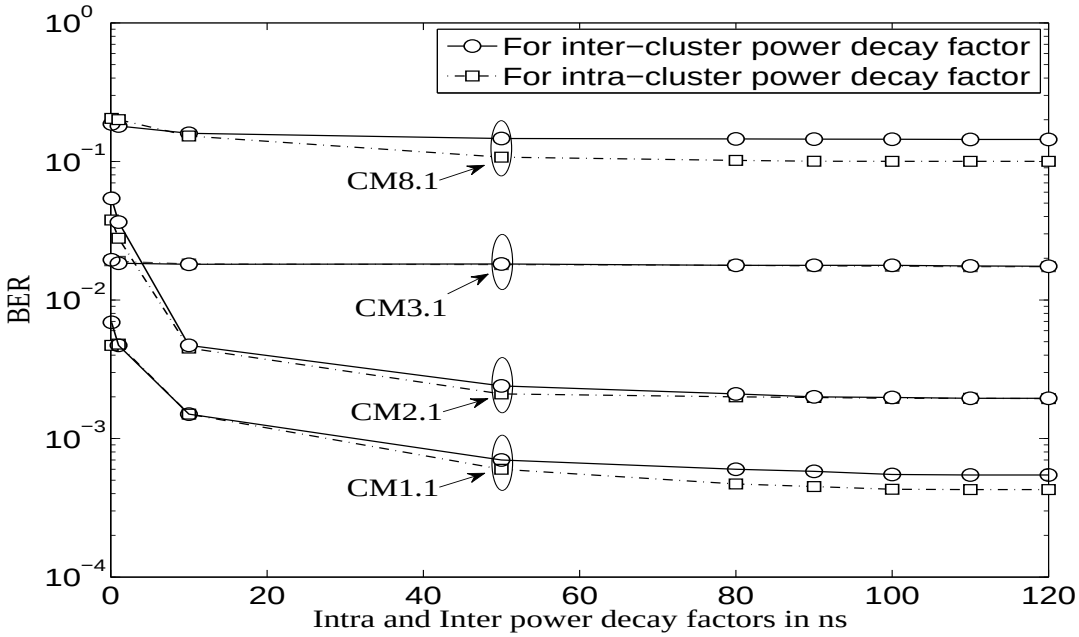

Figure 6.7: BER vs power decay factors for mm-Wave SISO system for SNR = 5dB

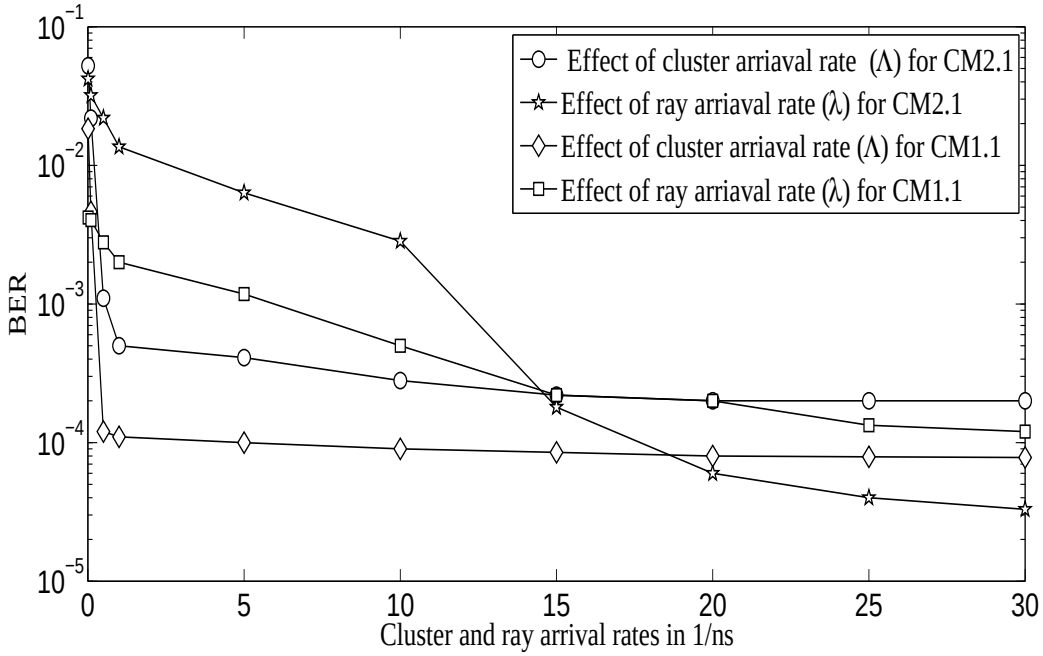

Figure 6.8: BER vs cluster and rays arrival rates of mm-Wave SISO system for SNR = 5dB

array. Therefore the differences between the simulated and the analytical BERs increase with the size of the antenna array as depicted in Fig. 6.5. The figure shows the effect of antenna array on the BER of the investigated mm-Wave system over the IEEE 802.15.3c CM8.1. For small antenna array configurations, the differences are small while for large antenna array configurations, i.e., for 8×8 and 16×16 antenna arrays, the differences are notable but is within acceptable limits. Fig. 6.6 shows the effect of HPBWs on the BER of mm-Wave SISO system over the IEEE 802.15.3c channel (CM2). According to TG3c channel report, HPBWs at Tx = 360°, 60°, 30°, 15° and HPBWs at Rx =15°, correspond to CM2.1, CM2.2, CM2.3 and CM2.4, respectively. It signifies a reduction in the omni-directionality and an increase in the directivity. A directional antenna sends more signal energy into a particular direction which leads to less power associated to cluster power level (Ω_0) in the multipath environment. As suggested in the report, Ω_0 (in dB)= -88.7, -108, -111 and -110.7 correspond to four different sub-categories of CM2. The Ω_0 has a direct effect on the energy collected by a Rake receiver (6.4), therefore, more HPBW accounts less BER.

Fig. 6.7 shows the effects of inter-cluster (Γ) and intra-cluster (γ) power decay factors on the BER of mm-Wave SISO communication system at SNR = 5 dB. Initially, when power decay factors increase, BER decreases, but for larger values of power decay factors BER curves become flat. From equation 6.4, it is clear that energy ($\mathcal{E}$) carried by MPCs increase with the Γ or γ. As a result, the total energy captured by a Rake receiver also increases, causing a decrease in BER. But beyond the certain value of power decay factor, the $\mathcal{E}$ remain. unchanged due to most of the energy carrying MPCs have already been captured by a Rake receiver. Therefore, BER curves become flat. Additionally, the similar trends of BER is also shown in Fig. 6.8, which shows the effects of cluster (Λ) and ray (λ) arrival rates on the BER. This is because, when arrival rates increase, the arrival times of MPCs decrease therefore, more MPCs arrive in the given time interval at the Rake receiver and $\mathcal{E}$ increases, thereby BER decreases. The result also indicates that the BER curves are less variant with a change in the λ and reaches the lower

saturation value slower than the change in Λ. This is because the ray arrival rate influences the rays within the cluster whereas cluster arrival rate influences the every cluster.

6.5 Summary

In this chapter, we have derived an expression of BER for antenna beamforming based mm-Wave MIMO communication system with the bank of coherent Rake receivers at 60 GHz band. In the antenna beamforming, we have considered the analog phase shifters employed at the Tx-ULAs and Rx-ULAs to overcome the high path loses experienced by the mm-Wave signals. We have plotted the simulation and analytical results of mm-Wave systems for different antenna arrays over various environment of the IEEE 802.15.3c channel model. The derived BER expression is a good match with the Monte-Carlo simulation results which validate the suitability of the analysis of this system. Additionally, we have discussed the impacts of power decay factors and arrival rates of the IEEE 802.15.3c channel model on the BER. We have also suggested a sufficient number of Rake fingers required to capture the energy of mm-Wave signal in various environments of the IEEE 802.15.3c channel model.

7

Conclusions and Future Work

Contents

The objective of the work presented in this thesis is to investigate the performance of the UWB and the mm-Wave indoor wireless communication systems with different diversity networks. In this chapter, we summarize the thesis, discuss its findings and contributions and also provide some suggestions for future extension of the presented work.

7.1 Conclusions

A brief summary of the thesis is as follows.

In this thesis, we have presented an approximate model of the lognormal shadowing by a Mixture of Gamma distributions using the moments matching with non-linear curve fitting method and the EM algorithm. Using this approximation, we have derived the CF based computable BER formulae of binary signals with a coherent Rake receiver for UWB and UWB-MIMO wireless communications systems over the IEEE 802.15.3a channel model. We have also derived the error performance of UWB and LR-UWB DF-relay systems with an antenna selection scheme over the IEEE 802.15.3a and the IEEE 802.15.4a channel models, respectively. Additionally, we have analysed the performance of mm-Wave wireless communication system at 60 GHz band. Furthermore, we have discussed the impacts of Rake fingers and other parameters of different channel models on the performance. The specific contributions of the thesis and its finding are enlisted below.

(a) The MG distribution is a good fit to the lognormal shadowing and the exactness of the MG distributions improves with addition of more Gamma components. To measure the exactness, we have generated the PDF and CDF plots of both the distributions (lognormal shadowing and MG distributions) and calculate the MSE for different number of mixing coefficients. We have also observed that, the parameter estimation using an EM algorithm is more efficient and accurate than the moment matching method.

(b) Using the MG approximation, we have derived the computable BER formula of binary signals with a coherent Rake receiver for UWB and TAS/MRC based UWB-MIMO systems

in Chapter 2 and Chapter 3, respectively. The results showed that, the accuracy of the derived BER expression for 5-MG distributions is better than the reported BER results. Additionally, the computer computation time of our BER expression is much less than the reported BER expressions and the Monte-Carlo simulation.

(c) We derived the error performance for the DF-relaying UWB and LR-UWB systems with an antenna selection scheme at the source and the relay terminals in Chapter 4 and Chapter 5, respectively. The results showed that the BER of investigated systems improves with the increase in number of antennas and the impact of shadow fading effect in the BER is quite significant and should not be ignored while evaluating the performance of UWB system. Additionally, the BER of investigated system over the IEEE 802.15.3a channel model has lesser than the IEEE 802.15.4a channel model.

(d) The derivation of BER for antenna beamforming based mm-Wave MIMO system over the IEEE 802.15.3c channel model at 60 GHz band is presented in Chapter 6. The effects of HPBWs and antenna configurations on the performance are also reported in the same chapter.

(e) The numerical results of the derived BER expressions are in close agreement with the Monte-Carlo simulation results, which validate our BER expressions and justify the assumptions and approximations taken in the analyses.

(f) In this work, we have also suggested the sufficient number of Rake fingers required to capture the signal energy in the various environments of investigated systems.

7.2 Suggestions for Future Work

Some of the possible future directions that can be taken up as an extension of this work are suggested below.

(a) Performance analysis of two hop UWB systems can be easily extended to the multi hop and multi user UWB systems with different cooperative strategies.

(b) The analysis of mm-Wave system for 60 GHz band can be done for the OFDM network with different beamforming techniques.

(c) The investigation of index modulation techniques in the OFDM-MIMO system for 60 GHz band can also be explored.

(d) The presented work can be explored for non-i.i.d channel and in the interference-limited conditions.

A

Gaussian-Quadrature Rule

A.1 Gauss Quadrature Rule

In numerical analysis, a quadrature rule is an approximate solution of the definite integral of a function, usually stated as a weighted sum of function values at specified points within the domain of integration. In this thesis, we have considered three types of quadrature formulae, which are given below.

A.1.1 Gauss-Hermite quadrature

$$\int_{-\infty}^{\infty} e^{-x^2} f(x)\, dx \approx \sum_{i=1}^{N^H} w_i^H f\left(x_i^H\right) \tag{A.1}$$

where N^H is the number of nodes and w_i^H denotes the weight coefficient associated with the i^{th} root $\left(x_i^H\right)$ of Hermite polynomial can be calculated as

$$w_i^H = \frac{N^H! 2^{(N^H-1)} \sqrt{\pi}}{N^{H2}\left[H_{N^H}\left(x_i^H\right)\right]^2}$$

and the Hermite polynomial is given as

$$H_{N^H}(x) = \left(2x - \frac{d}{dx}\right)^{N^H} .1$$

A.1.2 Gauss-Legendre quadrature

$$\int_a^b f(x)\, dx \approx \frac{b-a}{2} \sum_{j=1}^{N^L} w_j^L f\left(\frac{b-a}{2} x_j^L + \frac{a+b}{2}\right) \tag{A.2}$$

where N^L is the number of nodes and w_j^L are the weight coefficient associated with the j^{th} root $\left(x_j^L\right)$ of Legendre polynomials can be calculated as

$$w_i^L = \frac{2}{\left(1-\left(x_j^L\right)^2\right)\left[P'_{(N^L)}\left(x_j^L\right)\right]^2}$$

and the Legendre polynomials is given as

$$P_{N^L}(x) = \frac{1}{N^L! 2^{N^L}} \frac{d^{N^L}}{dx^{N^L}} \left[\left(x^2 - 1 \right)^{N^L} \right]$$

A.1.3 Gauss-Laguerre quadrature

$$\int_0^\infty e^{-x} f(x)\, dx \approx \sum_{s=1}^{S^L} w_s^L f\left(x_s^L \right) \tag{A.3}$$

where S^L is the number of nodes and w_s^L weight coefficients associated with the s^{th} root $\left(x_s^L \right)$ of Laguerre polynomials can be calculated as

$$w_s^L = \frac{x_s^L}{(S^L + 1)^2 [L_{S^L+1}(x_s^L)]^2}$$

and the Laguerre polynomials is given as

$$L_{S^L}(x) = \frac{1}{S^L!} \left(\frac{d}{dx} - 1 \right)^{S^L} x^{S^L}$$

B

Parametric Specification of the IEEE 802.15.4a Channel Model

B.1 IEEE 802.15.4a Channel Model

The experimentally measured values of channel parameters for various environments of the IEEE 802.15.4a channel model are given in the Tables B.1 and B.2, respectively.

Table B.1: Experimental values of the IEEE 802.15.4a channel parameters for residential and office environments

Channel Parameters	Residential		Indoor Office	
	LOS (CM1)	NLOS (CM2)	LOS (CM3)	NLOS (CM4)
Path Loss (PL_0)	43.9	48.7	36.6	51.4
Pathloss exponent (n)	1.70	4.58	1.63	3.07
Delay spread S[dB]	2.22	3.51	1.9	3.9
Antenna loss (A_{ant}) [dB]	3	3	3	3
Frequency dependence of the pathloss κ [dB/octave]	1.12+0.12	1.53+0.32	-3.5	5.3
Mean number of clusters $(\bar{L})$	3	3.5	5.4	1
Λ [1/ns]	0.047	0.12	0.016	NA
λ_1 [1/ns]	1.54	1.77	0.19	NA
λ_2 [1/ns]	0.15	0.15	2.97	NA
β	0.095	0.045	0.0184	NA
Γ [ns]	22.61	26.27	14.6	NA
k_γ	0	0	0	NA
γ_0 [dB]	12.53	17.50	6.4	NA
$\sigma_{cluster}$ [dB]	2.75	2.93	NA	NA
m_0 [dB]	0.67	0.69	0.42	0.50
k_m	0	0	0	0
$\hat{m}_0$ [dB]	0.28	0.32	0.31	0.25
$\hat{k}_m$	0	0	0	0
$\tilde{m}_0$	NA	NA	NA	NA
χ	NA	NA	NA	0.86
γ_{rise}	NA	NA	NA	15.21
γ_1	NA	NA	NA	11.84

Table B.2: Experimental values of the IEEE 802.15.4a channel parameters for outdoor and industrial environments

PARAMETERS	OUTDOOR		OPEN OUTDOOR	INDUSTRIAL	
	LOS (CM5)	NLOS (CM6)	NLOS (CM7)	LOS (CM8)	NLOS (CM9)
Path Loss (PL_0)	43.29	43.29	48.96	-56.7	-56.7
n	1.76	2.5	1.58	1.2	2.15
σ_s	0.83	2	3.96	6	6
A_{ant} [dB]	3	3	3	3	3
κ [dB/octave]	-1.6	0.4	NA	-5.6	-7.82
$\bar{L}$	13.6	10.6	3.31	4.75	1
Λ [1/ns]	0.0048	0.0243	0.0305	0.0709	NA
λ_1 [1/ns]	0.27	0.15	0.0225	NA	NA
λ_2 [1/ns]	2.41	1.13	0	NA	NA
β	0.0078	0.0062	0	NA	NA
Γ [ns]	31.7	104.7	56	13.47	NA
k_γ	0	0	0	0.926	NA
γ_0 [dB]	3.7	9.3	0.92	0.651	NA
$\sigma_{cluster}$ [dB]	NA	NA	NA	4.32	NA
m_0 [dB]	0.77	0.56	4.1	0.36	0.30
k_m	0	0	0	0	0
$\hat{m}_0$ [dB]	0.78	0.25	2.5	1.13	1.15
$\hat{k}_m$	0	0	0	0	0
$\tilde{m}_0$	NA	NA	0	12099	NA
χ	NA	NA	NA	NA	1
γ_{rise}	NA	NA	NA	NA	17.35
γ_1	NA	NA	NA	NA	85.36

C

Parametric Specification of the IEEE 802.15.3c Channel Model

C.1 IEEE 802.15.3c Channel Model

On the basis of practical measurements, the IEEE P802.15 WPAN channel modeling sub-committee has categorized the 60 GHz indoor communication environment into five categories defined in Table C.1. The detailed parametric specifications for various environments of the IEEE 802.15.3c channel model are given in Tables C.2, C.3 and C.4:

Table C.1: Channel environments of the IEEE 802.15.3c channel

CHANNEL MODEL (CM)	SCENARIO	ENVIRONMENT
CM1	LOS	Residential
CM2	NLOS	
CM3	LOS	Office
CM4	NLOS	
CM5	LOS	Library
CM6	NLOS	
CM7	LOS	Desktop
CM8	NLOS	
CM9	LOS	Kiosk

Table C.2: Parametric specifications of channel parameters for residential environment

PARAMETERS	RESIDENTIAL ENVIRONMENT								
	LOS (CM1)					NLOS (CM2)			
Tx-HPBW	360°	60°	30°	15°	360°	360°	60°	30°	15°
Rx-HPBW	15°	15°	15°	15°	15°	15°	15°	15°	15°
Λ [1/ns]	0.191	0.194	0.144	0.045	0.21	0.191	0.194	0.144	0.045
λ [1/ns]	1.22	0.9	1.17	0.93	0.77	1.22	0.9	1.17	0.93
Γ [ns]	4.46	8.98	21.5	12.6	4.19	4.46	8.98	21.5	12.6
γ [ns]	6.25	9.17	4.35	4.98	1.07	6.25	9.17	4.35	4.98
σ_1 [dB]	6.28	6.63	3.71	6.11	1.26	6.28	6.63	3.71	6.11
σ_2 [dB]	13	9.83	7.31	6.11	1.26	13.	9.83	7.31	6.11
σ_ϕ [degree]	49.8	119	46.2	107	8.32	49.8	119	46.2	107
L	9	11	8	4	4	9	11	8	4
Δk [degree]	18.8	17.4	11.9	4.6	NA	18.8	17.4	11.9	4.6
$\Omega(d)$ [dB]	-88.7	-108	-111	-110.7	NA	-88.7	-108	-111	-110.7
n	2	2	2	2	NA	2	2	2	2

Table C.3: Parametric specifications of channel parameters for office and desktop environments

PARAMETERS	OFFICE					DESKTOP				
	LOS (CM3)		NLOS (CM4)			LOS (CM7)			NLOS (CM8)	
Tx-HPBW	30°	60°	360°	30°	Omni	30°	60°	360°	30°	60°
Rx-HPBW	30°	60°	15°	15°	15°	30°	60°	15°	30°	60°
Λ [1/ns]	0.041	0.027	0.032	0.028	0.07	0.037	0.047	1.72	0.370	0.0474
λ [1/ns]	0.971	0.293	3.45	0.76	1.88	0.641	0.373	3.14	0.641	0.3731
Γ [ns]	49.8	38.8	109.2	134	19.44	21.1	22.3	4.01	21.1	22.3
γ [ns]	45.2	64.9	67.9	59.0	0.42	8.85	17.2	0.58	8.85	17.2
σ_1 [dB]	6.60	8.04	3.24	4.37	1.82	3.01	7.27	2.7	3.01	7.27
σ_2 [dB]	11.3	7.95	5.54	6.66	1.88	7.69	4.42	1.9	7.69	4.42
σ_ϕ [degree]	102	66.4	60.2	22.2	9.1	34.6	38.1	14	34.1	38.1
$\left(\bar{L}\right)$	6	5	5	5	6	3	3	14	3	3
Δk [degree]	21.9	11.4	19	19.2	NA	11	17.2	NA	11	17.2
$\Omega(d)$ [dB]	-3.27d -85.8	-0.303d -90.3	-109	-107.2	NA	4.44d -105.4	3.46d -98.4	NA	4.44d -105.4	3.46d -98.4
n	2	2	3.35	3.35	NA	2	2	NA	2	2
A_{NLOS}	0	0	5.56	5.56	NA	0	0	0	0	0
h_1 [m]	NA	NA	NA	NA	NA	0-0.3	0-0.3	NA	0-0.3	0-0.3
h_2 [m]	NA	NA	NA	NA	NA	0-0.3	0-0.3	NA	0-0.3	0-0.3
(d) [m]	NA	NA	NA	NA	NA	0.3	0.3	NA	0.3	0.3

Table C.4: Parametric specifications of channel parameters for kiosk environment

PARAMETERS	KIOSK	
	LOS (CM9)	
	Tx-30° & Rx-30°	Tx-30° & Rx-30°
Inter-cluster arrival rate [Λ in 1/ns]	0.0546	0.0442
Intra-cluster (ray) arrival rate [λ in 1/ns]	0.917	1.01
Inter-cluster (cluster) decay rate [Γ in ns]	30.2	64.2
Intra-cluster (ray) decay rate [γ in ns]	36.5	61.1
Cluster lognormal std deviation [σ_c in dB]	2.23	2.66
Ray lognormal std deviation [σ_r in dB]	6.88	4.39
Angle spread [σ_ϕ in degree]	34.2	45.8
Average number of clusters [$\bar{L}$]	5	7
Ray Rician factor [Δk in dB]	11	9.1
Average power of the first ray of the first cluster [$\Omega(d)$ in dB]	-98.0	-107.8
PL exponent [n]	2	2
Attenuation value for NLOS environments [A_{NLOS}]	0	0

Bibliography

[1] F. H. Henning, *Nonsinusoidal waves for radar and radio communication*, Academic press, 1981.

[2] M. Z. Win, D. Dardari, A. F. Molisch, W. Wiesbeck, and J. Zhang, "History and applications of UWB," in Proc. *IEEE*, vol. 97, no. 2, pp. 198–204, 2009.

[3] D. Benedetto, *Understanding ultra wide band radio fundamentals*, Pearson Education India, 2008.

[4] Federal Communications Commission, "First report and order in the matter of revision of part 15 of the Commissions rules regarding ultra-wideband transmission systems," *ET-Docket* 98-153, FCC02-48, April 2002.

[5] H. F. Engler Jr, "Technical issues in ultra-wideband radar systems," *Introduction to Ultra-Wideband Radar Systems*, pp. 11–50, 1995.

[6] T. W. Barrett, "History of Ultra-WideBand (UWB) Radar & Communications: Pioneers and Innovators. Part I, UWB communications," in Proc. *Progress In Electromagnetics Symposium Communication*, Cambridge, MA July 2000.

[7] S. Emami, *UWB Communication Systems: Conventional and 60 GHz*, Springer, 2013.

[8] J. Reed, *Introduction to ultra wideband communication systems*, Prentice Hall Press, 2005.

[9] IEEE 802.15 Overview, web site, (`http://standards.ieee.org/wireless/overview.html`).

[10] K.-I. Takizawa, L. Huan-Bang, I. Nishiyama, J.-I. Takada, and R. Kohno, "Overview of research, development, standardization, and regulation activities in NICT UWB project," *IEICE Trans. on Fundamentals of Elect., Commun. and Computer Sciences*, vol. 89, no. 11, pp. 2996–3005, 2006.

[11] A. F. Molisch, J. R. Foerster, and M. Pendergrass, Channel Modeling Sub-committee Report Final, *IEEE* P802.15-02/368r5-SG3a, IEEE P802.15 Working Group for WPAN, 2002.

[12] R. Fisher and others, IEEE 802.15 WPAN High Rate Alternative PHY Task Group 3a (TG3a) , web site (`http://ieee802.org/15/pub/TG3a.html`).

[13] A. F. Molisch, K. Balakrishnan, C.-C. Chong, S. Emami, A. Fort, J. Karedal, J. Kunisch, H. Schantz, U. Schuster, and K. Siwiak, "IEEE 802.15. 4a channel model-final report," *IEEE P802*, vol. 15, no. 04, p. 0662, 2004, (`http://www.ieee802.org/15/pub/TG4a.html`).

[14] LAN/MAN Standards Committee and others, "Part15.4: Wireless Medium Access Control (MAC) and Physical Layer (PHY) Specifications for Low-Rate Wireless Personal Area Networks (WPANs); Amendment I: Add Alternate PHYs," Mar. 2007.

[15] M. Hamalainen, *Wireless UWB Body Area Networks: Using the IEEE802. 15.4-2011*, Academic Press, 2014.

[16] K.-C. Huang and Z. Wang, *Millimeter wave communication systems*, John Wiley & Sons, vol. 29, 2011.

[17] S.-Q. Xiao and M.-T. Zhou, *Millimeter wave technology in wireless PAN, LAN, and MAN*, CRC Press, 2008.

[18] Z. Pi and F. Khan, "An introduction to millimeter-wave mobile broadband systems," *IEEE Commun. Mag.*, vol. 49, no. 6, pp. 101–107, 2011.

[19] S. Yong, "TG3c channel modeling sub-committee final report," *IEEE802. 15-07-0584-00-003c*, March 2007.

[20] H. Singh, J. Oh, C. Kweon, X. Qin, H.-R. Shao, and C. Ngo, "A 60 GHz wireless network for enabling uncompressed video communication," *IEEE Commun. Mag.*, vol. 46, no. 12, pp. 71–78, 2008.

[21] ETSI DTR/ERM-RM-049, "Electromagnetic Compatibility and Radio Spectrum Matter (ERM): System Reference Document: Technical Characteristics of Multiple Gigabit Wireless System in the 60 GHz Range," Mar 2006.

[22] E. Perahia, and M. X. Gong, "Gigabit wireless LANs: an overview of IEEE 802.11 ac and 802.11 ad," *ACM SIGMOBILE Mobile Computing and Communications Review*, vol. 15, no. 3, pp. 23-33, 2011.

[23] S. K. Yong, P. Xia and G. A. Valdes, *60GHz Technology for Gbps WLAN and WPAN: from Theory to Practice*, John Wiley & Sons, 2011.

[24] M. Marcus and B. Pattan, "Millimeter wave propagation: spectrum management implications," *IEEE Microwave Magazine*, vol. 6, no. 2, pp. 54–62, 2005.

[25] C. Cordeiro and S. Abu-Surra, "PHY/MAC complete proposal specification," 2010, (`http://www.ieee802.org/11/Reports/tgad_update.html`).

[26] J. P. Gilb, "IEEE Standards 802.15. 3c–Part 15.3: wireless medium access control (MAC) and physical layer (PHY) specifications for high rate wireless personal area networks (WPANs) Amendment 2: millimeter-wave-based alternative physical layer extension [S]," *IEEE Computer Society*, New York, 2009.

[27] H. Liu, "Error performance of a pulse amplitude and position modulated ultra-wideband system over lognormal fading channels," *IEEE Commun. Letters*, vol. 7, no. 11, pp. 531–533, 2003.

[28] C. Abou-Rjeily, "Performance analysis of UWB systems over the IEEE 802.15. 3a channel model," *IEEE Trans. Wireless Commun.*, vol. 59, no. 9, pp. 2377–2382, 2011.

[29] M. Di Renzo and F. Graziosi, "Approximating the linear combination of log-normal RVs via pearson type IV distribution for UWB performance analysis," *IEEE Trans. Commun.*, vol. 57, no. 2, pp. 388–403, 2009.

[30] I. Guvenc and H. Arslan, "Performance evaluation of UWB systems in the presence of timing jitter," in Proc. *IEEE Conf. Ultra Wideband Syst. and Technol.*, Virginia, Nov. 2003, pp. 136–141.

[31] T. Q. Quek and M. Z. Win, "Ultrawide bandwidth transmitted-reference signaling," in Proc. *IEEE Int. Conf. Commun.*, vol. 6, 2004, pp. 3409–3413.

[32] J. A. Gubner and K. Hao, "A computable formula for the average bit error probability as a function of window size for the IEEE 802.15. 3a UWB channel model," *IEEE Trans. on Microwave Theory and Techniques*, vol. 54, no. 4, pp. 1762–1768, 2006.

[33] W.-D. Wu, C.-C. Lee, C.-H. Wang, and C.-C. Chao, "Signal-to-Interference-Plus-Noise Ratio Analysis for Direct-Sequence Ultra-Wideband Systems in Generalized Saleh–Valenzuela Channels," *IEEE Journal of Selected Topics in Signal Processing*, vol. 1, no. 3, pp. 483–497, 2007.

[34] W. P. Siriwongpairat, W. Su, and K. R. Liu, "Performance characterization of multiband UWB communication systems using Poisson cluster arriving fading paths," *IEEE Journal on Selected Areas in Commun.*, vol. 24, no. 4, pp. 745–751, 2006.

[35] K. Hao and J. A. Gubner, "The distribution of sums of path gains in the IEEE 802.15.3a UWB channel model," *IEEE Trans. Wireless Commun.*, vol. 6, no. 3, pp. 811–816, 2007.

[36] L.-C. Wang and W.-C. Liu, "Bit error rate analysis in IEEE 802.15.3a UWB channels," *IEEE Trans. Wireless Commun.*, vol. 9, no. 5, pp. 1537–1542, 2010.

[37] A. Abdi and M. Kaveh, "On the utility of Gamma PDF in modeling shadow fading (slow fading)," in Proc. *IEEE Veh. Technol. Cof.,* Houston, TX., 1999, pp. 2308–2312.

[38] I. Kostic, "Analytical approach to performance analysis for channel subject to shadowing and fading," *IEE Proceedings-Commun.*, vol. 152, no. 6, pp. 821–827, 2005.

[39] J. Salo, L. Vuokko, H. M. El-Sallabi, and P. Vainikainen, "An additive model as a physical basis for shadow fading," *IEEE Trans. Veh. Technol.*, vol. 56, no. 1, pp. 13–26, 2007.

[40] S. Atapattu, C. Tellambura, and H. Jiang, "A mixture gamma distribution to model the SNR of wireless channels," *IEEE Trans. Wireless Commun.*, vol. 10, pp. 4193–4203, 2011.

[41] H. Al-Hmood and H. Al-Raweshidy, "On the Sum and the Maximum of Nonidentically Distributed Composite $(\eta - \mu)$/gamma Variates Using a Mixture Gamma Distribution With Applications to Diversity Receivers," *IEEE Trans. Veh. Technol.*, vol. 65, no. 12, pp. 10048–10052, 2016.

[42] S. Al-Ahmadi and H. Yanikomeroglu, "On the approximation of the generalized-K distribution by a gamma distribution for modeling composite fading channels," *IEEE Trans. Wireless Commun.*, vol. 9, no. 2, pp. 706–713, 2010.

[43] J. Almhana, Z. Liu, V. Choulakian, and R. McGorman, "A recursive algorithm for Gamma mixture models," in Proc. *IEEE ICC*, 2006, pp. 197–202.

[44] I. Gebru, X. Alameda-Pineda, F. Forbes, and R. Horaud, "EM algorithms for weighted-data clustering with application to audio-visual scene analysis," *IEEE Trans. on Pattern Analysis and Machine Intelligence*, vol. 30, no. 12, pp. 2402–2415, 2016.

[45] G. Celeux, S. Chrétien, F. Forbes, and A. Mkhadri, "A component-wise EM algorithm for mixtures," *Journal of Computational and Graphical Statistics*, vol. 10, no. 4, pp. 697–712, 2001.

[46] T. Skinner and J. Cavers, "Selective diversity for Rayleigh fading channels with a feedback link," *IEEE Trans. Commun.*, vol. 21, no. 2, pp. 117–126, 1973.

[47] S. Thoen, L. Van der Perre, B. Gyselinckx, and M. Engels, "Performance analysis of combined transmit-SC/receive-MRC," *IEEE Trans. Commun.*, vol. 49, no. 1, pp. 5–8, 2001.

[48] B. A. Bjerke, Z. Zvonar, and J. G. Proakis, "Antenna diversity combining schemes for WCDMA systems in fading multipath channels," *IEEE Trans. Wireless Commun.*, vol. 3, pp. 97–106, Jan 2004.

[49] Z. Chen, Z. Chi, Y. Li, and B. Vucetic, "Error performance of maximal-ratio combining with transmit antenna selection in flat Nakagami-m fading channels," *IEEE Trans. Wireless Commun.*, vol. 8, no. 1, pp. 424–431, Jan 2009.

[50] Z. Chen, J. Yuan, and B. Vucetic, "Analysis of transmit antenna selection/maximal-ratio combining in Rayleigh fading channels," *IEEE Trans. Veh. Technol.*, vol. 54, no. 4, pp. 1312–1321, July 2005.

[51] Z. Yan and P. Yu, "Performance analysis of the MB-OFDM ultra-wide band communication system with space-time block coding and antenna selection," in Proc. 3rd *IEEE/IFIP Int. Conference in Central Asia*, 2007, pp. 1–5.

[52] A. Mertins and L. C. Tran, "Space-time-frequency code implementation in MB-OFDM UWB communications: design criteria and performance," *IEEE Trans. Wireless Commun.*, vol. 8, no. 2, pp. 701–713, 2009.

[53] H. Liu, R. C. Qiu, and Z. Tian, "Error performance of pulse-based ultra-wideband MIMO systems over indoor wireless channels," *IEEE Trans Wireless Commun.*, vol. 4, no. 6, pp. 2939–2944, 2005.

[54] W. Q. Malik and D. J. Edwards, "Measured MIMO capacity and diversity gain with spatial and polar arrays in ultrawideband channels," *IEEE Trans. Commun.*, vol. 55, no. 12, pp. 2361–2370, 2007.

[55] H. Nguyen, F. Zheng, and T. Kaiser, "Antenna selection for time reversal MIMO-UWB systems," in Proc. *IEEE* 69^{th} *VTC*, 2009, pp. 1–5.

[56] E. C. Van Der Meulen, "Three-terminal communication channels," *Advances in Applied Probability*, pp. 120–154, 1971.

[57] T. Cover and A. E. Gamal, "Capacity theorems for the relay channel," *IEEE Trans. on Inform. Theory*, vol. 25, no. 5, pp. 572–584, 1979.

[58] A. Sendonaris, E. Erkip, and B. Aazhang, "User cooperation diversity. Part I and part II," *IEEE Trans. Commun.*, vol. 51, no. 11, pp. 1927–1948, 2003.

[59] A. Nosratinia, T. E. Hunter, and A. Hedayat, "Cooperative communication in wireless networks," *IEEE commun. Mag.*, vol. 42, no. 10, pp. 74–80, 2004.

[60] K. R. Liu, *Cooperative communications and networking*, Cambridge university press, 2009.

[61] Y.-W. P. Hong, W.-J. Huang, and C.-C. J. Kuo, *Cooperative communications and networking: technologies and system design*, Springer Science & Business Media, 2010.

[62] J. N. Laneman, D. N. Tse, and G. W. Wornell, "Cooperative diversity in wireless networks: Efficient protocols and outage behavior," *IEEE Trans. on Inform. theory*, vol. 50, no. 12, pp. 3062–3080, 2004.

[63] R. Pabst, B. H. Walke, D. C. Schultz, P. Herhold, H. Yanikomeroglu, S. Mukherjee, H. Viswanathan, M. Lott, W. Zirwas, M. Dohler, and others, "Relay-based deployment concepts for wireless and mobile broadband radio," *IEEE Commun. Mag.*, vol. 42, no. 9, pp. 80–89, 2004.

[64] M. O. Hasna and M.-S. Alouini, "End-to-end performance of transmission systems with relays over Rayleigh-fading channels," *IEEE Trans. Wireless Commun.*, vol. 2, no. 6, pp. 1126–1131, 2003.

[65] C. Cho, H. Zhang, and M. Nakagawa, "A UWB repeater with a short relaying-delay for range extension," in Proc. *Wireless Commun. and Networking Conf.*, vol. 2, 2004, pp. 1154–1158.

[66] C. Abou-Rjeily, N. Daniele, and J.-C. Belfiore, "On the decode-and-forward cooperative diversity with coherent and non-coherent UWB systems," in Proc. *IEEE Int. Conf. Ultra-Wideband,*, 2006, pp. 435–440.

[67] C. Chihong, H. Zhang, and M. Nakagawa, "A short delay relay scheme using shared frequency repeater for UWB impulse radio," *IEICE Trans. on Fundamentals of Electronics, Commun. and Computer Sciences*, vol. 90, no. 7, pp. 1444–1451, 2007.

[68] G. Pan, E. Ekici, and Q. Feng, "Performance analysis of cooperative time hopping UWB systems with multi-user interference," *IEEE Trans. Wireless Commun.*, vol. 11, no. 6, pp. 1969–1975, 2012.

[69] K. Maichalernnukul, T. Kaiser, and F. Zheng, "Performance investigation of a UWB relay system using multiple relays with multiple antennas in IEEE 802.15. 3a channel," in Proc. 69th *IEEE Veh. Technol. Conf.*, 2009, pp. 1–6.

[70] Y. Fan and J. Thompson, "MIMO configurations for relay channels: Theory and practice," *IEEE Trans. Wireless Commun.*, vol. 6, no. 5, pp. 1774–1786, 2007.

[71] W.-C. Liu and L.-C. Wang, "BER analysis of the IEEE 802.15. 4a channel model with RAKE receiver," in Proc. 64th *IEEE Veh. Technol. Conf.*, 2006, pp. 1–5.

[72] Z. Ahmadian and L. Lampe, "Performance analysis of the IEEE 802.15.4a UWB system," *IEEE Trans. Commun.*, vol. 57, no. 5, pp. 1474–1485, 2009.

[73] Z. Zeinalpour-Yazdi, M. Nasiri-Kenari, and B. Aazhang, "Bit error probability analysis of UWB communications with a relay node," *IEEE Trans. Wireless Commun.*, vol. 9, no. 2, pp. 802–813, 2010.

[74] P. L. Yeoh, M. Elkashlan, and I. B. Collings, "MIMO relaying: distributed TAS/MRC in Nakagami-m fading," *IEEE Trans. Commun.*, vol. 59, no. 10, pp. 2678–2682, 2011.

[75] B. Kumbhani, L. N. B. Reddy, and R. S. Kshetrimayum, "Approximate symbol error rate of cooperative communication over generalised κ- μ and η- μ fading channels," *The Journal of Engineering*, vol. 1, no. 1, 2014.

[76] R. C. Daniels and R. W. Heath Jr, "60 GHz wireless communications: emerging requirements and design recommendations," *IEEE Veh. Technol. Mag.*, vol. 2, no. 3, pp. 41–50, 2007.

[77] S. K. Yong and C.-C. Chong, "An overview of multigigabit wireless through millimeter wave technology: potentials and technical challenges," *EURASIP Journal on Wireless Commun. and Networking*, vol. 2007, no. 1, pp. 1–10, 2006.

[78] T. S. Rappaport, S. Sun, R. Mayzus, H. Zhao, Y. Azar, K. Wang, G. N. Wong, J. K. Schulz, M. Samimi, and F. Gutierrez, "Millimeter wave mobile communications for 5G cellular: It will work," *IEEE Access*, vol. 1, pp. 335–349, 2013.

[79] H.-Y. Hsu, T.-H. Tsai, W.-D. Wu, and C.-C. Chao, "Performance Analysis of OFDM Systems over 60 GHz Indoor Channels," in Proc. *IEEE Veh. Technol. Conf.*, 2012, pp. 1–5.

[80] C. Yiu and S. Singh, "Empirical capacity of mmWave WLANs," *IEEE Journal on Selected Areas in Commun.*, vol. 27, no. 8, pp. 1479–1487, 2009.

[81] X. Zhu, A. Doufexi, and T. Kocak, "On the Performance of IEEE 802.15. 3c millimeterwave WPANs: PHY and MAC," in Proc. 6th *Conf. on Wireless Advanced (WiAD)*, 2010.

[82] T. V. Nguyen, E. Masry, and L. B. Milstein, "Channel model and performance analysis of QAM multiple antenna systems at 60-GHz in the presence of human activity," in Proc. *IEEE Global Telecommunications Conference (GLOBECOM)*, 2011, pp. 1–6.

[83] O. El Ayach, S. Rajagopal, S. Abu-Surra, Z. Pi, and R. W. Heath, "Spatially sparse precoding in millimeter wave MIMO systems," *IEEE Trans. Wireless Commun.*, vol. 13, no. 3, pp. 1499–1513, 2014.

[84] R. Rajashekar and L. Hanzo, "Hybrid Beamforming in mm-Wave MIMO Systems Having a Finite Input Alphabet," *IEEE Trans. Commun.*, vol. 64, no. 8, pp. 3337–3349, 2016.

[85] A. Alkhateeb, O. El Ayach, G. Leus, and R. W. Heath, "Channel estimation and hybrid precoding for millimeter wave cellular systems," *IEEE Journal of Selected Topics in Signal Processing*, vol. 8, no. 5, pp. 831–846, 2014.

[86] R. Valentini, M. Levorato, and C. Fischione, "Performance analysis of IEEE 802.15.3c Based mm-Wave wireless networks," in Proc. 49th *Annual Conf. Information Sciences and Systems (CISS)*, 2015, pp. 1–6.

[87] M. H. Al-Ali and K. C. Ho, "Transmit precoding in underlay MIMO cognitive radio with unavailable or imperfect knowledge of primary interference channel," *IEEE Trans. on Wireless Commun.*, vol. 15, no. 8, pp. 5143-5155, 2016.

[88] S. Hur, T. Kim, D. J. Love, J. V. Krogmeier, T. A. Thomas, and A. Ghosh, "Millimeter wave beamforming for wireless backhaul and access in small cell networks," *IEEE Trans. Commun.* , vol. 61, no. 10, pp. 43914403, Oct. 2013.

[89] G. Lee, Y. Sung, J. Seo, "Randomly-directional beamforming in millimeter-wave multiuser MISO downlink," *IEEE Trans. Wireless Commun.*, vol. 15, no. 2, pp. 1086–1100, 2016.

[90] X. Zhu, A. Doufexi, and T. Kocak, "Beamforming performance analysis for OFDM based IEEE 802.11 ad millimeter-wave WPANs," in Proc. 8th *IEEE International Workshop on Multi-Carrier Systems & Solutions (MC-SS)*, 2011, pp. 1–5.

[91] J. G. Proakis, *Digital communications*, McGraw-Hill, New York, 1995.

[92] M. Chiani, D. Dardari, and M. K. Simon, "New exponential bounds and approximations for the computation of error probability in fading channels," *IEEE Trans. Wireless Commun.*, vol. 2, no. 4, pp. 840–845, 2003.

[93] H. A. David and H. N. Nagaraja, *Order statistics*, Wiley, 1970.

[94] J. Suarez, G. Llano, and G. Hernandez, "Development of an analytic model that characterizes the fade depth of IEEE 802.15. 4a UWB channels," *IEEE Latin America Trans.*, vol. 9, no. 5, pp. 644–648, 2011.

List of Publications

Journal Publications

1. **A. Agrawal** and R. S. Kshetrimayum, "Analysis of UWB Communication over IEEE 802.15.3a Channel by Superseding Lognormal Shadowing by Mixture of Gamma Distributions," *AEU International Journal of Electronics and Communications*, vol. 69, no. 12, pp. 1795-1799, 2015.

2. **A. Agrawal** and R. S. Kshetrimayum, "Transmit Antenna Selection in the Cooperative Communication based UWB System," *Wireless Personal Communications*, vol. 94, no. 4, pp. 3001-3015, 2017.

3. **A. Agrawal** and R. S. Kshetrimayum, "Analytical BER Calculation of TAS/MRC based Two-Hop UWB Communication System over IEEE 802.15.4a Channel," accepted for publication, *IETE Technical Review*. DOI: 10.1080/02564602.2017.1331759

4. **A. Agrawal** and R. S. Kshetrimayum, "Performance Analysis of Beamforming based mm-Wave MIMO Communication System over IEEE 802.15.3c Channel at 60 GHz," under review for *IET Communication*.

Conference Publications

1. **A. Agrawal** and R. S. Kshetrimayum, "Transmit Antenna Selection for UWB Communication System over IEEE 802.15.3a Channel," in Proc. *IEEE CONNECT*, Bangalore, July 2015.

2. **A. Agrawal** and R. S. Kshetrimayum, "Average SINR Analysis of mm-Wave System at 60 GHz Band Using First and Second-order Moments," in Proc. *IEEE ANTS*, Bhubaneswar, December 2017 (Third Best Paper Award).

Bio-Data

1	Name:	Anand Agrawal
2	Date of Birth:	10-October-1985
3	Educational Qualifications:	B.E., RGPV Bhopal (2004-08) Electronics & Communication Engg. M.Tech, NIT Bhopal (2008-10) Digital Communication Engg. Ph.D, IIT Guwahati (2012-Present) Electronics and Electrical Engg.
4	Experience:	Visiting Scholar (Sept. 2015- Jan. 2016) National Tsing Hua University, Taiwan
5	Award:	Best paper award at IEEE ANTS 2017, Bhubaneswar Best poster at Research Conclave-2017, IIT Guwahati Best poster at WIP-ICDAW-2016, AEC Guwahati
6	Student Membership:	IEEE (92620870) IEICE (148396)
7	Permanent Address:	S/o Munna Lal Agrawal Subhash Puri Ghash Mandi Gwalior Madhya Pradesh, India Pincode-474 003
8	Contact Address:	Anand Agrawal Room No. G-207, Brahmaputra Hostel Indian Institute of Technology Guwahati Assam, India Pincode-781 039
9	Email:	anand.agrawal@iitg.ernet.in anand.agrawal482@gmail.com
10	Contact Number:	(+91)-94767-99216 (+91)-97069-69684